PRIMITIVE KIMBERLITE MAGMAS FROM JERICHO, N.W.T., CANADA: CONSTRAINTS ON PRIMARY MAGMA CHEMISTRY

by

SUSANNAH ELOISE PRICE

B.Sc. (Hons), James Cook University, 1994

A THESIS SUBMITTED IN PARTIAL FULFILMENT OF THE REQUIREMENTS FOR THE DEGREE OF

MASTER OF SCIENCE

in

THE FACULTY OF GRADUATE STUDIES
(Geological Sciences Division, Department of Earth And Ocean Sciences)

We accept this thesis as conforming to the required standard

THE UNIVERSITY OF BRITISH COLUMBIA

December, 1998

In presenting this thesis in partial fulfilment of the requirements for an advanced degree at the University of British Columbia, I agree that the Library shall make it freely available for reference and study. I further agree that permission for extensive copying of this thesis for scholarly purposes may be granted by the head of my department or by his or her representatives. It is understood that copying or publication of this thesis for financial gain shall not be allowed without my written permission.

Department of Earth + Ocean Sciences

The University of British Columbia
Vancouver, Canada

Date 16 Dec. '98

ABSTRACT

In this thesis I present petrographic and geochemical data for six aphanitic kimberlite samples from the Jericho kimberlite pipe, N. W. T., Canada. Three samples derive from chilled margins where kimberlite dykes cooled against wall rock; three samples represent flow differentiated margins of a kimberlite diatreme. The chilled margin samples (JD51, JD69 and JD82) are texturally representative of a melt phase with relatively few microphenocrysts (<30 vol%) set in a groundmass of predominantly calcite and serpentine. The other samples (LGS07, 4S and 4SA) are similar in texture to typical macrocrystal kimberlite (Phase 1 kimberlite at Jericho); they are a mixture of melt and small crystals, although with a higher proportion of melt than macrocrystal kimberlite. Crustal contamination was identified in samples 4S, 4SA, and weakly in JD51, with samples having elevated U and Th attributed to contamination by the U- and Th-bearing host granite (Contwoyto batholith).

Based on petrographic and geochemical evidence, samples JD69 and JD82 represent the most primitive melts identified within the Jericho kimberlite to date, with several characteristics indicative of primary melts. They have high Mg#s (86-88), high Cr (1300-1900 ppm) and Ni (800-1400 ppm) contents indicative of primary melts. They also have high CO_2 contents (10-17 wt%) suggesting they have suffered little devolatilization, and these values are a minimum for the primary magma. Furthermore, incompatible element contents (Nb, Zr, Y) of aphanitic samples are high relative to other phases of the Jericho kimberlite, suggesting these samples are the closest to a primary magma. The microphenocrysts in these samples are, however, completely serpentinized (and partly altered to other Mg-silicate hydroxides and chlorite), which affects the Mg/Si ratio of the rock.

Geochemical comparisons with experimentally generated partial melts from a carbonated garnet lherzolite source indicate that the primary kimberlite magma at Jericho may have been generated from a similar source at a pressure of 6 GPa (approximately 200 km). The Jericho geotherm suggests that the kimberlite melt may have been generated at slightly higher pressures (6.5 GPa; 220 km) and at temperatures greater than 1300°C.

TABLE OF CONTENTS

LIST OF FIGURES

LIST OF TABLES

ACKNOWLEDGEMENTS

Many thanks to my supervisor, Dr. Kelly Russell for his great ideas, sound scientific argument and abundant enthusiasm. Dr. Maya Kopylova is also thanked for being a great role model for a young "kimberlitologist" and for her many helpful discussions and suggestions. Dr. Harrison Cookenboo is thanked for encouraging me to pursue kimberlite research and for all his many helpful comments. Dr. Ian Coulson is thanked for reviewing the thesis and for many helpful suggestions. Dr. Greg Dipple and Dr. Kurt Kyser are thanked for their discussion of stable isotopes. Dr. Mati Raudsepp is thanked for help with the SEM and for reviewing the thesis. Lytton Minerals Ltd (particularly Mr. Stefan Lopatka) are thanked for access to samples and permission to publish this data.

Thanks also to the friends I've made at UBC - you've made my stay most pleasurable, and last, but not least, thanks to Toby Hobbs for providing distraction whenever it was needed.

Chapter 1

INTRODUCTION

1.1 INTRODUCTION

The chemical and physical properties of primary kimberlite melts remain enigmatic due to the lack of quenched 'glassy' kimberlite (Mitchell, 1986). In particular, it is difficult to determine the nature of primary, or even primitive, kimberlite melts because of their hybrid nature, which includes substantial amounts of xenolithic material. Unfortunately, the difference between cognate and xenolithic material is not obvious. Olivine macrocysts which are ubiquitous throughout macrocrystal kimberlite, and occupy approximately 50% by volume, might be cognate or derived from the disaggregation of peridotite nodules (Mitchell, 1986). The rounded nature of many of these macrocrysts (non-genetic name) suggests that they are xenocrysts that were milled during transport and emplacement.

In the absence of glassy kimberlite, aphanitic kimberlite represents the next best approximation to the melt phase. It is scientifically and economically important to determine the nature of primary kimberlite magmas. As kimberlite magmas originate in the mantle, the composition of primary kimberlite magmas will give us an insight into the composition of the mantle. Economically, if primary magmas can be identified at individual kimberlite deposits, it may be possible to determine whether that particular kimberlite magma sampled diamondiferous mantle. For example, did the kimberlite have a low enough fO_2 and/or temperature such that diamonds would not be completely resorbed. Thus, characterizing the primary magma allows speculation on diamond content, which may help in determining the economic potential of the

kimberlite.

There are two approaches to obtaining information about primary kimberlite magma from available kimberlite samples. The first approach is to take macrocrystal kimberlite and attempt to remove the xenolithic components. This is troublesome due to 1) the uncertainty in which material is xenolithic, e.g. choosing which olivine crystals are phenocrysts or xenocrysts, and 2) the practical difficulty of extracting these crystals, considering they make up approximately 40-60 vol% of a typical kimberlite sample. The second option is to obtain aphanitic kimberlite samples, from which either crystals have been physically removed or were never present. Once these samples have been investigated, it may be possible to model whether phenocrysts have been lost from these samples. This second option is more realistic and this study focuses on aphanitic samples.

Aphanitic volcanic rocks are produced in at least two fundamentally different ways. The first involves the cooling of aphyric magma at rates rapid enough to suppress the growth of larger crystals. The second involves the removal of crystals by processes such as 1) gravity separation reflecting density differences between melt and crystals, 2) flow differentiation (Bhattacharji, 1967) where particles tend to migrate into the region of higher flow velocity, and away from conduit walls, and 3) filter pressing, where the fluid phase is squeezed through small conduits, leaving crystals behind (like a sieve).

Aphanitic kimberlite is commonly interpreted to be a result of crystal separation mechanisms (Mitchell, 1986; Scott Smith, 1996). However, Scott Smith (1996) notes that if crystal separation processes have not occurred, aphanitic kimberlite samples represent the closest approximation of a true erupting liquid.

Samples of aphanitic kimberlite are relatively rare, especially in hypabyssal facies

kimberlite (Scott Smith, 1996), and only a few examples have been described in the literature. These include samples from the Wesselton mine, South Africa (Shee, 1986), Benfontein, South Africa (Mitchell, 1997), the Jericho kimberlite, northern Canada (Kopylova *et al.*, 1998), the Aries kimberlite, Western Australia (Edwards *et al.*, 1992), the Koidu kimberlite complex, West Africa (Taylor *et al.*, 1994), and the Mayeng Kimberlite Sill Complex, South Africa (Apter *et al.*, 1984). Of these kimberlites, only the Wesselton, Benfontein and Jericho aphanitic kimberlites are Group I kimberlites; all others are Group II kimberlites (orangeites). Group I and Group II kimberlites are chemically distinct, and only Group I kimberlites are considered in this study.

The Wesselton aphanitic kimberlite is considered to be one of the closest estimates of relatively unfractionated kimberlite (Mitchell, 1995; Edgar *et al.*, 1988; Edgar and Charbonneau, 1993). Edgar *et al.* (1988) and Edgar and Charbonneau (1993) have used it in to model the nature of kimberlite liquids. They suggest that the absence of olivine macrocrysts, the low abundances of xenoliths and xenocrysts, the high Mg# (83.9), low SiO_2 (25.6 wt%), high Ni (810 ppm) and high Cr (2410 ppm) contents are indicative of unfractionated kimberlite. The Wesselton aphanitic kimberlite has also been used in experimental studies by Arima *et al.* (1993) and Arima and Inoue (1995).

More recently, Berg (1998) has suggested that the hypabyssal Dutoitspan monticellite kimberlite and the hypabyssal Leslie monticellite kimberlite (Berg and Carlson, 1998) represent relatively primitive kimberlite magmas, being low in Al_2O_3 and considered uncontaminated by crustal material. Both these examples are macrocrystal kimberlite (i.e. not aphanitic) and Berg (1998) suggests that many of the olivine macrocrysts are derived from peridotites, and therefore not part of the original primary melt.

The only documented example of aphanitic kimberlite in Canada to date is a chilled

margin from the Jericho kimberlite pipe in the Northwest Territories, reported by Kopylova *et al.* (1998). With the completion of an underground bulk sampling program at Jericho and re-examination of the drill core sample, more examples of aphanitic kimberlite have been identified. The purpose of this study is to report the petrography and chemical composition of a suite of aphanitic kimberlite samples from the Jericho pipe. Based on textural and compositional evidence, I argue that this sample suite contains compositions representative of kimberlite melt at the time of emplacement. These samples also provide the best estimate of the nature of the primary magma composition at Jericho and potentially for the Slave craton.

1.2 GEOLOGICAL SETTING AND SAMPLE SELECTION

1.2.1 Geology of the Jericho kimberlite

The Jericho kimberlite is one of the kimberlite pipes recently discovered in the Slave craton of northern Canada. Located 400 km northeast of Yellowknife on the northwest edge of Contwoyto Lake (Fig. 1.1), Jericho is a diamondiferous pipe with 17 million tonnes of kimberlite grading between 0.7 and 1.0 carats per metric tonne, at an estimated value of $60 US per carat based on the recovery of 10,539 carats of diamonds in 9,401 tonnes of processed kimberlite (Lytton Minerals Ltd press release, June 1998). JD-2 and JD-3 are two other pipes which have been identified near the Jericho (JD-1) pipe. JD-2 is a small satellite pipe located 250 m to the north which is connected to Jericho by a 1 m wide kimberlite dyke, and JD-3 is a larger pipe 7 km to the southwest (Cookenboo, 1998). Recent drilling has identified another kimberlite intrusion (Lytton Minerals Ltd press release, September, 1998). Heaman *et al.* (1998) have determined an emplacement age for Jericho and the JD-3 pipe of 173±1 Ma, based on Rb-Sr isotope results for phlogopite macrocrysts and one eclogite xenolith.

The Jericho kimberlite intrudes Archean granitic rocks of the Slave craton, specifically the Contwoyto batholith, which is dated at 2.58-2.59 Ma (van Breemen *et al.*, 1989). The Contwoyto batholith consists of granodiorite and, more rarely, granite which are cross-cut by numerous thin (30cm) pegmatite dykes. Generally, the granitic rocks are unaltered and competent (with only minor fractures), but a 60 cm zone of friable and weathered granite occurs locally at the contact with the kimberlite pipe (Cookenboo, 1998). The Contwoyto batholith intrudes Archean supracrustal rocks of the Yellowknife Supergroup (2.66 - 2.71 Ga; Hoffman and Hall, 1993). Exposures of the Contwoyto Formation (part of the Yellowknife Supergroup) are found 8 km south of the pipe. This formation consists of meta-turbidites and iron formation. During the Proterozoic, the Mackenzie dyke swarm (1.27 Ga) and the Malley-Mackey dyke swarm (2.23-2.21 Ga) intruded the Slave craton (LeCheminant and Heaman, 1989; Davis, 1997). Mafic dykes found in contact with kimberlite at depth may be related to these dyke swarms.

Jericho is a non-micaceous kimberlite and has been chemically classified as a Group Ia kimberlite (Kopylova *et al.*, 1998). Cookenboo (1998) has distinguished three major phases of kimberlite intrusion at Jericho based on colour, degree of olivine macrocryst serpentinization, competency, groundmass appearance, texture, mantle xenolith and xenocryst content, magnetic susceptibility and density (Fig. 1.2). Mineralogical descriptions of each phase are given in Table 1.1. The first phase (Phase 1) involves the formation of a precursor dyke, which formed from several pulses of magma. The second and third phases (Phases 2 and 3) are diatreme-forming phases. Although the three phases are petrologically and chemically distinct, Kopylova *et al.* (1998) suggest they derive from a single magma. The Jericho kimberlite incorporates both mantle and crustal xenoliths. Crustal xenoliths include granite and Middle Devonian fossiliferous limestone xenoliths (Cookenboo *et al.*, 1998). Phase 1 hypabyssal kimberlite has lower

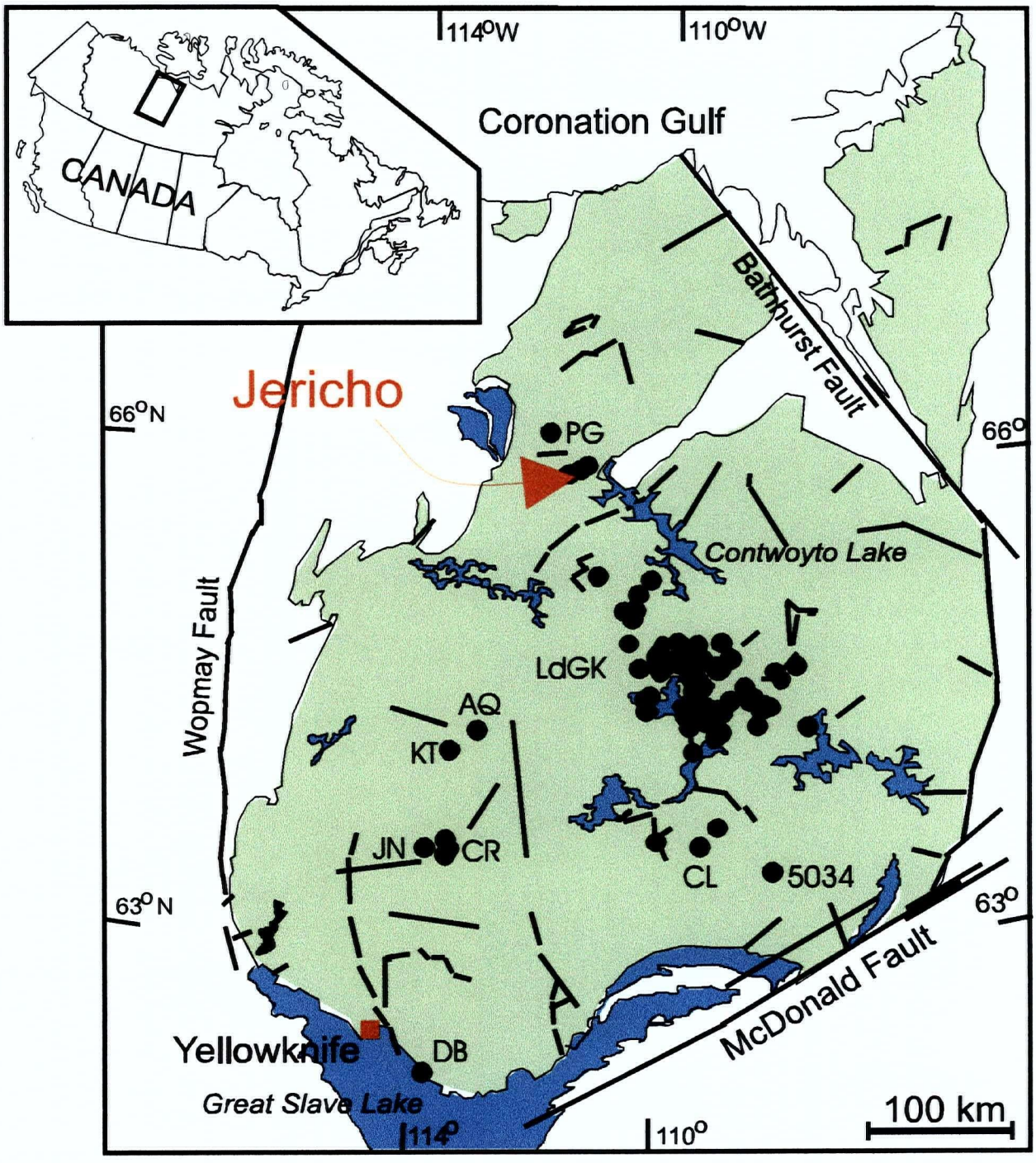

Figure 1.1 Location of kimberlite pipes (circles) in the Slave craton (green), NW Canada (see inset), including the Jericho pipes. PG = Peregrine; LdGK = Lac de Gras kimberlite field; AQ = Aquila; KT = Kent; JN = Jean; CR = Cross cluster; CL = CL-25; DB = Drybones.

concentrations of crustal rock fragments than the Phase 2 and 3 diatreme facies kimberlite.

1.2.2 Sample Selection

A suite of six aphanitic kimberlite samples were collected at Jericho with the objective of characterizing the melt phase. Three samples of aphanitic kimberlite were selected from drill core (JD51, JD69, JD82), and two from material excavated from the underground decline (4S, 4SA).

Table 1.1: *Description of the three kimberlite phases distinguished within the Jericho pipe (compiled from Kopylova et al., 1998 and Cookenboo, 1998).*

Phase /Facies; Name	Mineralogy	Other[1]
Phase 1 /Hypabyssal facies Hypabyssal, macrocrystal, calcite serpentine kimberlite	Blue-grey kimberlite containing >60% pale yellow rounded olivine macrocrysts (unserpentinized), orthopyroxene, clinopyroxene, garnet and ilmenite. Magmatic and macrocrystal, with a generally uniform texture. This phase has autoliths of previously crystallized kimberlite (which are similar to Phase 1 except with less macrocrysts and oval concave segregations of calcite). **Groundmass:** Olivine microphenocrysts (9-12%), anhedral serpentine (46-64%), primary anhedral calcite (18-36%), euhedral oxides (<20μ) including spinel, ilmenite and perovskite (2-5%), euhedral skeletal apatite (0-2%) and laths of phlogopite (0-1%).	ms: high ρ: high v: high ♦: low
Phase 2 /Diatreme facies Tuffisitic carbonatized, serpentinized kimberlite	Dark green kimberlite containing olivine macrocrysts (completely serpentinized), chromian-pyrope (lherzolitic) garnet, chromian diopside, ilmenite, enstatite, and orange (eclogitic) garnet. Pelletal lapilli are common. Autoliths of Phase 1 are present within this phase. **Matrix:** Serpentine (97%), oxides including spinel, ilmenite and perovskite (3%). Late-stage carbonate (magnesite to calcite) occurs in interclast pore space.	ms: low ρ: mod v: mod ♦: mod.
Phase 3 /Diatreme facies Tuffisitic carbonatized, serpentinized kimberlite	Greenish-grey kimberlite containing olivine macrocrysts (fresh to weakly serpentinized), Cr-pyrope (lherzolitic) garnet, chromian diopside, ilmenite, enstatite, and orange (eclogitic) garnet. Pelletal lapilli are abundant. Autoliths of Phase 1 and 2 are common. **Matrix:** Serpentine (55-60%), oxides including spinel, ilmenite and perovskite (5%), late carbonate (11-20%), and late mixed-layer Mg-rich clay mineral (20%).	ms: mod ρ: low v: low ♦: high

[1]Other: Relative ms (magnetic susceptibility), ρ (density), v (volatile content) and ♦(Diamond Content)

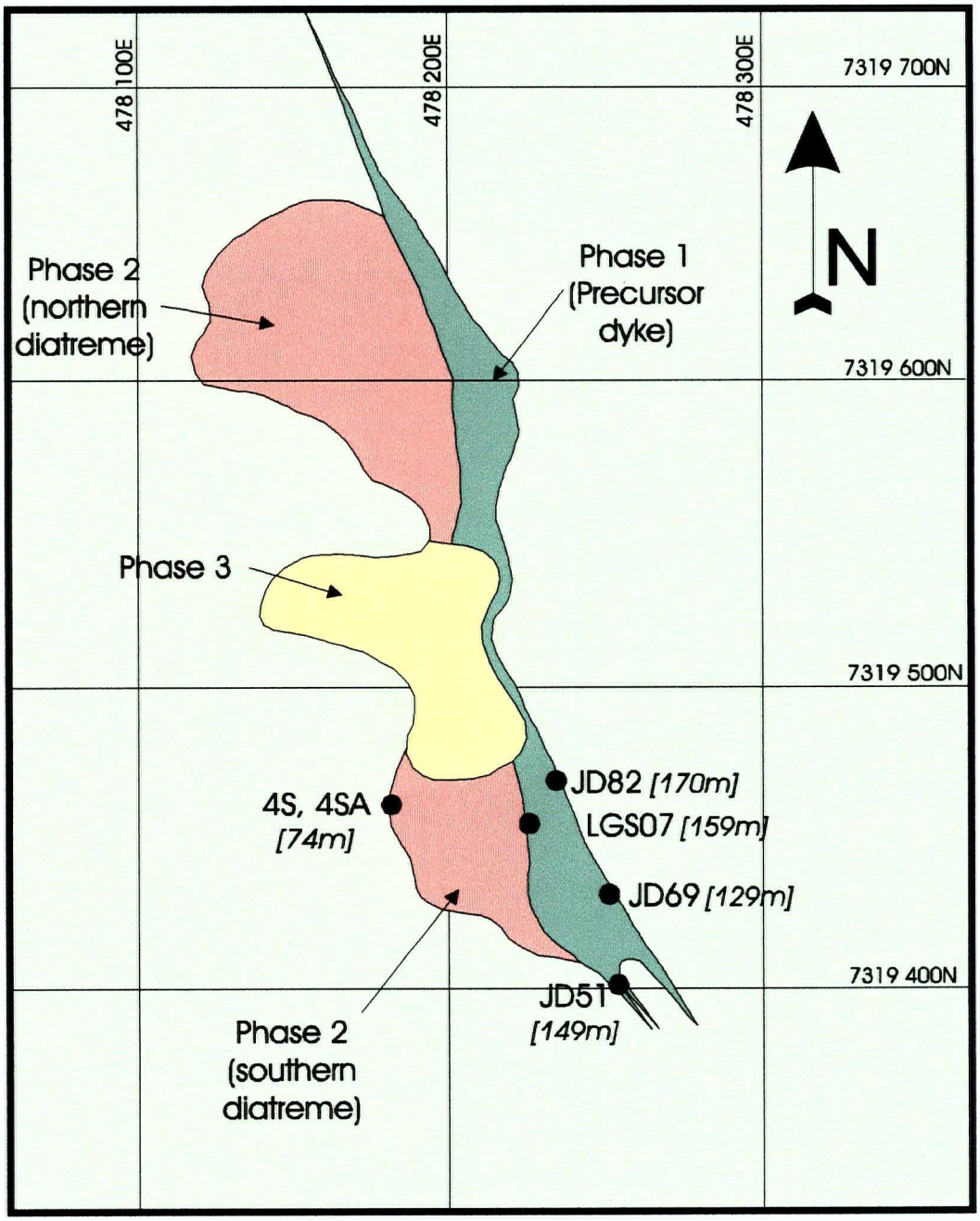

Figure 1.2 Plan view of the Jericho kimberlite pipe at 50 m depth showing the three kimberlite emplacement phases proposed by Cookenboo (1998). The aphanitic kimberlite sample locations and depths are also shown. Sample depths have been recalculated for an average surface elevation of 493 metres above sea level.

Three splits were made of JD69 and JD82 and analysed separately to investigate sample heterogeneity. Together with three splits of sample LGS07 (from drill core), described by Kopylova et al. (1998), these are the only aphanitic kimberlite samples presently identified at Jericho. Sample descriptions and locations are presented in Table 1.2.

Table 1.2: *Description of samples of aphanitic kimberlite collected from the Jericho pipe.*

Sample	Drill hole/ Round#[1]	Depth (m)[2]	Sample size	Sample Description and Contact Relationships
JD51 (DC)	95-JD051	149.3	≈100 cm^3	Light grey, competent, aphanitic kimberlite with no obvious alteration. Bounded by macrocrystal Phase 1 kimberlite above (with gradual contact over 0.5cm) and bounded below by a thin mafic dyke (sharp contact with no obvious brecciation). The mafic dyke is bounded by granite on the other side.
JD69 (DC)	96-JD069	128.7	≈560 cm^3	Light grey, moderately friable, aphanitic kimberlite. Microphenocrysts appear to be completely serpentinized. Bounded by macrocrystal Phase 1 kimberlite above (with gradual contact over approx. 10cm) and by a mafic dyke below (brecciated contact with fragments of mafic dyke within the kimberlite, then the strongly sheared mafic dyke). The mafic dyke is bounded by granite on the other side. This sample was split into three samples (JD69-1, JD69-2, JD69-3).
JD82 (DC)	96-JD082	169.7	≈560 cm^3	Light grey, moderately friable, aphanitic kimberlite. Microphenocrysts appear to be completely serpentinized. Bounded by macrocrystal Phase 1 kimberlite above (with gradual contact over approx. 10cm) and by a mafic dyke below (brecciated contact with fragments of mafic dyke within the kimberlite, then the strongly sheared mafic dyke). This sample was split into three samples (JD82-1, JD82-2, JD82-3).
LGS07 (DC)	96-LGS07	159.2	≈200 cm^3	Dark grey, competent, aphanitic kimberlite. Bounded by macrocrystal Phase 1 kimberlite above (with gradually coarsening contact over approx. 10cm) and by macrocrystal Phase 1 kimberlite below (sharp contact). This sample was split into three samples (LGS07-1, LGS07-2, LGS07-3) by Kopylova *et al.* (1998).
4S (UD)	Round #120	74	≈200 cm^3	Light grey, moderately friable, aphanitic kimberlite. Olivine phenocrysts are partly altered. Bounded on one side by macrocrystal Phase 2 kimberlite (contact is gradual over 0.5 cm) and on the other side by the slightly bleached host granite (Contwoyto batholith).
4SA (UD)	Round #120	74	≈200 cm^3	Light grey to brown, highly friable, aphanitic kimberlite. Olivine phenocrysts are partly altered and are brown-red in colour (suggesting oxidation). Bounded on one side by macrocrystal Phase 2 kimberlite (contact is gradual over 0.5 cm) and on the other side by the slightly bleached host granite (Contwoyto batholith).

DC = Drill core sample; UD = Underground decline sample
[1]For location of samples, see Fig. 1.2
[2]Depths calculated from average surface elevation of 493.0 metres.

Chapter 2

PETROGRAPHIC DESCRIPTIONS

2.1 INTRODUCTION

Basic petrographic features of all samples were determined by transmitted and reflected light microscopy of polished thin sections. Groundmass mineralogy was determined using a Philips XL30 Scanning Electron Microscope (SEM) located at the University of British Columbia. Semi-quantitative chemical analyses of minerals were obtained using a Princeton Gamma-Tech energy-dispersive spectrometer (EDS) attached to the SEM. False colour images were produced using the image analysis (IAS) system to aid in the identification of groundmass minerals and to determine their modal abundances (Appendix A). Standard kimberlite terminology has been used in the following descriptions after Scott Smith (1996). Macrocrysts refer to phenocrysts or xenocrysts which are 0.5 - 10 mm, and microphenocrysts refer to crystals <0.5 mm which are interpreted as having crystallized from the melt. 'Aphanitic kimberlite' refers to a kimberlite with less than 5% macrocrysts (Mitchell, 1986; Scott Smith 1996).

The aphanitic samples collected for this study can be split into two broad groups based on macroscopic observations: chilled margin samples and flow differentiated samples. Samples JD51, JD69 and JD82 have been interpreted as kimberlitic chilled margins. LGS07 has also been interpreted as a chilled margin (by Kopylova *et al.*, 1998) but is petrologically distinct from the other chilled margin samples and will be discussed separately. Samples 4S and 4SA have been interpreted as flow differentiated samples whereby crystals were removed by flow processes.

2.2 CHILLED MARGIN SAMPLES

The chilled margin samples (JD51, JD69 and JD82) are from 128-170 metres below the present surface (Table 1.2), and occur at the south end of the kimberlite pipe, where the pipe tapers at depth. These samples are interpreted as kimberlitic chilled margin as they are very fine-grained, occur at the contact with other rocks, and show no obvious mineral alignment or other features indicative of flow differentiation. The aphanitic samples are from the edges of thin (<5m) dykes of macrocrystal Phase 1 kimberlite which intrude highly sheared mafic dykes. The contact between the aphanitic kimberlite and wall rock is generally sharp, but is occasionally brecciated with small fragments of wall rock occurring within the kimberlite. Sample JD51 forms a narrow selvedge between macrocrystal Phase 1 kimberlite and a mafic dyke. The contact with the macrocrystal kimberlite is fairly sharp, grading over 0.5 cm. Samples JD69 and JD82 are from wider selvedges of aphanitic kimberlite (up to 40 cm) which have gradational contacts with macrocrystal Phase 1 kimberlite over 10 cm.

The chilled margin samples are texturally uniform; they are hypabyssal with altered (serpentinized) microphenocrysts set in a serpentine-, calcite-, oxide-rich groundmass (Fig. 2.1, 2.2). Microphenocrysts are evenly distributed throughout the samples and show no preferred orientation. There are relatively few (less than 30%) microphenocrysts in these samples and they are subangular to subrounded and range in size up to 0.3 mm. These microphenocrysts probably originally consisted of olivine, but have been completely replaced by Fe-bearing serpentine and other Mg silicate hydroxides. Some microphenocrysts (and macrocrysts) are highly strained (Fig. 2.3) and others are layered with light green serpentine layers and blue-green Fe- and Al- rich chlorite layers (Fig. 2.4).

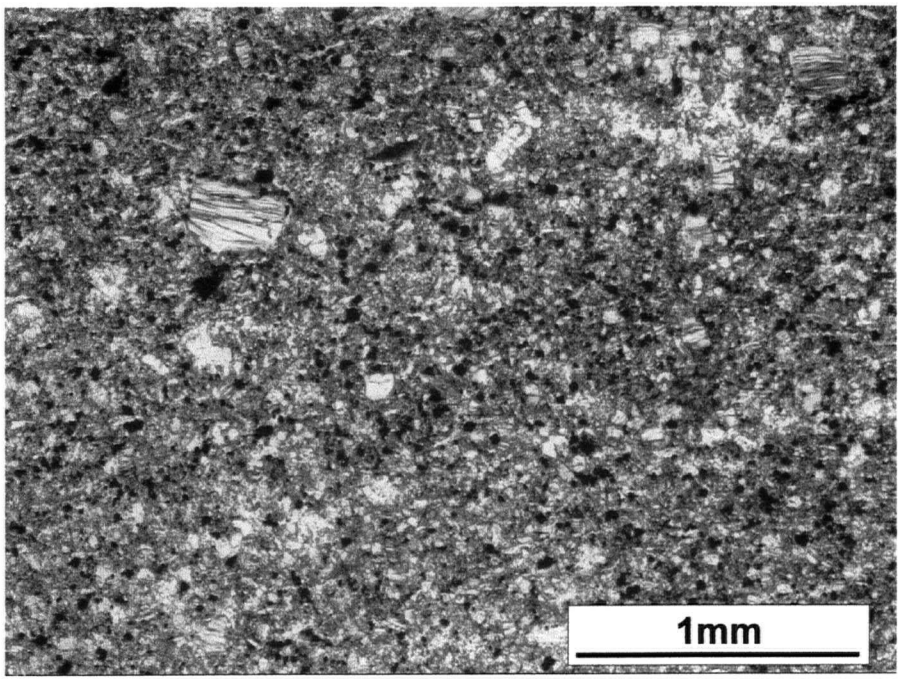

Figure 2.1 Photomicrograph of JD51 showing hypabyssal texture. Olivine microphenocrysts are completely altered (*ppl*).

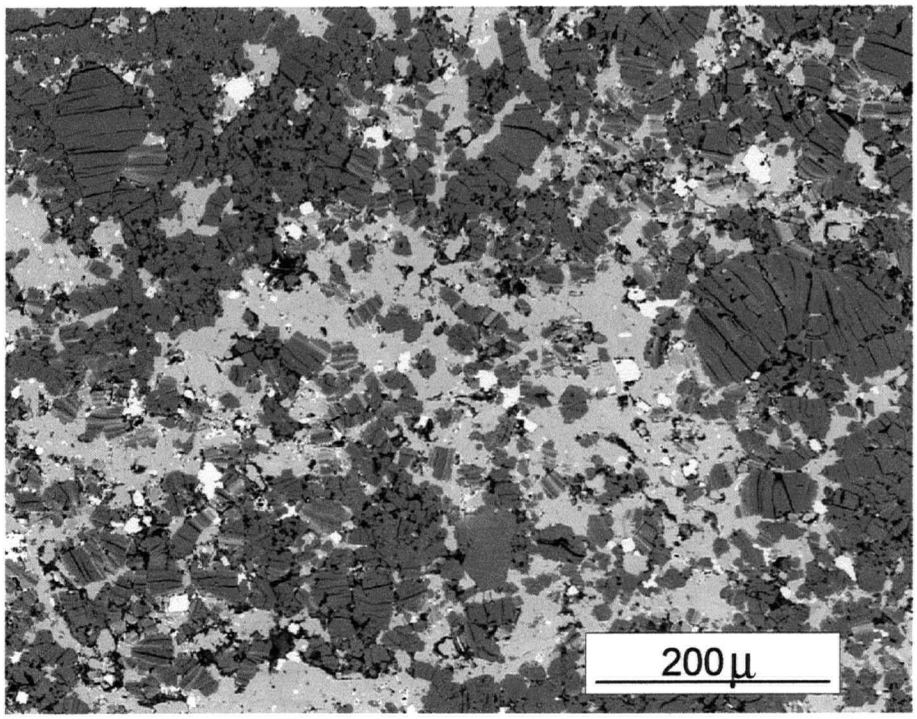

Figure 2.2 BSE image of JD69 showing serpentine as both microphenocrysts and interstitial groundmass (dark grey), and interstitial calcite (light grey) and oxides (white).

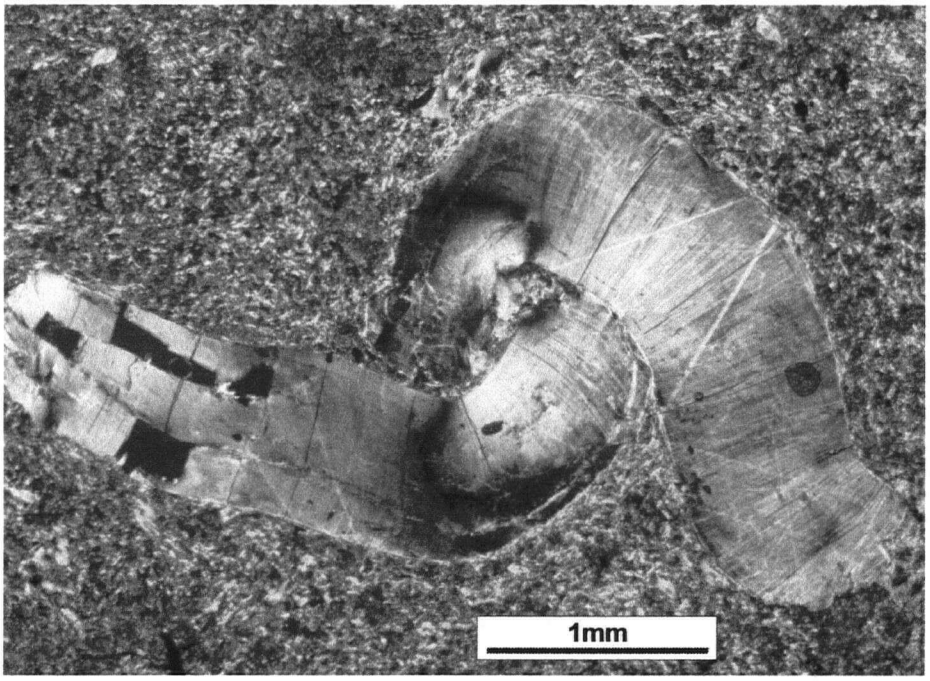

Figure 2.3 Photomicrograph of strained Mg-silicate hydroxide altered macrocryst in JD69 (*xpl*).

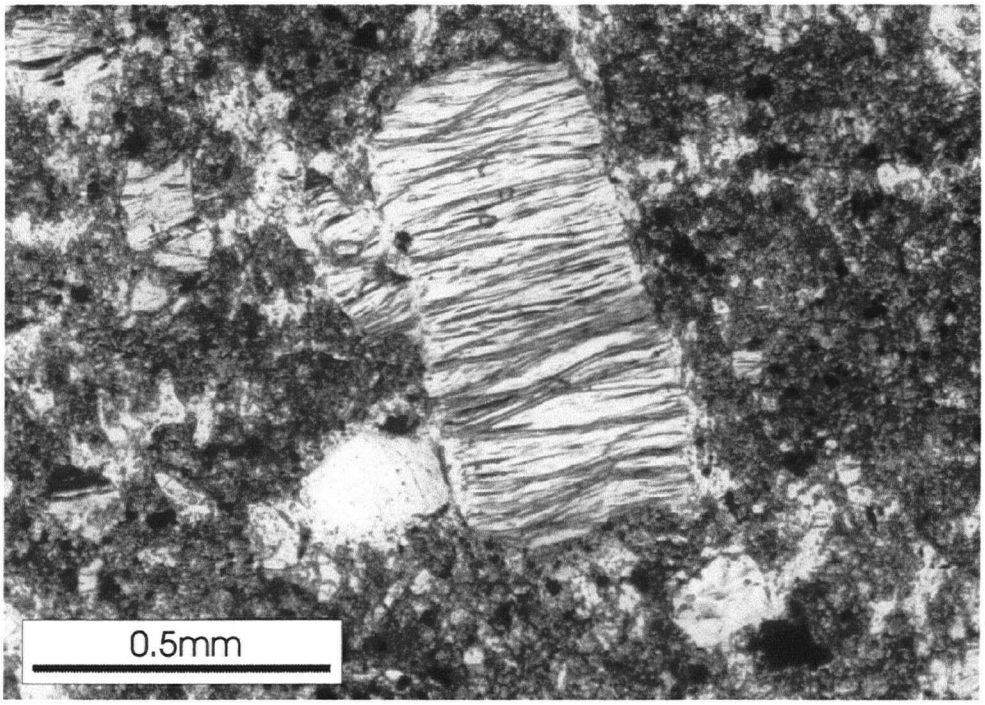

Figure 2.4 Photomicrograph of banded serpentine and chlorite microphenocryst in JD51 (*ppl*) The serpentine layers are colourless and the chlorite layers are blue-green in ppl.

The groundmass of these samples consists of primary calcite and serpentine (> 95 vol.%), and minor accessory minerals including perovskite, chromian spinel, ilmenite, Ni- Fe- sulphides, apatite, phlogopite and barite (Fig. 2.5). Details of the mineralogy and trace element composition of the groundmass minerals are presented in Appendix B. Sample JD51 has the highest proportion of calcite (39 vol.%), then JD69 (30 vol.%), and JD82 (26 vol.%), and all samples have similar modes of accessory minerals (Table 2.1). Calcite-serpentine segregations are present in JD51 (Fig. 2.6), and are typical of hypabyssal facies kimberlite (Mitchell, 1986).

Xenoliths and xenocrysts are rare within these samples. One quartz crystal (0.5mm) was identified in sample JD51. A garnet crystal, which may a xenocryst, was identified in JD69 with a strongly developed kelyphitic rim. Both crystals have sharp edges and it is not obvious if any significant dissolution has occurred. A strongly corroded phlogopite crystal was also found in JD69.

Table 2.1: *Volume % groundmass mineralogy and olivine microphenocryst alteration assemblages of samples*

Sample	Groundmass mineralogy[1] (vol%)				MP[2]	Olivine microphenocryst alteration
	Ol.	Serp.	Calcite	Access.		
JD51	-	58	39	2	<30	Complete replacement by serpentine ± Mg-silicate hydroxides ± chlorite. Some crystals are highly strained.
JD69	-	68	30	2		
JD82	-	70	26	4		
4S	39	53	<1	8	≈50	Large crystals are weakly replaced by serpentine (thin rims) and small crystals are completely replaced.
4SA	39	56	<1	5		Extensive silica alteration (hydrothermal alteration) - possibly overprinting serpentine replacement.
LGS07	15	52	21	12	≈50	No alteration - fresh, euhedral-subhedral olivine.

[1]Modal abundances of groundmass determined using false colour images of BSE images; Ol. = olivine; Serp. = serpentine; Access = accessory minerals
[2]MP=microphenocrysts.

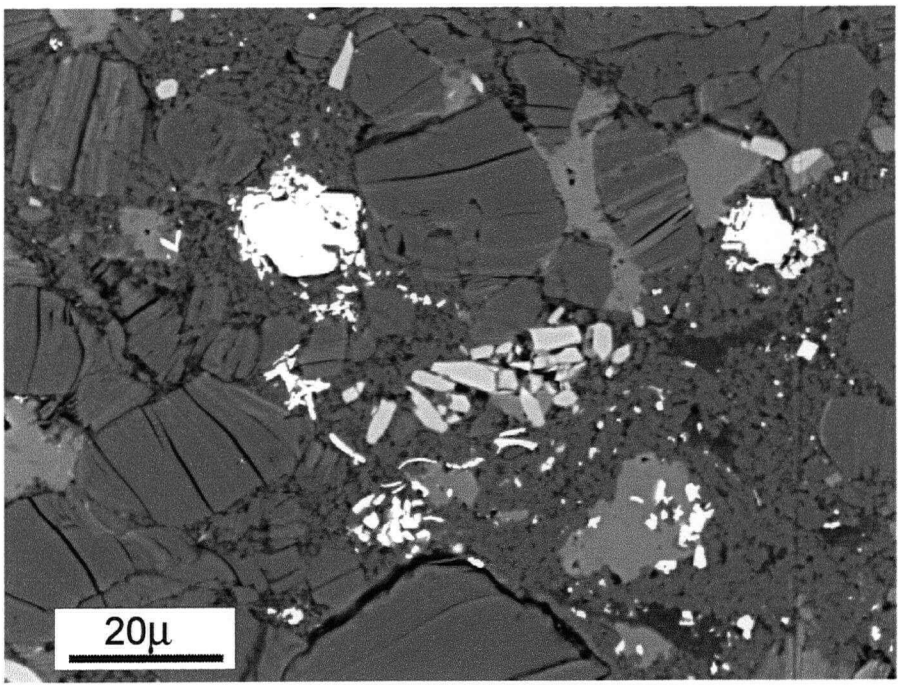

Figure 2.5 BSE image of JD82 groundmass showing serpentine microphenocrysts with minor interstitial calcite (light grey) and serpentine (dark grey). Bright grains are chromian spinels and Fe- Ni- sulphides, and apatite forms light grey stubby grains.

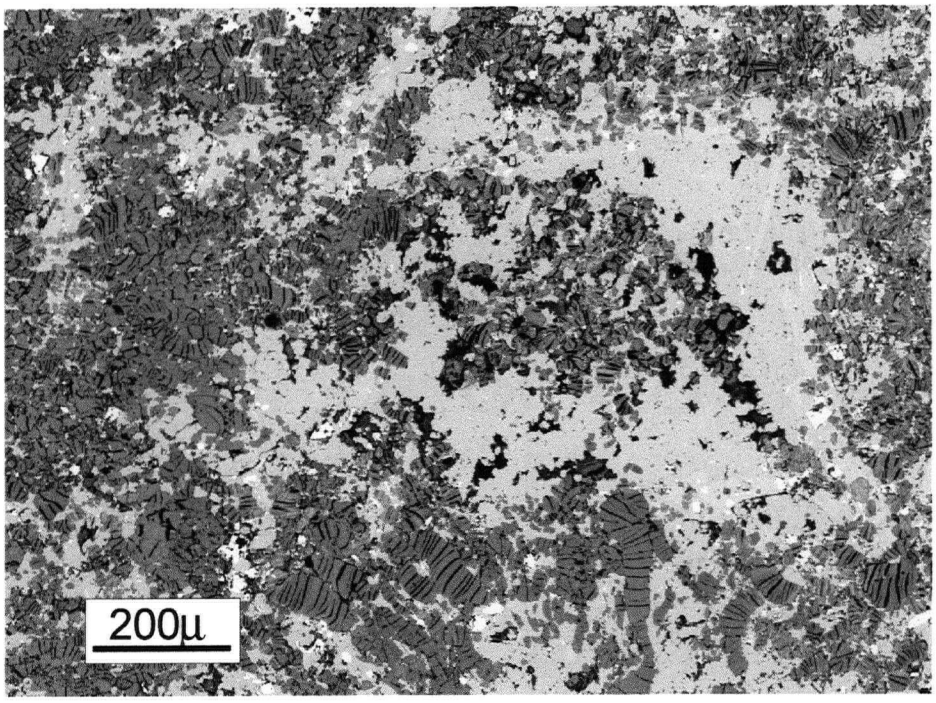

Figure 2.6 BSE image of segregation texture involving calcite (light grey) and serpentine (dark grey) in sample JD51.

2.3 FLOW DIFFERENTIATED SAMPLES

2.3.1 Samples 4S and 4SA

Samples 4S and 4SA derive from the underground decline at 74 metres below the present surface. They occur at the southwest edge of the Phase 2 diatreme where the kimberlite is in contact with granite (Contwoyto batholith). These samples form thin (up to 20 cm) selvedges between Phase 2 (diatreme facies) macrocrystal kimberlite and the granite, which is slightly bleached at the contact. The contact between the aphanitic and macrocrystal kimberlite is fairly sharp, grading over 0.5 cm. Due to the friable nature of both the kimberlite and granite at the contact, it is difficult to determine the exact nature of the contact. The aphanitic texture of these samples is interpreted to be a result of flow differentiation processes occurring near the edge of the diatreme. Mineral alignment in some areas of these samples suggest flow processes may have occurred, and the aphanitic texture was likely a result of the large crystals being sorted away from the edges of the diatreme. Fig. 2.7 is a photograph of aphanitic sample 4SA in contact with macrocrystal Phase 2 kimberlite. In some areas of the aphanitic portion, larger crystals still remain. The granite is located beside the aphanitic kimberlite, but due to the friable nature of the contact zone, it was not possible to preserve this piece. This sample appears to have been oxidized, possibly from hydrothermal fluids, as has orange-brown (Fe-stained) microphenocrysts (Fig. 2.7). Sample 4S, which occurs within a metre of sample 4SA, does not have orange-brown microphenocrysts, and was possibly further from the granite contact.

The flow differentiated samples have hypabyssal textures with fresh to moderately serpentinized olivine microphenocrysts set in a serpentine, oxide-rich groundmass (Fig. 2.8). Generally the microphenocrysts are randomly oriented, although there appears to be a weak mineral alignment (defined by the olivine microphenocrysts) in some parts of the samples. There

is no visible calcite in the groundmass of these samples, and the accessory minerals are the same as in the chilled margin samples, although there is a higher proportion (5-8 vol%; Table 3). The microphenocrysts range in size up to 0.5 mm and comprise approximately 50% of the samples. There are two size classes of olivine with larger, subhedral to rounded olivine microphenocrysts (0.05-0.5 mm), and smaller rounded microphenocrysts (0.01-0.05 mm). The larger microphenocrysts are partially serpentinized (at the rims), and the smaller microphenocrysts are completely serpentinized (Fig. 2.9). From EDS analysis, it was determined that there is extensive Fe-silica alteration overprinting all microphenocrysts in sample 4SA. This appears to be a secondary alteration which overprints earlier serpentinization (Fig. 2.10).

These samples have a macrocrystal texture, although finer grained, similar to more coarse-grained kimberlite. This suggests there may be a significant proportion of the olivines may be xenocrysts.

2.3.2 Sample LGS07

Sample LGS07 is from 159 metres below the present surface, and represents a thin selvedge of aphanitic kimberlite, which has intruded against previously emplaced kimberlite (Phase 1 macrocrystal kimberlite). This sample has been interpreted as a chilled margin by Kopylova *et al.* (1998). It has a hypabyssal texture with fresh, subhedral to rounded, olivine microphenocrysts set in a serpentine, calcite (21%) groundmass with a high proportion (12 vol%) of accessory minerals (Fig. 2.11). This sample has a much higher proportion of microphenocrysts (approx. 50 vol%) than the other chilled margin samples identified in this study and is not as fine-grained (microphenocrysts up to 0.5mm). This sample still has a macrocrystal, 'porphyritic' texture, typical of macrocrystal Phase 1 kimberlite (Fig. 2.12). The crystals are quite rounded suggesting

they may have been milled during emplacement. As this sample is similar to macrocrystal kimberlite, it is likely the olivine is largely xenolithic, and therefore this sample is not a good representation of the melt phase. The aphanitic texture of this sample is therefore interpreted to be a result of flow differentiation processes occurring at the edge of the dyke during emplacement.

Figure 2.7 Aphanitic flow-differentiated kimberlite margin (sample 4SA) in contact with macrocrystal Phase 2 kimberlite. The granite is located beside the aphanitic portion of the sample. Note that this sample is quite friable and has been set in epoxy. Scale bar is in centimetres.

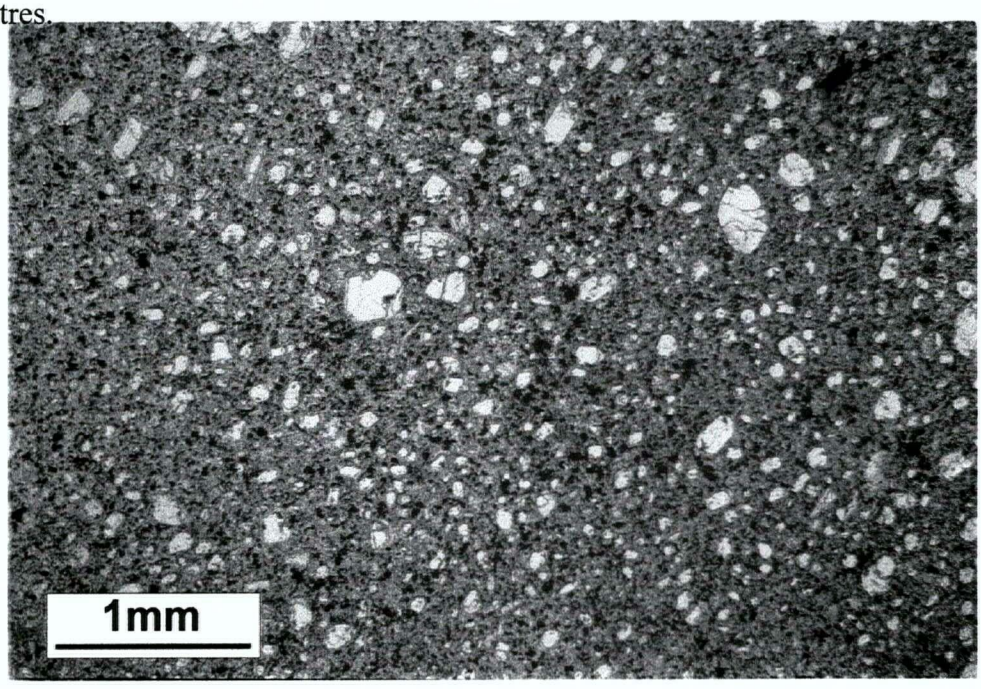

Figure 2.8 Photomicrograph of 4S showing hypabyssal texture, with olivine microphenocrysts (*ppl*).

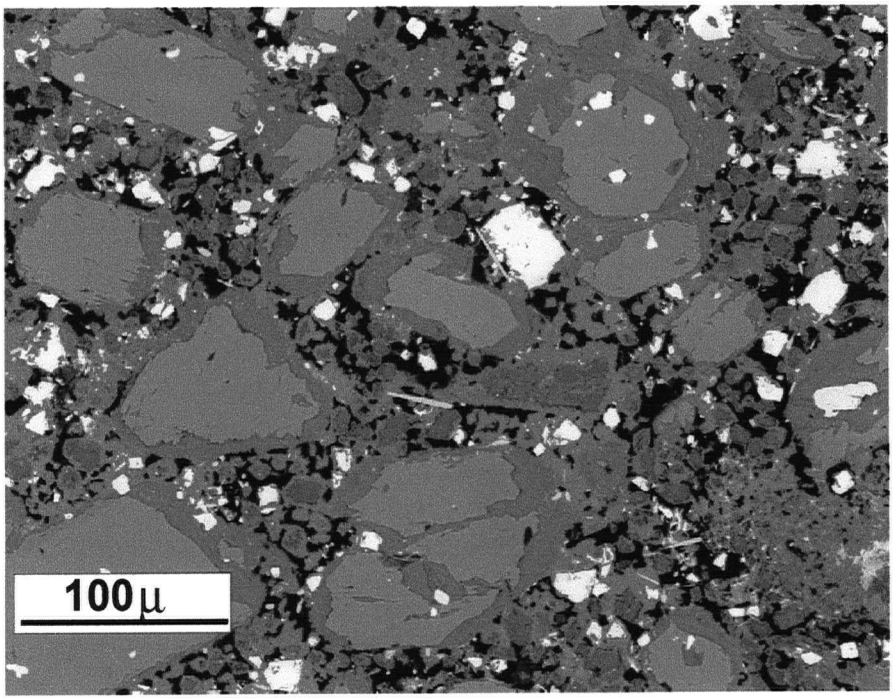

Figure 2.9 BSE image of 4S showing olivine microphenocrysts with serpentine rims. Note that the smaller microphenocrysts are completely serpentinized. Bright grains are oxide minerals, consisting of mostly chromian spinel; small laths are apatite.

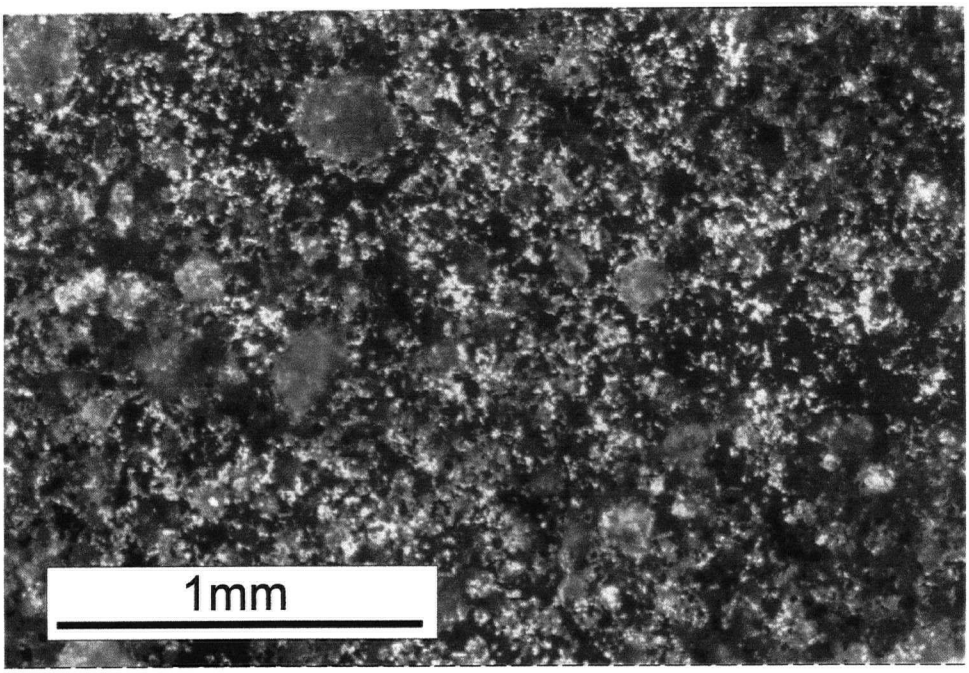

Figure 2.10 Photomicrograph of 4SA. Microphenocrysts are Fe-silica altered and they appear blurred due to the strong orange-brown colouration (*ppl*).

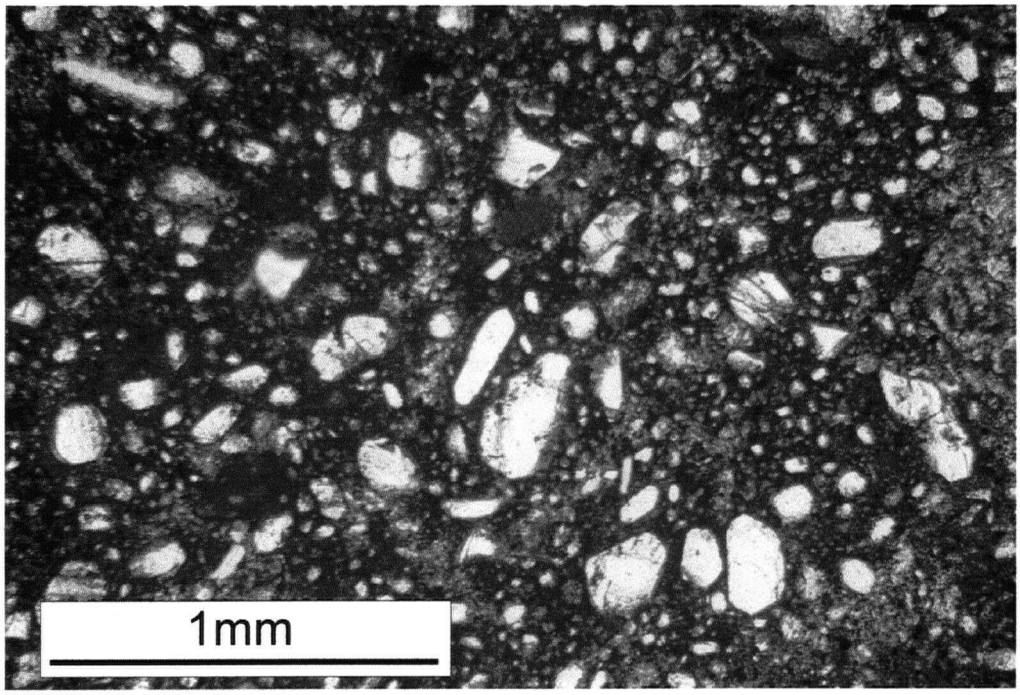

Figure 2.11 Photomicrograph of LGS07 showing hypabyssal texture. Olivine microphenocrysts are subhedral to rounded (*ppl*).

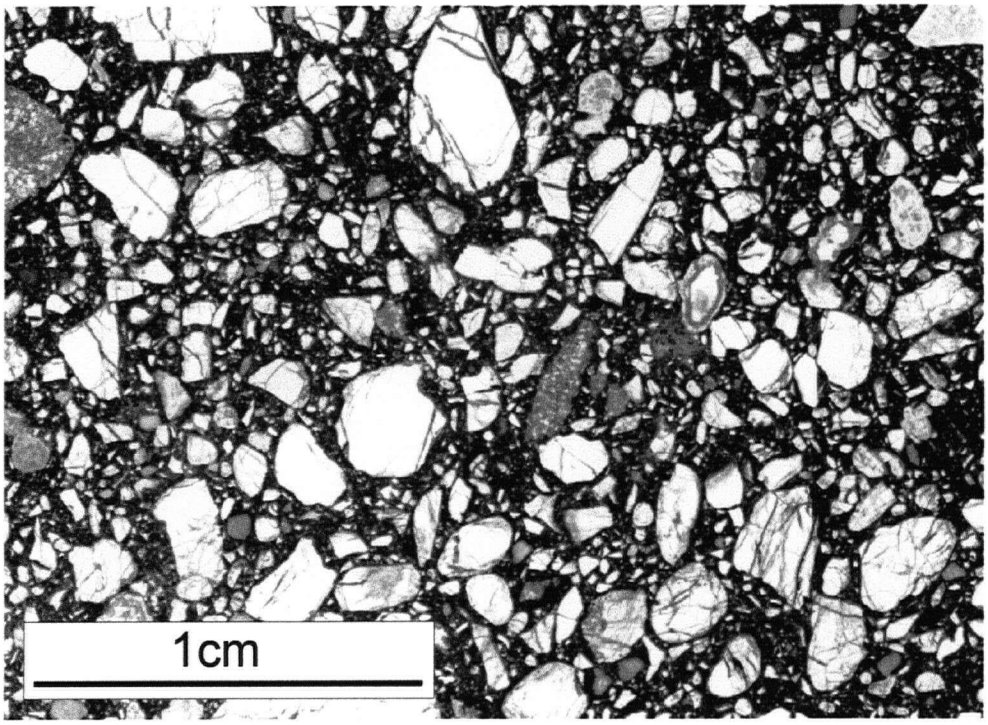

Figure 2.12 Photomicrograph of typical Phase 1 macrocrystal kimberlite from Jericho. Note the texture is similar to LGS07 above, but the olivine crystals are more abundant and larger (*ppl*)

2.4 COMPARISONS BETWEEN CHILLED MARGIN AND FLOW DIFFERENTIATED SAMPLES

All samples exhibit an aphanitic hypabyssal texture and comprise microphenocrysts set in a uniform groundmass of predominantly serpentine and calcite, with minor oxides (perovskite, chromian spinels, ilmenite), apatite, phlogopite, barite and Ni- Fe- sulphides. Macrocrysts, consisting of fresh and altered olivine, are rare (<3%). The chilled margin samples have <30 vol% microphenocrysts (completely altered), low proportions of accessory minerals (2-4%), and high calcite modes (26-39%). The flow differentiated samples 4S and 4SA have a higher proportion (≈50%) of microphenocrysts (fresh to weakly altered), a higher proportion of accessory minerals (5-8%), and no calcite. Sample LGS07 also has ≈50% microphenocrysts (fresh olivine), a very high proportion of accessory minerals (12%) and significant proportions of calcite (21%). The microphenocrysts are generally randomly oriented throughout the samples, however some areas of samples 4S and 4SA show a weak mineral alignment, as defined by the olivine microphenocrysts.

The chilled margin samples have a texture consistent with the rapid crystallization of a relatively crystal-free melt, being very fine-grained with few subangular to subrounded microphenocrysts. In contrast, the flow differentiated samples have a macrocrystal texture similar, although finer grained, than typical kimberlite (Fig. 2.8). This suggests they have a significant olivine xenocryst component.

Up to 5 vol.% void space occurs within these samples. Tiny holes (<20μ), similar in size and shape to the groundmass grains, occur throughout the groundmass. These may represent holes which were once vapour-filled or be a result of plucking during thin section preparation. Void space also occurs within the serpentinized microphenocrysts, possibly as a result of

dehydration of the hydroxide minerals.

In summary, the chilled margin samples represent good examples of liquids, with negligible amounts of macrocrystic or xenolithic material. These samples appear to be good examples of rapidly cooled kimberlite melt. The flow differentiated samples should be treated with more caution as they appear to have significant numbers of xenocrysts.

Chapter 3

WHOLE-ROCK AND ISOTOPE GEOCHEMISTRY

3.1 ANALYTICAL TECHNIQUES

All samples have been analysed for major, minor, rare earth element concentrations and for oxygen and carbon isotope concentrations. Major element, trace element, CO_2, H_2O+, H_2O-, and loss on ignition (LOI) abundances were determined at the Geochemical Laboratories of McGill University in Montreal, Canada. Major and trace elements were measured by X-ray fluorescence (XRF) spectrometry using a Philips PW2400 Spectrometer. The major elements Si, Ti, Al, Fe, Mn, Mg, Ca, Na, K, and P and the trace elements Ba, Cr, Ni and V were analysed for using fused beads, and the trace elements Rb, Sr, Nb, Zr, Y, Pb, Ga, Th and U were analysed for using pressed pellets. Total iron was determined by XRF as Fe_2O_3, and ferrous iron was determined volumetrically. H_2O- was determined at 105 °C, H_2O+ was determined by difference, and CO_2 analyses were done using a LECO induction furnace and absorption bulb. Rare earth element (REE) concentrations were measured on an Elan-5000 inductively coupled plasma - mass spectrometer (ICP-MS) at the Department of Geological Sciences at the University of Saskatchewan, following procedures described by Jenner *et al.* (1990). Details of the laboratory accuracy and precision are given in Appendix C.

Carbon and oxygen isotopes were measured at the Department of Geological Sciences at Queens University in Kingston, Canada using a MAT 252, multi-collector isotope-ratio mass spectrometer. Carbon and oxygen isotope ratios were determined for the carbonate fraction, and oxygen isotope ratios were determined for the silicate fraction. To prepare the silicate fraction, calcite was removed prior to analysis by reacting with 10% HCl. From EDS analysis, it was

determined that all carbonates in the samples were calcite, with no Mg-bearing carbonates. The powdered samples were allowed to react for approx. 2 hours, then centrifuged to allow removal of the liquid. This process was repeated again with HCl to ensure all calcite was removed, then repeated twice with deionized H_2O to ensure all residual HCl was removed. No attempt was made to remove the silicate fraction from the calcite fraction.

In order to prepare the samples for analysis, all large xenolithic material was removed. The samples were then cleaned and passed through a steel-faced jaw crusher to reduce the size to <0.5 cm. As the aim of this study was to investigate the nature of the kimberlite melt, any visible crystals (>0.5 mm) were hand-picked from the sample prior to geochemical analysis. The samples contained up to 3% macrocrysts (crystals >0.5 mm), and many were removed such that less than 1% of the crystals were left in the samples. Although some of these crystals were probably phenocrysts, removal of all macrocrysts ensured the melt phase was sampled. Crystals removed included dark pink and orange garnets (probably of peridotitic and eclogitic origins, respectively), partly serpentinized olivine, and dark green serpentine books (probably pseudomorphs after olivine). The crystal-poor samples (<1% crystals) were powdered to approximately 100 mesh using a tungsten carbide ring mill.

3.2 SAMPLE HETEROGENEITY

Samples JD69 and JD82 were divided into three splits and analysed separately to investigate the degree of sample heterogeneity. The major element chemistry within each sample showed only minor variations (generally <5%) suggesting these samples crystallized from a fairly homogeneous melt. Variations might be due to 1) the proportion of microphenocrysts to groundmass, and the extent to which the macrocrysts were removed, or 2) small variations in the

volatile content of the melt, resulting in variations in the modal abundances of calcite or serpentine in the groundmass. Within the JD82 samples, JD82-1 has a substantially higher Fe_2O_3 concentration (5.27 wt%) and a lower FeO concentration (1.51 wt%) than JD82-2 and JD82-3, possibly resulting from xenolith contamination.

3.3 MAJOR ELEMENT CHEMISTRY

The major element abundances for the aphanitic kimberlite samples are presented in Table 3.1; the chemical compositions for bulk samples of the three phases of the Jericho kimberlite (Kopylova *et al.*, 1998) are summarized in Table 3.2. Extended results are presented in Appendix D.

The aphanitic kimberlite samples are characterized by low Na_2O/K_2O ratios (<6), which is typical for kimberlites (Mitchell, 1986). Plots of SiO_2, FeO(t), H_2O, CaO and CO_2 vs. MgO show linear correlations (Fig. 3.1a-e) reflecting the proportions of olivine and serpentine to calcite. Figure 3.1a shows serpentine- (Si/Mg = 0.67 for pure serpentine) and olivine- (Si/Mg = 0.5 for forsterite) control lines, drawn through the median datapoint (JD69-2 for the serpentine line and LGS07-2 for the olivine line). All samples lying along the olivine-control line (LGS07, 4S, autoliths and Phases 1 and 3) have fresh olivine microphenocrysts, and samples lying along the serpentine-control line (JD51, JD69, JD82, Phase 2) have extensively serpentinized microphenocrysts. Sample 4SA has a very high SiO_2 content, lying well above the serpentine-control line. This anomalous value is probably a result of the secondary Fe-silica alteration of 4SA, detected during EDS analysis (Chapter 2).

Table 3.1: *Measured major and trace element (in wt% and ppm respectively) concentrations of samples of Jericho aphanitic kimberlite.*

	JD51	JD69			JD82			Rnd 120		LGS07			1σ[1]
Sample	51	69-1	69-2	69-3	82-1	82-2	82-3	4S	4SA	07-1	07-2	07-3	
SiO_2	20.77	24.15	27.00	29.06	28.83	28.13	30.31	34.56	35.50	34.04	32.90	31.86	0.197
TiO_2	0.89	0.51	0.51	0.49	0.57	0.71	0.77	2.96	4.45	0.82	1.05	1.19	0.005
Al_2O_3	1.82	1.14	1.33	1.38	1.39	1.61	1.75	3.19	5.00	2.10	2.06	2.25	0.056
Fe_2O_3	6.47	2.23	2.15	2.13	5.27	2.69	2.95	5.55	4.97	2.16	2.57	2.82	0.063
FeO	0.57	3.58	3.50	3.79	1.51	4.17	4.64	5.67	12.03	5.36	5.17	5.15	-
MnO	0.19	0.16	0.14	0.13	0.16	0.16	0.15	0.32	0.50	0.17	0.19	0.20	0.004
MgO	16.65	19.71	22.39	23.69	23.25	23.09	25.14	37.06	24.95	35.28	34.41	33.98	0.217
CaO	25.45	22.25	19.37	16.69	16.86	16.66	13.32	2.03	3.19	7.12	7.49	8.73	0.109
Na_2O	0.10	0.14	0.15	0.13	0.12	0.19	0.24	0.24	0.31	0.15	0.20	0.18	0.012
K_2O	0.17	0.33	0.43	0.45	0.43	0.46	0.42	0.51	0.70	0.41	0.26	0.26	0.012
P_2O_5	0.85	0.67	0.61	0.56	0.71	0.78	0.75	0.59	0.67	0.68	0.84	0.96	0.005
CO_2	18.82	16.91	14.01	12.97	12.39	12.06	9.80	0.65	0.28	4.84	4.91	5.76	0.01
H_2O+	5.30	6.40	7.10	6.40	6.00	6.70	7.50	5.80	4.50	5.24	5.80	5.05	0.04
H_2O-	1.02	0.71	0.76	0.76	1.15	1.04	1.05	1.02	2.54	0.67	0.81	0.56	
Total	99.07	98.89	99.45	98.63	98.64	98.45	98.79	100.15	99.59	99.04	98.66	98.95	
LOI[7]	25.45	24.04	21.98	20.40	20.40	20.11	18.54	6.97	6.21	10.35	11.37	11.21	
C.I.[2]	1.34	1.25	1.22	1.24	1.26	1.25	1.24	1.00	1.55	1.01	1.01	0.99	
Ilm. Ind.[3]	0.43	0.3	0.26	0.25	0.28	0.3	0.31	0.36	0.79	0.23	0.24	0.26	
Fe ratio[4]	11.35	0.62	0.61	0.56	3.49	0.65	0.64	0.98	0.41	0.40	0.50	0.55	
Si/Mg	0.97	0.95	0.93	0.95	0.96	0.94	0.93	0.72	1.10	0.75	0.74	0.73	
Mg#	82.3	86.3	88.0	88.1	86.9	86.2	86.0	86.1	72.9	89.6	89.1	88.7	
Cr[6] (ppm)	2013	1301	1312	1570	1513	1803	1891	5255	7612	2121	2463	2874	18
Ba	666	2889	4026	7274	3351	2820	3318	1200	2933	2160	2100	2370	28
Rb	13.4	23.8	30.0	30.7	26.8	29.3	27.6	37.9	46.2	66	56	54	0.2
Sr	472.0	948.9	692.8	571.7	498.5	423.4	297.2	123.9	162.6	840	670	958	2.7
Nb	263.0	168.7	165.4	142.6	182.0	207.5	231.8	398.6	568.1	196	246	274	1.3
Zr	125.1	71.6	71.3	67.8	73.0	93.8	108.8	137.3	200.0	96	120	135	0.6
Y	12.8	9.6	10.3	11.1	10.2	10.9	11.3	16.9	21.7	12	12	12	0.07
Pb	23.5	13.1	15.7	14.3	15.9	13.2	16.2	16.2	22.9	10	12	10	0.09
Ni	598	789	1099	1151	1291	1367	1396	1300	1535	1350	1200	1100	14
V	107	87	87	95	90	85	87	221	271	-	-	-	0.9
Ga	5.0	1.9	1.8	b.d.	2.8	3.2	3.0	6.8	9.9	-	-	-	0.02
Th	35.1	18.5	16.6	15.0	19.8	25.7	28.8	41.8	61.4	-	-	-	0.2
U	5.0	1.0	b.d.	b.d.	b.d.	b.d.	b.d.	126.2	46.9	-	-	-	0.3

b.d. below detection (Detection limits for U and Th is 1.0 ppm)

[1]Analytical uncertainty for major elements is after Russell and Snyder (1997), and for trace elements is from laboratory precision. LGS07 samples were analysed by Kopylova *et al.* (1998) and have different uncertainties. See Appendix C for details.

[2]C.I. (Contamination Index) = $(SiO_2 + Al_2O_3 + Na_2O)/(MgO + 2K_2O)$, after Clement (1982).

[3]Ilm. I. (Ilmenite Index) = $(FeO(t) + TiO_2)/(MgO + 2K_2O)$, after Taylor *et al.* (1994).

[4]Fe ratio = Fe_2O_3/FeO.

[5]Mg# = 100. $Mg/(Mg + Fe^{2+})$ where Fe^{2+} is calculated from FeO(t).

[6]Cr (ppm) for LGS07 samples was recalculated from Cr_2O_3 (wt%).

[7]LOI = Loss on ignition

Table 3.2: *Average bulk chemistry of Phases 1-3 and autoliths of the Jericho kimberlite (after Kopylova et al., 1998).*

	Phase 1		Autoliths		Phase 2		Phase 3	
Sample	Mean (*N*=18)	1σ[1]	Mean (*N*=10)	1σ	Mean (*N*=10)	1σ	Mean (*N*=9)	1σ
SiO_2 (wt%)	33.04	1.48	30.51	2.82	35.25	2.02	33.57	1.58
TiO_2	0.99	0.31	1.03	0.15	0.79	0.27	0.77	0.25
Al_2O_3	1.78	0.28	2.02	0.35	2.76	0.51	1.88	0.42
Fe_2O_3	2.50	0.55	2.93	0.49	2.68	0.26	2.66	0.71
FeO	5.51	0.45	4.89	0.46	4.38	0.78	4.72	0.72
MnO	0.16	0.02	0.17	0.03	0.13	0.03	0.14	0.02
MgO	36.12	2.08	32.91	3.10	30.62	2.23	34.78	2.67
CaO	6.79	2.02	9.46	3.34	6.56	2.10	6.64	2.22
Na_2O	0.12	0.04	0.12	0.04	0.16	0.03	0.12	0.09
K_2O	0.16	0.09	0.14	0.04	0.62	0.19	0.22	0.20
P_2O_5	0.43	0.10	0.48	0.12	0.30	0.18	0.24	0.18
CO_2	4.75	1.76	6.96	2.58	4.40	1.56	5.03	1.55
H_2O+	5.31	1.16	6.19	1.40	7.65	2.00	6.89	1.61
H_2O-	0.88	0.57	1.11	0.77	2.05	1.06	1.01	0.40
Total	98.54		98.92		98.35		98.67	
LOI[7]	10.91	1.24	14.12	2.89	14.40	2.18	12.85	2.37
C.I.[2]	0.96	0.07	0.98	0.44	1.20	0.09	1.01	0.06
Ilm. Ind.[3]	0.24	0.03	0.26	0.03	0.24	0.04	0.22	0.02
Fe ratio[4]	0.46	0.11	0.61	0.14	0.62	0.08	0.59	0.26
Si/Mg	0.71	0.05	0.72	0.02	0.89	0.07	0.75	0.03
Mg#	89.2	1.11	88.6	1.00	88.9	1.50	89.7	0.58
Cr[6] (ppm)	1916	342	1916	274	1711	342	1847	616
Ba	1637	576	1188	919	1173	665	1054	885
Rb	29	13	20	14	66	21	34	36
Sr	577	226	373	274	413	171	326	270
Nb	143	32	110	78	105	40	96	41
Zr	66	15	49	35	61	19	47	23
Y	7	2	6	5	8	2	6	3
S (wt%)	0.09	0.05	0	0	0.12	0.11	0.17	0.08
Pb	6	4	4	3	6	3	6	7
Ni	1383	111	936	678	1315	158	1478	205
F	557	181	673	268	511	230	440	231

b.d. below detection (U = 1.0 ppm)

[1]1σ is one standard deviation of all samples

[2]C.I. (Contamination Index) = $(SiO_2 + Al_2O_3 + Na_2O)/(MgO + 2K_2O)$, after Clement (1982).

[3]Ilm. I. (Ilmenite Index) = $(FeO(t) + TiO_2)/(MgO + 2K_2O)$, after Taylor *et al.* (1994).

[4]Fe ratio = Fe_2O_3/FeO.

[5]Mg# = 100. $Mg/(Mg + Fe^{2+})$ where Fe^{2+} is calculated from FeO(t).

[6]Cr (ppm) was recalculated from Cr_2O_3 (wt%).

[7]LOI = Loss on ignition

[8]$Fe_2O_{3(T)}$ = measured total Fe

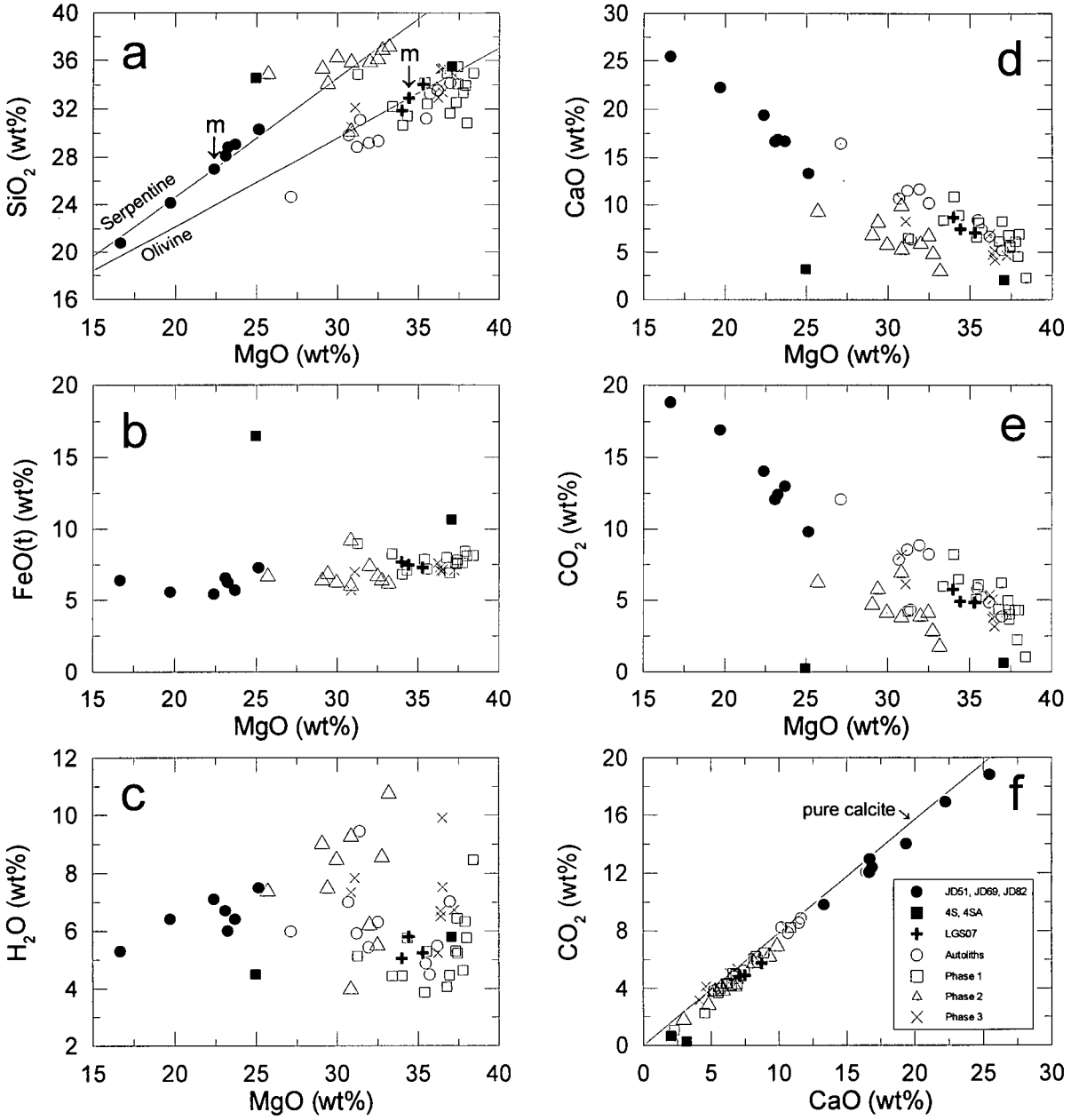

Figure 3.1 Bivariate plots of selected major elements for the aphanitic and major phases of the Jericho kimberlite, demonstrating the control by the proportions of olivine or serpentine to calcite. (a) SiO_2 vs. MgO shows control by olivine or serpentine. The slope of the control lines is determined by the molar ratio of Si/Mg for end-member serpentine ($Mg_3Si_2O_5(OH)_4$) and forsterite (Mg_2SiO_4), and is drawn through the median datapoint (m); (b) Total iron, FeO(t) vs. MgO. (c) H_2O vs. MgO; (d, e) CaO and CO_2 vs. MgO; (f) CO_2 vs CaO. The straight line represents pure calcite, with a CaO/CO_2 molar ratio = 1. Data for sample LGS07, autoliths, and Phases 1-3 are from Kopylova *et al.* (1998).

The most striking geochemical difference between the aphanitic samples is the wide range of CO_2 contents, from 0.3 wt% in sample 4SA to 18.8 wt% in sample JD51. Samples JD51, JD69 and JD82 have the highest CO_2 values (from 9.8 - 18.9 wt%), LGS07 has a moderate value (≈5.2 wt%) and 4S and 4SA have anomalously low values (0.3 - 0.7 wt%). This is consistent with the amount of calcite observed in these samples. There is a strong linear relationship between CO_2 and CaO (Fig. 3.1f), with all samples lying just below a 1:1 CaO:CO_2 line representing pure calcite. While CaO predominantly exists within calcite, it is also present in the accessory phases apatite and perovskite. Samples JD69 and JD82 have higher H_2O contents (6.0 - 7.5 wt%) than samples JD51, 4S, 4SA and LGS07 (4.5 - 5.8 wt%). This H_2O is present as serpentine, other Mg-silicate hydroxides and chlorite (after olivine) in JD69 and JD82. JD51 is also extensively serpentinized but probably has a lower H_2O content due to the lower proportion of serpentine to calcite. Sample 4SA has a low H_2O content (4.5 wt%), with serpentinization partially overprinted by an Fe-silica alteration.

The Fe_2O_3/FeO ratios of the aphanitic samples are between 0.4 - 0.7, which is similar to the bulk kimberlite samples (0.3 - 0.8; Table 3.2). These values are slightly higher than for unaltered basaltic rocks (Fe_2O_3/FeO ≈0.15-2). Sample 4S is more oxidized (Fe_2O_3/FeO = 1) and sample JD51 has an extremely high Fe_2O_3/FeO ratio of 11.35. As sample JD51 is mineralogically similar to samples JD69 and JD82, which do not have such high Fe_2O_3/FeO ratios, it is probable that an Fe^{3+}-bearing mineral such as spinel was incorporated into the geochemical aliquot. One of the JD82 samples (JD82-1) also has a very high Fe ratio, which might also be attributable to the presence of spinel. Although sample 4SA is high in Fe_2O_3, it is also high in FeO and therefore does not have an unusual Fe ratio.

Magnesium numbers for the aphanitic and bulk kimberlite samples are very high (Table 3.1, Table 3.2). Most samples have Mg#s of 86 - 91, except JD51 and 4SA, which have lower Mg#s of 82 and 73, respectively. This is due to JD51 having a relatively low MgO, and 4SA having a very high total Fe content.

The three Jericho kimberlite phases have been distinguished on a plot of P_2O_5 vs. K_2O (Fig. 3.2) by Kopylova *et al.* (1998). The aphanitic samples are different from the other phases, with high P_2O_5 contents and variable K_2O contents. The high P_2O_5 content possibly reflects the initial volatile contents. 4S and 4SA may have originally been high in CO_2, and a secondary process has removed calcite, but not apatite (P-mineral) from the samples. The aphanitic samples have variable K_2O contents, which span the range of compositions of Phases 1, 2 and 3. Variations in K could be an intrinsic kimberlite melt property or represent alteration which has affected both the aphanitic and macrocrystal phases of Phase 1 or Phase 2. Samples 4S and 4SA also have anomalously high Ti, Fe, Na and Mn concentrations.

3.3.1 Crustal Contamination Indices

Several indices have been devised using major element oxide geochemistry to try and identify contamination (usually crustal) in kimberlites. Ilupin and Lutz (1971) suggested that kimberlites contaminated with crustal rocks would have elevated Si/Mg and lowered Mg/(Mg+Fe) atomic ratios (Mg#/100) due to crustal rocks having significantly higher Si and lower Mg concentrations than kimberlite. They proposed that kimberlites with Si/Mg>0.88 and/or Mg/(Mg+Fe)<0.85 were significantly contaminated. Fesq *et al.* (1975) argued that, based on the Si/Mg ratios of olivine (Fo_{87-93} ≈0.60) and phlogopite (≈1.21), contamination was only obvious when Si/Mg was greater than 1.2. Clement (1982) developed a "Contamination Index"

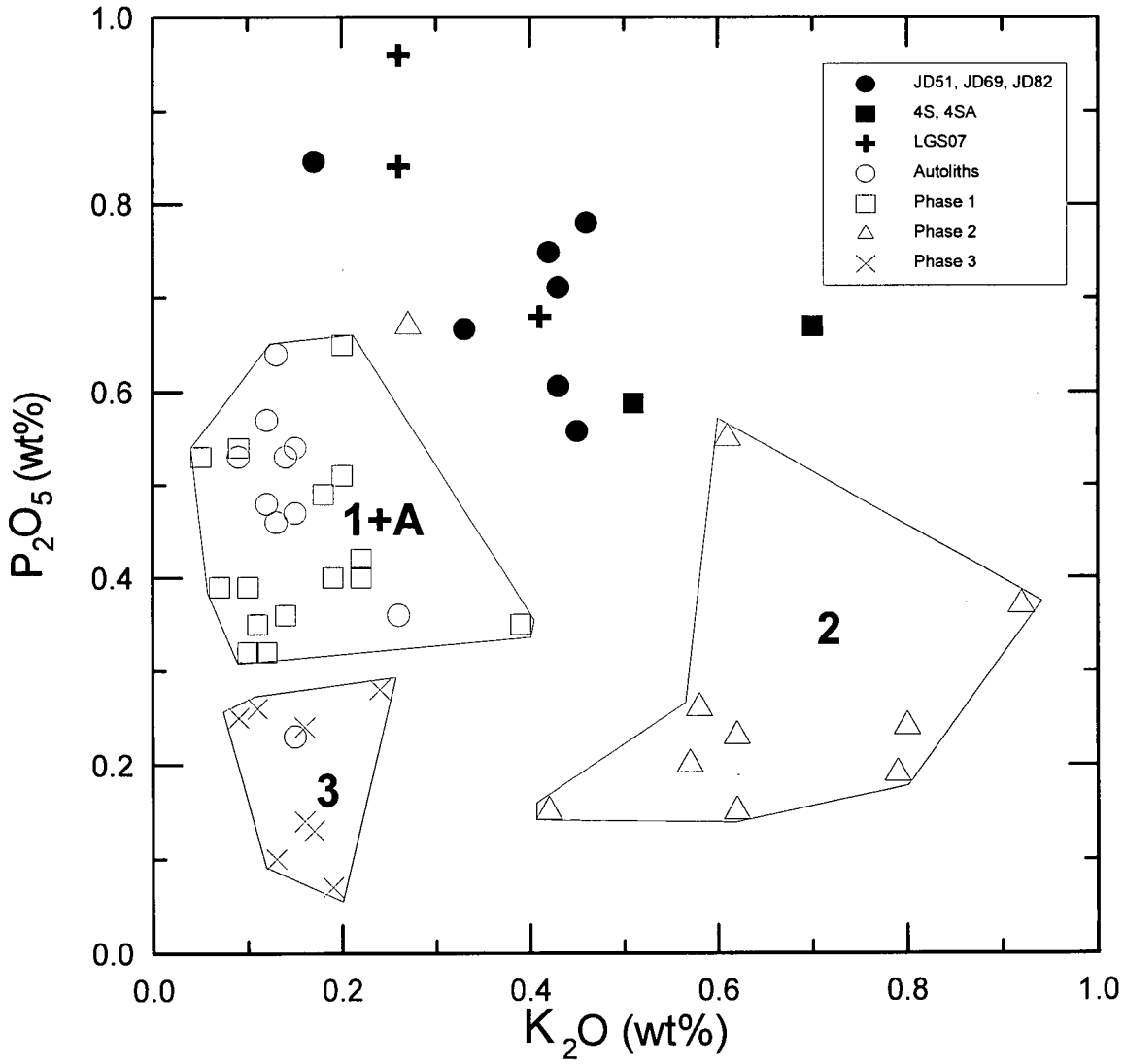

Figure 3.2 Plot of P_2O_5 vs. K_2O for all Jericho samples. 1+A is Phase 1 kimberlite and autoliths, 2 and 3 are Phases 2 and 3 respectively.

(C.I. = (SiO_2 + Al_2O_3 + Na_2O) / (MgO + $2K_2O$)) to evaluate the extent of crustal contamination and weathering in the KIMFIK intrusions (De Beers, Wesselton, Dutoitspan, Bultfontein, Finsch and Koffiefontein pipes, South Africa). This index is based on the KIMFIK crustal xenolith suite which includes shales, dolerites, basalts, andesites and other acid basement rocks. If the kimberlite sample is uncontaminated (and unweathered) the C.I. should be less than 1.5. Taylor *et al.* (1994) devised the "Ilmenite Index" (Ilm. I. = $FeO_{(t)}$ + TiO_2 / MgO + $2K_2O$) to determine the extent of ilmenite (xenocryst or megacryst) contamination. They suggested that for Type 1a non-micaceous kimberlites (as at Jericho), the Ilm. I. should not exceed 0.52.

Based on these four contamination indices, all Jericho aphanitic and bulk kimberlite samples, except samples 4SA and JD51, appear uncontaminated (Fig. 3.3). The Mg/(Mg+Fe) ratio, contamination and ilmenite indices suggest that sample 4SA is contaminated. Low Mg/(Mg+Fe) values in sample JD51 suggest the possibility of contamination although this is not supported by the other indices.

3.4 TRACE ELEMENT CHEMISTRY

3.4.1 Incompatible and compatible elements

The trace element abundances for the Jericho chilled margin samples are presented in Table 3.1, and a summary of the results of the Jericho bulk chemistry is presented in Table 3.2, with extended results in Appendix D. Primitive mantle-normalized multi-element diagrams show there is significant variation between the aphanitic samples.

In general, the aphanitic samples show strong LILE (with the exception of K) and HFSE enrichment, coupled with high LREE (Fig. 3.4). Samples are generally depleted in K, Sr, Zr, Ti and Y. Pb is anomalously high in all aphanitic samples. JD69 and JD82 demonstrate very similar

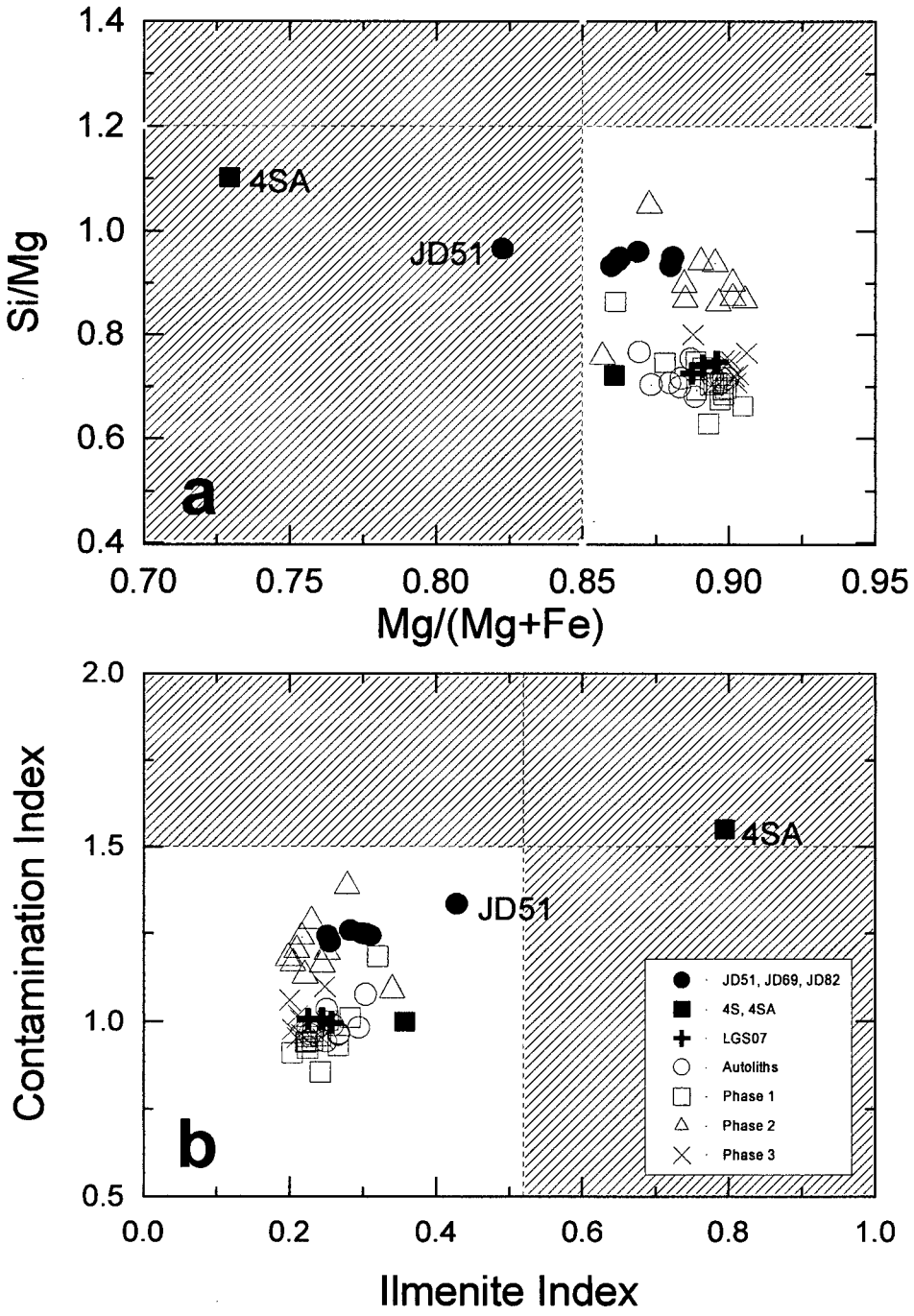

Figure 3.3 Jericho kimberlite samples plotted on current contamination indices (after Fesq *et al.*, 1975, Ilupin and Lutz, 1971, Clement, 1982, Taylor *et al.*, 1994). Contaminated samples plot in the shaded region with a) Si/Mg>1.2 and Mg/(Mg+Fe) <0.85, and b) Contamination Index >1.5, and Ilmenite Index >0.52.

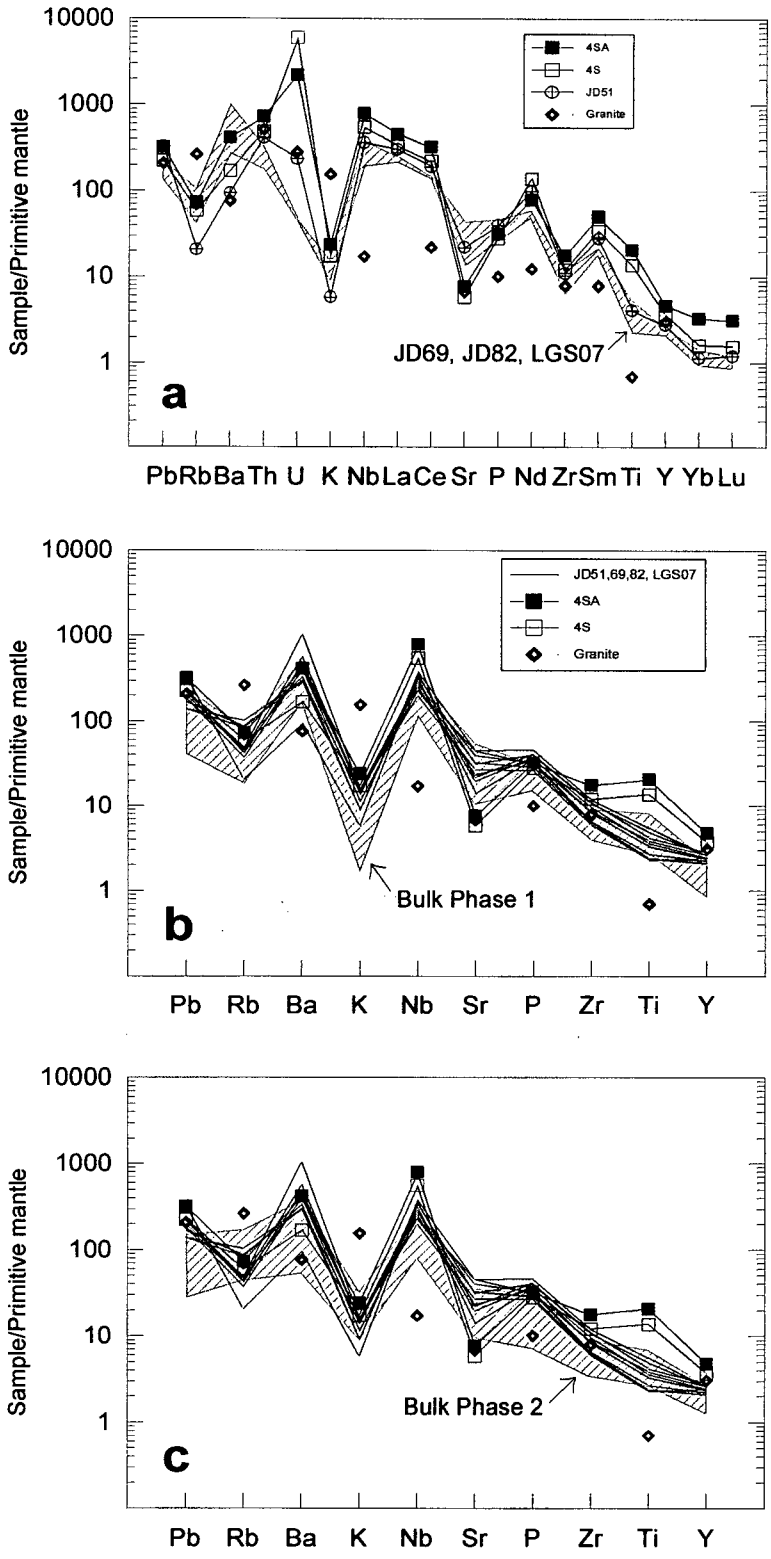

Figure 3.4 Primitive mantle normalized multi-element diagrams. (a) all aphanitic kimberlite phases with shaded region outlining results of JD69 and JD82 analyses, (b) Aphanitic samples with bulk Phase 1 chemistry (cross-hatched), (c) Aphanitic samples with bulk Phase 2 chemistry (cross-hatched). Primitive mantle normalizing values are from McDonough *et al.* (1992), except for P (Sun,1980) and Yb and Lu (Taylor and McLennan, 1985). The host granite (Contwoyto batholith) is also represented (Legault and Charbonneau, B. Davies, pers. comm.).

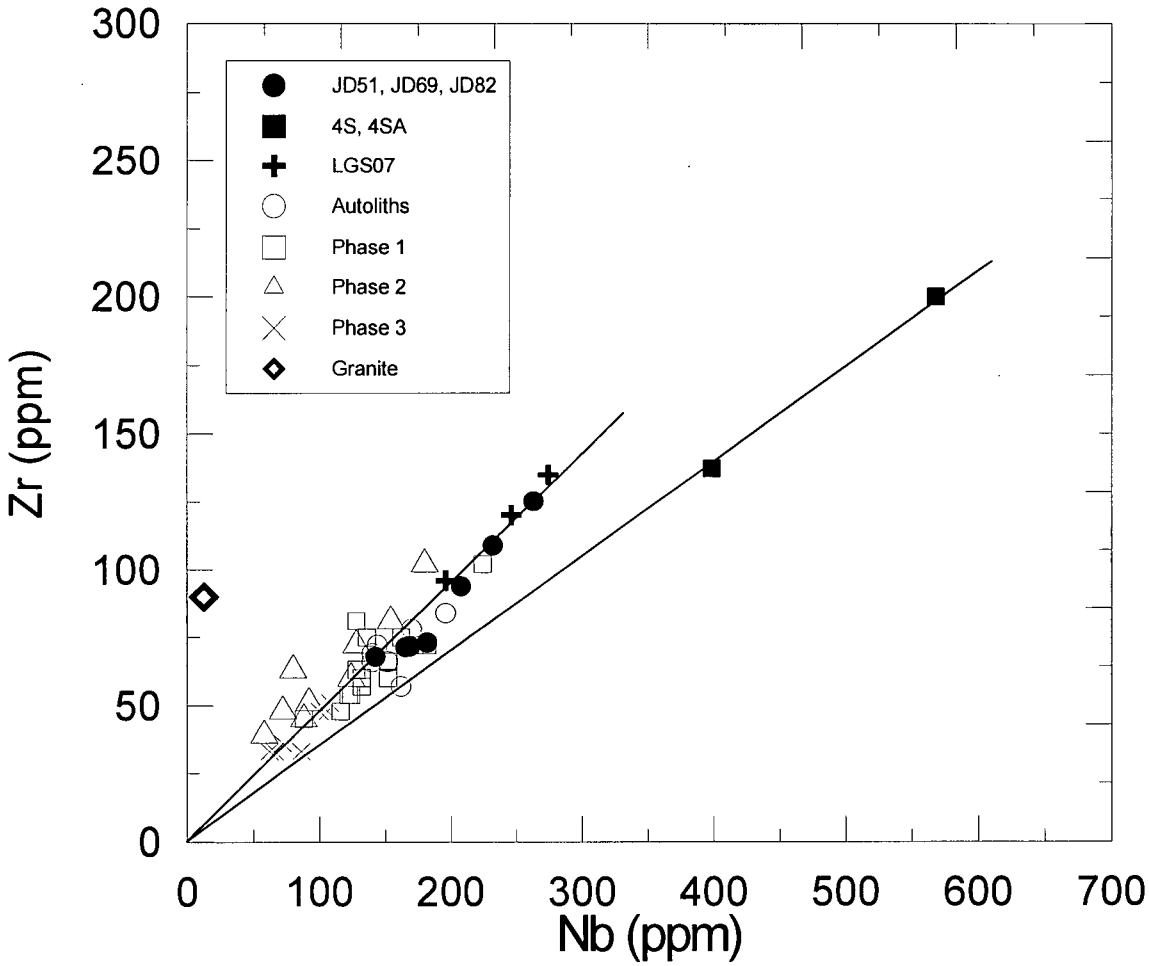

Figure 3.5 Trace element plot of Zr vs. Nb for Jericho aphanitic and bulk rock samples. Lines have been drawn through the data to estimate the Zr/Nb ratios. All samples, except 4S and 4SA have similar Zr/Nb ratios of approximately 0.48 (solid line). Samples 4S and 4SA have lower Zr/Nb ratios of approximately 0.35 (dashed line). The host granite (Contwoyto batholith) is also represented (Legault and Charbonneau, B. Davies, pers. comm.).

patterns, while JD51, 4S and 4SA are strongly enriched in U and Th and moderately enriched in the other incompatible elements, except Rb, Ba and Sr in which they are depleted. The enrichment in U and Th may be a result of granite contamination as the host granite (Contwoyto Batholith) is U and Th-bearing (Legault and Charbonneau, 1993; B. Davies, pers. comm.; Appendix F).

Cr and Ni concentrations are high in the aphanitic samples (Table 3.1) with Cr concentrations ranging between 1300-7600 ppm (highest in samples 4S and 4SA) and Ni concentrations ranging between 600-1500 ppm. These high values are similar to those of the bulk Jericho samples (Appendix D).

Comparing the aphanitic samples to Phase 1 and Phase 2 bulk Jericho samples (which are associated with aphanitic samples) shows that JD51, JD69 and JD82 are very similar to both Phase 1 and Phase 2, while samples 4S and 4SA are different from both of them. Therefore samples 4S and 4SA do not appear to be genetically linked to Phase 2, although their compositions may have been affected by contamination and/or alteration.

Kopylova *et al.* (1998) established a linear correlation between Nb and Zr for the Jericho kimberlite samples, and suggested there was a temporal and chemically continuous trend from high Nb and Zr magmas, to magmas depleted in these elements. The aphanitic samples have the highest Nb and Zr values, followed by the autoliths, then Phase 1, 2, and 3 (Fig. 3.5). Samples 4S and 4SA have the highest values, and lie slightly off the trend. Nb and Zr are good examples of incompatible elements in this system.

3.4.2 Rare earth elements

Rare earth element (REE) abundances for the Jericho aphanitic samples are listed in Table 3.3 and chondrite normalized (Taylor and McLennan, 1985) patterns are shown in Fig. 3.6. REE abundances were not determined for the bulk Jericho samples of Kopylova *et al.* (1998).

The aphanitic samples all have steep chondrite-normalized patterns with extreme light rare earth element (LREE) enrichment (400-900 times chondrite abundances for La); this steep pattern is typical of kimberlites worldwide (Mitchell, 1986). All samples show a similar pattern with a linear trend in the LREE, a kink in the middle REE with slightly elevated Gd and slightly depleted Tb values, and an enrichment towards the heavy rare earth elements (HREE) with the patterns flattening towards Lu. Comparisons with other kimberlite analyses do not show a Gd enrichment (Mitchell, 1986), however Gd is seldom analysed for. Sample 4SA is the most enriched in REE, then 4S and JD51. JD69 and JD82 have very similar abundances. Most of the samples have $(La/Yb)_N$ ratios between 232-299 except JD51 and 4SA which have elevated (344) and lowered (179) values respectively. There is a slight enrichment in the HREE with $(Tb/Lu)_N$ = 4.2 - 5.9 compared to the LREE with $(La/Sm)_N$ = 9.2 -11.9.

The similar REE patterns and abundances of the aphanitic samples suggest that the REE have not been affected by contamination or alteration. Mitchell (1986) suggests that contaminated kimberlites are generally enriched in HREE. However, the Contwoyto granite has a generally lower abundance of REE than Jericho aphanitic kimberlite (Fig. 3.6), and therefore if contamination has affected the REE, they should be reduced. Although the minor element geochemistry suggests that samples JD51, 4S and 4SA are affected by granite contamination, the enriched REE patterns cannot be explained by granite contamination.

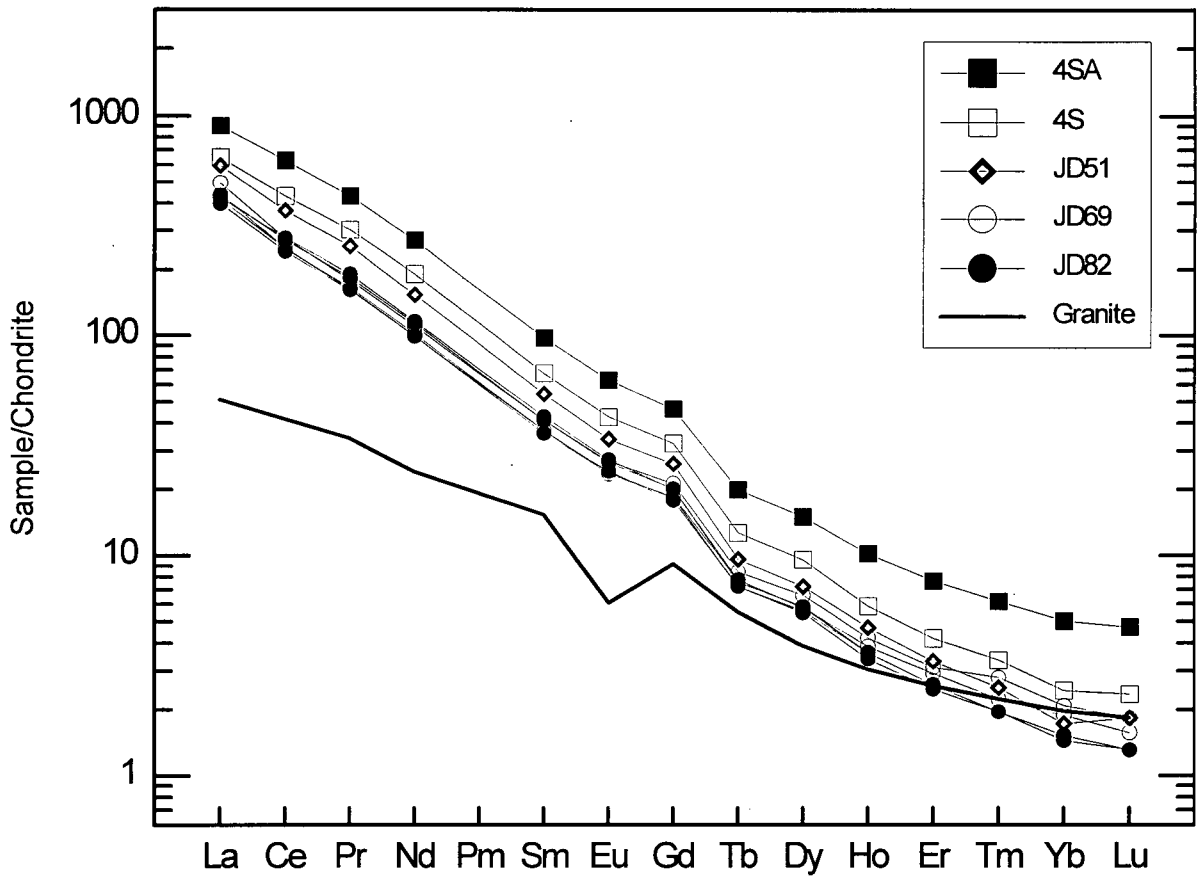

Figure 3.6 Chondrite normalized REE diagram for aphanitic kimberlite samples analysed in this study. Chondrite values are from Taylor and McLennan (1985). Error values are within the size of the symbol plotted. The host granite (Contwoyto batholith) is also represented (from B. Davies, pers. comm.).

Table 3.3: *Measured REE abundances (ppm) of samples of Jericho aphanitic kimberlite.*

	JD51	JD69			JD82			Rnd 120		1σ[1]
Sample	51	69-1	69-2	69-3	82-1	82-2	82-3	4S	4SA	
La	218.73	154.51	161.45	182.5	146.2	159.12	155.79	238.25	331.05	1.659
Ce	353.76	236.85	238.11	263.19	230.6	258.73	264.62	413.03	601.27	3.681
Pr	34.81	22.81	22.4	24.69	22.2	25.3	26.19	41.38	59.12	0.584
Nd	109.48	72.26	70.51	78.32	70.6	80.79	82.36	135.91	191.81	1.376
Sm	12.59	8.58	8.56	9.53	8.32	9.52	9.91	15.62	22.59	0.057
Eu	2.95	2.08	2.05	2.34	2.11	2.31	2.38	3.72	5.49	0.046
Gd	8.03	5.61	5.69	6.53	5.46	6.19	6.14	9.97	14.24	0.128
Tb	0.56	0.42	0.45	0.49	0.42	0.45	0.44	0.74	1.16	0.0058
Dy	2.76	2.13	2.19	2.51	2.09	2.2	2.23	3.66	5.72	0.0058
Ho	0.4	0.31	0.33	0.36	0.29	0.31	0.31	0.5	0.87	0.0058
Er	0.83	0.65	0.73	0.78	0.62	0.65	0.65	1.05	1.91	0.032
Tm	0.09	0.07	0.08	0.1	0.07	0.07	0.07	0.12	0.22	0.000
Yb	0.43	0.38	0.47	0.52	0.38	0.36	0.36	0.61	1.25	0.026
Lu	0.07	0.05	0.06	0.07	0.05	0.05	0.05	0.09	0.18	0.006
$(La/Yb)_N$	343.7	274.8	232.1	237.2	260.0	298.7	292.4	263.9	178.9	
$(La/Sm)_N$	10.9	11.3	11.9	12.1	11.1	10.5	9.9	9.6	9.2	
$(Tb/Lu)_N$	5.3	5.5	4.9	4.6	5.5	5.9	5.8	5.4	4.2	

[1] Standard deviation (σ) based on 3 replicate analyses of JD051 (see Appendix C for details).

3.4.3 Stable Isotopes

Stable isotope analyses were used to assess the potential effects of post-magmatic alteration. Samples JD51, JD69(-2), JD82(-2), 4S and 4SA were analysed for oxygen and carbon isotopes, and the results are presented in Table 3.3. Standard 'δ' notation in parts per thousand (‰) is used relative to the Pee Dee Belemnite (PDB) standard for carbon isotope ratios, and the Standard Mean Ocean Water (SMOW) standard for oxygen isotope ratios.

Oxygen isotope ratios ($\delta^{18}O_{SMOW}$) for the silicate fractions range between 4.2-11.9‰. Errors in these results are significant with a duplicate sample of JD69 varying by 2‰ (Appendix C). The yields of samples JD51, JD69 and JD82 are high and are greater than 90% of the calculated theoretical yields (Appendix E), however samples 4S and 4SA have much lower yields (64% and 82% respectively) and these values, especially for 4S need to be considered with caution. The low yields are probably a result of the presence of olivine, which is difficult to

dissolve (K. Kyser, pers. comm.). Figure 3.7a shows $\delta^{18}O_{SMOW}$ as a function of water content. All samples lie within the ranges determined for kimberlite groundmass mica and serpentine (Sheppard and Dawson, 1975). Petrographically, sample 4SA is the only aphanitic sample which appears to have any post-magmatic alteration. The $\delta^{18}O_{SMOW}$ results suggest it may have interacted with a fluid equilibrated with the granite, although the results are not conclusive. Samples JD51, JD69 and JD82 are extensively altered, and the oxygen isotope values suggest this is magmatic, rather than meteoric water, alteration. The extremely low yield of sample 4S meant the result was unreliable.

Carbon and oxygen isotope ratios for the carbonate fraction of samples JD51, JD69 and JD82 were similar with a mean value ($\pm 1\sigma$) of $\delta^{13}C_{PDB}$= -4.6 ± 0.4‰, and for $\delta^{18}O_{SMOW}$ =16.2 ± 0.4‰ (Fig. 3.7b). The extracted yields of these samples were high (88-96% of theoretical yields). These values indicate low temperature magmatic waters (K. Kyser, pers. comm., 1998) and fall within the typical range of fresh hypabyssal kimberlites (Kobelski *et al.*, 1979; Kirkley *et al.*, 1989). The low calcite contents of samples 4S and 4SA meant low yields were obtained, and therefore the results for these samples are highly suspect, and will not be further discussed.

Table 3.4: *Measured carbon and oxygen isotopes (‰) of samples of Jericho aphanitic kimberlite.*

	JD51	JD69(-2)	JD82(-2)	4S	4SA	1σ[1]
Calcite fraction						
$\delta^{13}C_{PDB}$	-5.2	-4.5	-4.8	*(-9.3)*[2]	*(-7.6)*[2]	0.1
$\delta^{18}O_{SMOW}$	16.6	16.1	16.3	*(14.2)*[2]	*(17.5)*[2]	1.4
%Yield[3]	88%	91%	96%	-	-	
Silicate fraction						
$\delta^{18}O_{SMOW}$	8.2	6.2	6.4	4.2	11.9	0.2
%Yield[3]	91%	95%	96%	64%	82%	

[1] Standard deviation (σ) based on replicate analyses of JD69(-2); see Appendix C for details.
[2] Yields for samples 4S and 4SA are negligible due to low calcite concentrations and are highly suspect.
[3] %Yield = actual yield/theoretical yield (*100). See Appendix E for calculations.

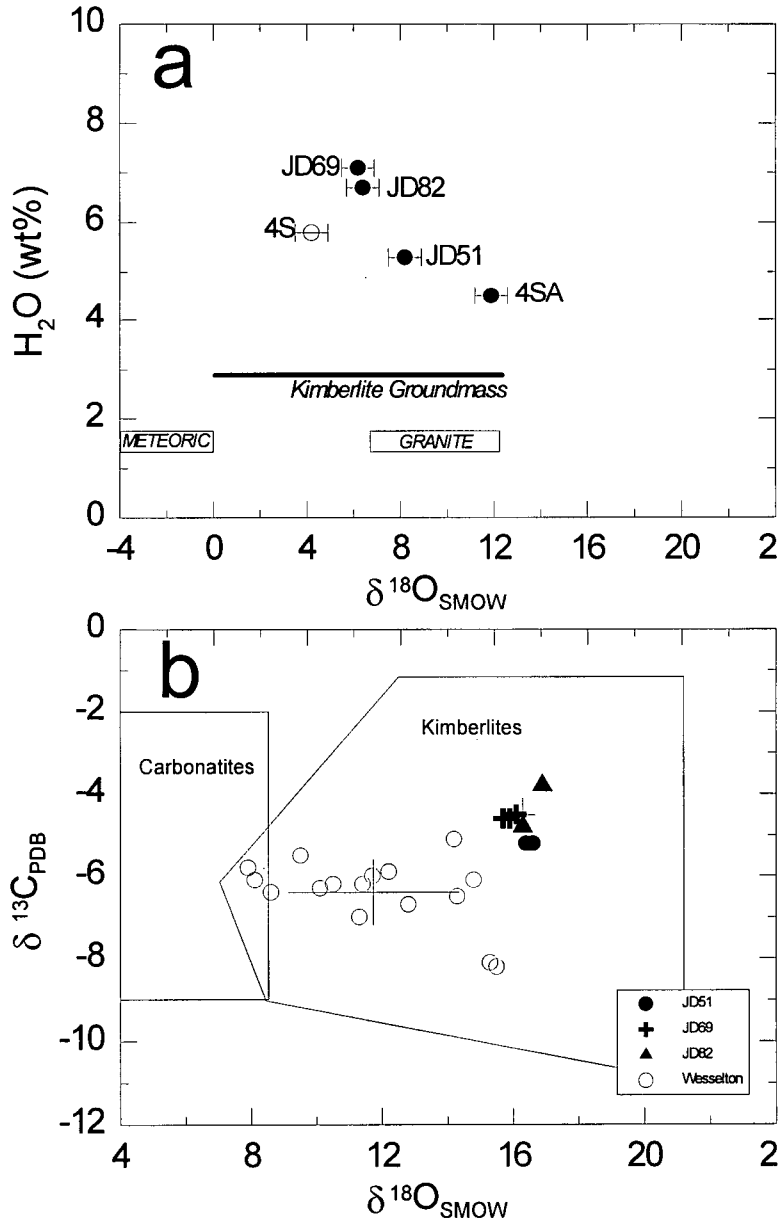

Figure 3.7 Carbon and oxygen isotopes of Jericho aphanitic samples. a) Oxygen isotope ratios of the silicate fractions as a function of H_2O (wt%). The yield of sample 4S is very low and, therefore this result is unreliable. All samples plot within values typical of kimberlite serpentine and mica groundmass (Sheppard and Dawson, 1975). Error bars represent 1 σ based on duplicate analyses. b) Carbon and oxygen isotopic composition of Jericho calcite compared with carbonates from kimberlites worldwide. Jericho samples are shown as bold symbols and the cross represents the arithmetic mean and one standard deviation. The shaded box is the field of primary carbonatite (from Deines and Gold, 1973). The kimberlite field is compiled from Kobelski *et al.* (1979) and Kirkley *et al.* (1989) and includes the Wesselton kimberlite (shown as open circles with a cross indicating the mean and 1 σ).

3.5 PEARCE ELEMENT RATIOS

To investigate whether the differences in geochemistry between the aphanitic samples and the bulk Jericho samples could be explained in terms of mineralogical stoichiometry, the chemical data (Table 3.1, Appendix D) were plotted as Pearce element ratio diagrams (Pearce, 1968; Russell and Nichols, 1988; Nichols and Russell 1991, Cui and Russell 1995). This requires the selection of an appropriate conserved element for the denominator, and a set of numerator elements for the x and y axes that can model the effects of the target mineral assemblage (Stanley and Russell, 1989; Nicholls and Gordon, 1994).

Zirconium and Niobium are believed to be conserved elements within these systems. Zirconium was chosen in this study as the denominator element. Zr has a low analytical error and is absent in the major macrocrystal phases. Within the groundmass phases, Zr is mostly present within perovskite. Contamination by ilmenite macrocrysts or megacrysts, which might be rich in Zr, could significantly increase this value, however, no macrocrysts or megacrysts of ilmenite were identified in these samples. In a geochemical study of altered and unaltered kimberlite samples, Taylor *et al.* (1994) determined the order of mobility of incompatible elements during alteration to be Sr ≈ Rb > La ≈ Ce > P ≈ Zr > Nb. According to this order, Zr is highly immobile. Plotted as Zr vs. Nb, all Jericho samples, except 4S and 4SA, define a trend that passes through the origin (Fig. 3.5). This is also consistent with Zr being incompatible.

The axes ½(Mg+Fe) and Si were chosen to investigate the stoichiometric controls on rock chemistry. For example, the accumulation or loss of olivine [$(Mg,Fe)_2SiO_4$] would cause samples to distribute themselves along a line with a slope of 1. Conversely, samples in which the olivine has been replaced by serpentine [$Mg_3Si_2O_5(OH)_4$], and in which the Mg+Fe/Si ratio have been adjusted by this process, should plot along a line with a slope of 0.75. Fig. 3.8 shows that

differences within the aphanitic samples LGS07, 4S and 4SA and the bulk Phase 1, autoliths and Phase 3 kimberlite can be explained as a result of either olivine accumulation or fractionation. Aphanitic samples JD51, JD69 and JD82 and bulk Phase 2 sample clearly show the chemical effects of serpentinization processes.

There are two interpretations for the position of the aphanitic samples in Fig. 3.8. One interpretation is that the aphanitic samples represent primitive magma and all other samples have accumulated olivine xenocrysts, and the other interpretation is that the bulk chemistry samples represent the more primitive kimberlites and the aphanitic samples have fractionated olivine. I argue that the aphanitic samples represent primitive melts and that the other phases at Jericho represent primitive melt with additional crystals.

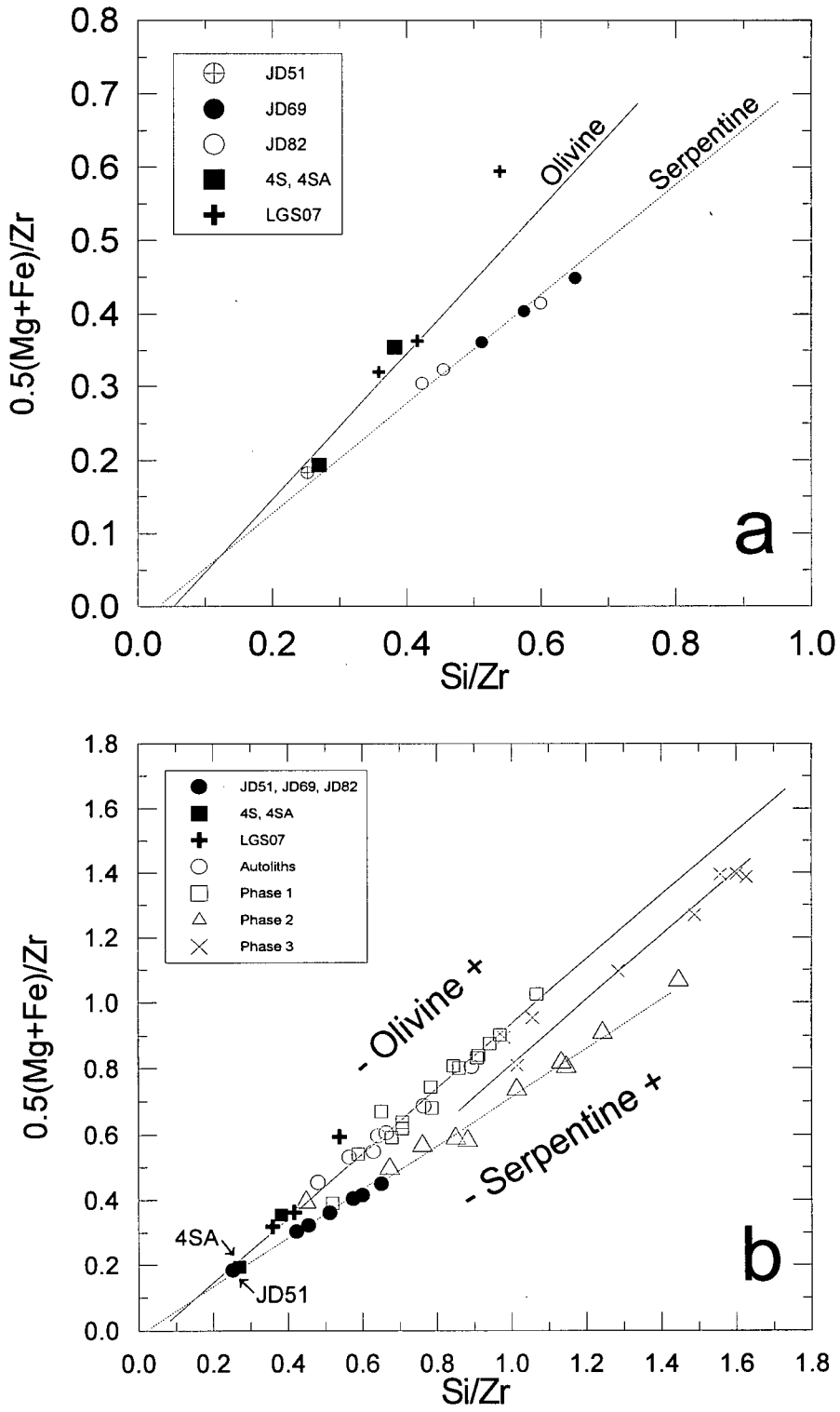

Figure 3.8 Pearce element ratio diagrams showing olivine (m = 1; full line) and serpentine (m = 0.75; dashed line) control lines as a function of ½(Mg+Fe)/Zr vs. Si/Zr. a) is a close up of the Jericho aphanitic samples and b) represents all Jericho samples. The position along the line can suggest either olivine accumulation or fractionation from a primitive magma. Control lines are drawn through median data points.

Chapter 4

DISCUSSION

4.1 INTRODUCTION

The aim of this study is to sample aphanitic kimberlite from Jericho and evaluate their compositions as to what degree they represent primitive, or perhaps primary, magmas. In previous chapters, I described the aphanitic kimberlite suite and compared these samples to macrocrystal bulk Jericho kimberlite samples. In the first part of this chapter I will argue that some of the aphanitic kimberlite samples from Jericho are representative of primitive kimberlite melts, and compare them to other 'primitive' kimberlite magmas worldwide. In the second part of this chapter I discuss the primary nature of the Jericho primitive melts.

4.2 PRIMITIVE KIMBERLITE MELTS

4.2.1 Jericho aphanitic kimberlite suite

Based on petrographical and geochemical evidence, several properties of the aphanitic samples indicate they are representative of primitive kimberlite melt. The attributes and shortcomings of the aphanitic samples as primitive melts are summarized in Table 4.1, and more fully discussed below.

Textural features

The chilled margin samples are from thin (<5 m) kimberlite dykes. Their fine-grained nature and location at the edge of thin macrocrystal dykes suggest they are kimberlite chilled

Table 4.1: *Summary of primitive melt attributes and shortcomings of Jericho aphanitic kimberlite samples.*

	Attributes						Shortcomings		
Sample	Hypabyssal texture	High CO_2	High Nb, Zr	High Cr, Ni	High Mg#	Fresh microphenocrysts	Secondary Alteration	Evidence of flow differentiation	Crustal contamination
JD51	✔	✔✔	✔	✔	✔	✘	✘	✘	✔
JD69	✔	✔✔	✔	✔	✔✔	✘	✘	✘	✘
JD82	✔	✔✔	✔	✔	✔✔	✘	✘	✘	✘
LGS07	✔	✔	✔	✔	✔✔	✔✔	✘	✘	✘
4S	✔	✘	✔✔	✔✔	✔✔	✔	✔	✔	✔✔
4SA	✔	✘	✔✔	✔✔	✘	✘	✔✔	✔	✔✔

✔ = sample has this attribute or shortcoming
✘ = sample does not have this attribute or shortcoming

margins. The aphanitic texture is interpreted as being produced from the rapid cooling of a relatively crystal-free magma against the relatively cool host rock. Sample LGS07 is slightly coarser-grained than the other chilled margin samples, and has a 'microporphyritic' texture similar to macrocrystal kimberlite. Olivine macrocrysts in macrocrystal kimberlite are interpreted to be, at least partially, xenocrysts and therefore it is likely that the olivine crystals in LGS07 are also xenocrysts.

Samples 4S and 4SA have a weakly developed mineral alignment and are associated with the diatreme facies. As the magma is moving through the diatreme, crystals tend to migrate away from the margins (Bhattacharji, 1967). This produces a relatively crystal-free kimberlite margin at the edge of the diatreme, which cools to form a fine-grained rock. There are, however, small olivine crystals present within these samples (up to 50%) and these crystals are quite rounded (Fig. 2.8). This rounding might have been produced from milling during emplacement, indicating that these crystals might be xenocrysts.

The chilled margin samples, except LGS07, are more primitive magmas that have not been fractionated to the extent of the flow differentiated samples. However, if the crystal phase in the flow differentiated samples are xenocrysts, the removal of this phase leaves a melt phase. Scott Smith (1996) suggests there is greater potential for textural modifications to the erupting magma during diatreme formation than during dyke emplacement. Therefore, the diatreme association of the flow differentiation samples suggests they may be less reliable as examples of primitive melts than the chilled margin samples.

Geochemical characteristics

In order to get the best estimate of the chemistry of the melt phase, an effort was made to hand-remove the small macrocrystal component (<3%) of these samples. Three splits were also taken of three of the chilled margin samples (JD69, JD82 and LGS07) and analysed separately. The similar geochemistry (Table 3.1) of these splits indicate the samples crystallized from a fairly homogeneous melt phase.

All the Jericho aphanitic samples, except JD51 and 4SA, have high Mg#s (86-91) suggestive of primitive magmas. JD51 and 4SA have lower Mg#s of 82 and 73 respectively. This is due to JD51 having a relatively low MgO, and 4SA having a very high total Fe content.

The aphanitic samples have high Cr (1300-7600 ppm) and Ni (600-1500 ppm) contents, which are also characteristics of primitive magmas. Samples 4S and 4SA have anomalously high Cr contents (5300-7600ppm). All samples have high incompatible element contents, particularly Zr, Nb and Y concentrations. The flow differentiated samples have anomalously high values and different Zr/Nb ratios than both the chilled margin samples and bulk Jericho samples. This suggests the Zr and Nb values have been affected by secondary processes, most likely by granite contamination.

Volatile content

The aphanitic samples have variable CO_2 contents (<1 - 19 wt%) and similar H_2O contents (5-7 wt%). The chilled margin samples have high CO_2 concentrations (5-19 wt%), with JD51, JD69 and JD82 having particularly high values (10-19 wt%), and the flow differentiated samples have anomalously low CO_2 concentrations (<1 wt%). As calcite appears primary in thin section, and there is no evidence for recrystallization, it is likely that CO_2 was an original phase

within the magma.

The high CO_2 contents of the chilled margin samples suggests these magmas have not undergone extensive devolatilization during emplacement. The low CO_2 contents of the flow differentiated samples suggests the magma either devolatilized prior to solidification (as would be expected during diatreme formation), or that calcite has been subsequently removed by post-emplacement processes. There is some void space in these samples (up to 5%) which may have once held calcite, however the origin of the void space is not obvious, and may be a result of expansion of hydrous minerals during alteration. The low volatile contents in the flow differentiated samples are not indicative of primitive kimberlite magmas.

Secondary processes: Alteration and contamination

Some of the Jericho aphanitic samples are affected by secondary processes. Processes identified within some of these samples include the replacement of olivine by serpentine, Fe- Si-rich alteration, and crustal contamination.

Microphenocrysts in the chilled margin samples, except LGS07, and the flow differentiation samples have serpentinized microphenocrysts. Sample 4SA also has an overprinting Fe- Si- rich alteration (seen in elevated Fe and Si contents).

The chilled margin samples, except JD51, appear uncontaminated by crustal material. The Ilupin and Lutz (1971) crustal contamination index suggests JD51 is contaminated, however, the slightly elevated U, Th and Ti concentrations suggest contamination by the host granite (Contwoyto batholith). This sample also has an extremely high Fe_2O_3/FeO ratio (11.35), indicating either oxidation or incorporation of an Fe^{3+} bearing mineral, which suggests the composition should be treated with caution.

The flow differentiated samples appear to be crustal rock contaminated. The Ilupin and Lutz (1971) index, and the C.I. and Ilm. I. suggest that sample 4SA is contaminated, and both 4S and 4SA have elevated U, Th and Ti values indicative of host granite (Contwoyto batholith) contamination.

Summary

The chilled margin samples JD69 and JD82 are the best estimates of primitive kimberlite magma with textures representative of a liquid phase, high CO_2 content and Mg#s, high Cr, Ni and incompatible element concentrations. They also appear to be free of contamination by crustal material. Sample JD51, although similar to primitive samples JD69 and JD82, appears to be weakly contaminated by crustal material (granite). Therefore, it is not as representative of a primitive magma as the other chilled margin samples. The aphanitic samples LGS07, 4S and 4SA have a higher proportion of olivine microphenocrysts than JD69 and JD82 and have an almost macrocrystal texture, though finer-grained. The olivine microphenocrysts are quite rounded, possibly representing milling during emplacement. This suggests they may be xenocrysts. Samples 4S and 4SA appear to have been affected by crustal contamination, and/or secondary alteration, and therefore are not as good representatives of primitive magmas.

4.2.2 Aphanitic sample suite vs. macrocrystal Jericho samples

Geochemical and textural evidence suggests that the chilled margin samples JD69 and JD82 represent more primitive kimberlite magmas than Jericho Phase 1, 2 and 3 macrocrystal kimberlite described in Chapter 1. The macrocrystal kimberlite phases are hybrid rocks that include large proportions of xenocrysts, particularly peridotitic olivines. Therefore, they are poor representatives of primitive melts. Also, the aphanitic samples generally have much higher CO_2 contents (10 - 20 wt%) than the macrocrystal kimberlite phases (average is 4 - 5 wt%), suggesting the aphanitic samples have suffered less devolatilization. This makes the aphanitic kimberlite samples better estimates of primitive melts than the macrocrystal samples.

Pearce Element Ratio (PER) analysis of both the aphanitic and macrocrystal Jericho samples demonstrated that the different Mg, Fe and Si concentrations in these samples (together >50 wt% of the rock) can be explained by olivine, or serpentinized olivine, sorting (Fig. 3.8). This represents microphenocryst sorting in the aphanitic samples and macrocryst sorting in the macrocrystal samples. The aphanitic samples have consistently low olivine or serpentine values and this suggests they are more primitive than the macrocrystal Jericho samples which have had olivine, probably xenocrysts, added to them.

Both the aphanitic and macrocrystal samples from Jericho have similar high Mg#s and high Cr and Ni contents (Table 3.1, Appendix D). The low modal content of macrocrysts in the aphanitic samples suggests the high observed Mg#s and Cr and Ni contents are not caused by olivine accumulation, but instead are primary characteristics of the magma.

The aphanitic samples have higher incompatible elements, especially Nb, Zr and Y, than the macrocrystal kimberlite samples. Kopylova *et al.* (1998) identified a trend within the Nb-Zr data from magmas high in Nb and Zr through to magmas low in Nb and Zr. Their "chilled

margin" sample (LGS07) had the highest values, followed by the autoliths, then Phase 1, 2 and 3. The aphanitic samples of this study also have high Nb and Zr values, similar to LGS07 (Fig. 3.5). The flow differentiated samples have anomalously high values, lying off the general trend, and are interpreted as having been affected by secondary processes, probably due to granite contamination. As a temporal trend of kimberlite emplacement has been identified by Cookenboo (1998) from Phase 1 to 3, with Phase 1 being the earliest intrusion and Phase 3 the latest intrusion, this suggests the aphanitic samples were emplaced earlier than Phase 1. This is another good argument that the chilled margin samples represent primitive magmas.

In summary, the textural and geochemical evidence outlined above suggests that the chilled margin samples represent more primitive kimberlite magmas than any of the macrocrystal samples.

4.2.3 Comparison with other 'Primitive' Kimberlites

The Wesselton aphanitic kimberlite (South Africa) is thought to be the best example of an unfractionated 'primitive' kimberlite (Mitchell, 1995; Edgar *et al.,* 1988; Edgar and Charbonneau, 1993). The major and trace element chemistry of the Wesselton aphanitic kimberlite is listed in Table 4.2. This kimberlite has an absence of olivine xenocrysts, low abundances of xenoliths and xenocrysts (Edgar *et al.,* 1988), high Mg# (83.9), low SiO_2 (25.6 wt%), high Ni (810 ppm) and high Cr (2410 ppm). In comparison, the Jericho primitive kimberlite samples JD69 and JD82 have higher Mg#s (86-88), similar SiO_2 (24-30 wt%), higher Ni (800-1400 ppm) and higher Cr (1300-1900 ppm). The Wesselton kimberlite has approximately 5 wt% CO_2 whereas the Jericho primitive samples have between 10 - 17 wt%. Therefore, the Jericho samples appear to be geochemically more primitive than the Wesselton

kimberlite. The Wesselton kimberlite also has a microporphyritic texture (Fig. 4.1) similar to the Jericho chill margin sample LGS07 and the flow differentiated samples which suggests the smaller olivines may be xenocrysts.

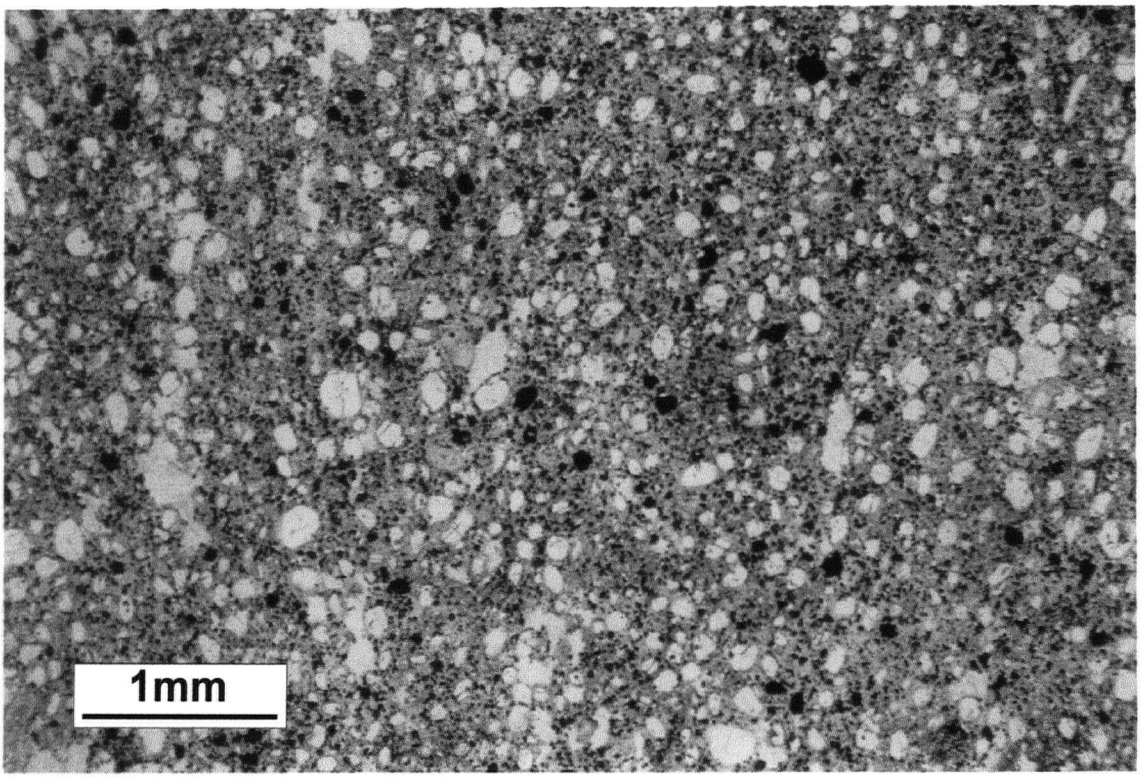

Figure 4.1 Photomicrograph of the Wesselton aphanitic kimberlite, from Mitchell (1998).

Berg (1998) suggests the Dutoitspan (KDT) macrocrystal monticellite kimberlite (South Africa) and the Leslie hypabyssal monticellite kimberlite, NWT, Canada (Berg and Carlson, 1998) represent relatively primitive kimberlite magmas, being low in Al_2O_3 and considered uncontaminated by crustal material. Both these examples are macrocrystal, not aphanitic, kimberlite and Berg (1998) suggests that many of the olivine macrocrysts are derived from peridotites, and therefore not part of the primary melt. Major element geochemistry of the KDT

(Dutoitspan) and Leslie kimberlites are presented in Table 4.2 with average compositions of Group 1A (off-craton; Scott *et al.*, 1985), Group 1B (on-craton; Smith *et al.*, 1985)), Kimberley (Clement, 1982) and Siberian kimberlites (Ilupin and Lutz, 1971). Unfortunately, Berg (1998) and Berg and Carlson (1998) do not give present CO_2 analyses, so it is difficult to directly compare the CO_2 content.

In order to directly compare the geochemistry of Jericho primitive kimberlite to other primitive and average kimberlites, the analyses were normalized without the volatiles CO_2 and H_2O. As the volatile concentrations are highly variable within the samples, and are affected by emplacement processes, removing these phases allows for a more direct comparison of the other phases in the melt. Fig. 4.2 shows volatile-normalized SiO_2 *vs.* MgO and CaO *vs.* Al_2O_3 plots for the Jericho aphanitic samples, the Wesselton, Dutoitspan (KDT) and Leslie primitive kimberlites, and average bulk samples of kimberlites worldwide. On both plots, the Jericho chill margin sample LGS07 and the KDT and Leslie kimberlites have similar geochemistry, different from the Wesselton kimberlite and the primitive Jericho samples JD69 and JD82. The Wesselton kimberlite has a very low SiO_2 content and has low MgO contents, similar to the primitive Jericho samples JD69 and JD82. The position of the primitive Jericho samples in SiO_2-MgO space has possibly been affected by serpentinization. The Jericho aphanitic samples JD69 and JD82 have the highest CaO values, along with the Wesselton kimberlite. The Wesselton kimberlite has the highest Al_2O_3 content, which could possibly be reflecting crustal contamination.

Without knowing the composition of a primary kimberlite magma, I can only compare these results. If the Wesselton kimberlite is a good example of a primary kimberlite magma, perhaps the differences in the chemistry of the Wesselton and Jericho kimberlites are giving us

an insight into the nature of partial melts (and the nature of the mantle) in South Africa and Canada, respectively.

Table 4.2: *Compositions of primitive kimberlites from Jericho and worldwide, and average Group I kimberlites.*

	Jericho primitive kimberlites		Other primitive kimberlites			Average Group I kimberlites			
	1	2	3	4	5	6	7	8	9
Source	JD69(-2)	JD82 (-2)	Wesselton	Leslie	Dutoitspan	Group IA	South Africa	Group IB	Siberia
SiO_2 (wt%)	27.00	28.13	25.60	31.67	31.73	32.1	30	25.7	27.6
TiO_2	0.51	0.71	3.35	0.66	1.55	2.0	1.8	3.0	1.6
Al_2O_3	1.33	1.61	3.31	1.23	1.94	2.6	2.6	3.1	3.2
Fe_2O_3[a]	2.15	2.69	-	9.24(t)	8.76(t)	9.2(t)	9.4(t)	12.7(t)	8.4(t)
FeO[a]	3.50	4.17	10.30(t)	-	-	-	-	-	-
MnO	0.14	0.16	0.21	0.17	0.16	0.2	0.2	0.2	0.1
MgO	22.39	23.09	27.20	40.93	36.17	28.5	29.4	23.8	24.3
CaO	19.37	16.66	15.30	8.09	7.98	8.2	10.9	14.1	14.1
Na_2O	0.15	0.19	0.28	0.00	0.37	0.2	0.3	0.2	0.2
K_2O	0.43	0.46	0.70	0.397	0.74	1.1	1.2	0.6	0.8
P_2O_5	0.61	0.78	1.83	0.258	0.80	1.1	1.6	1.1	0.5
CO_2	14.01	12.06	4.77			4.3	5.4	8.6	10.8
H_2O+	7.10	6.70	6.20			8.6	7.3	7.2	7.9
LOI	21.98	20.11		5.59	9.85				
Total	99.44	98.45	99.05	99.45	101.24				
Cr (ppm)	1312	1803	2410			1400	1398	1000	
F			2500						
Cl			800						
Ni	1099	1367	810			1360	1018	800	
Rb	30	29	20			50	66	30	
Sr	693	423	1180			825	1145	1020	
Y	10	11	10			13	17	30	
Zr	71	94	580			200	308	385	
Nb	165	208	250			165	168	210	
Ba	4026	2820	1000			1000	915	850	
Th	17	26				18		27	
Zn						56	63	75	
Cu						54	52	79	
Co						83	85	79	
V	87	85				75	91	170	

1-2: Jericho primitive kimberlite (median compositions); 3: Wesselton kimberlite (Shee, 1986); 4: Leslie kimberlite (Berg and Carlson, 1998); 5: Dutoitspan kimberlite (Berg, 1998); 6: average of 10 Group IA off-craton southern African kimberlites (Scott *et al.*, 1985); 7: average of 30 kimberlite pipe and dykes from the Kimberley area, South Africa (Clement, 1982); 8: average of 7 Group IB on-craton southern African kimberlites (Smith *et al.*, 1985); 9: average of 623 analyses of Siberian kimberlites (Ilupin and Lutz, 1971).

[a] Fe_2O_3(t) and FeO(t) indicates Fe was calculated as either total Fe_2O_3 or FeO respectively.

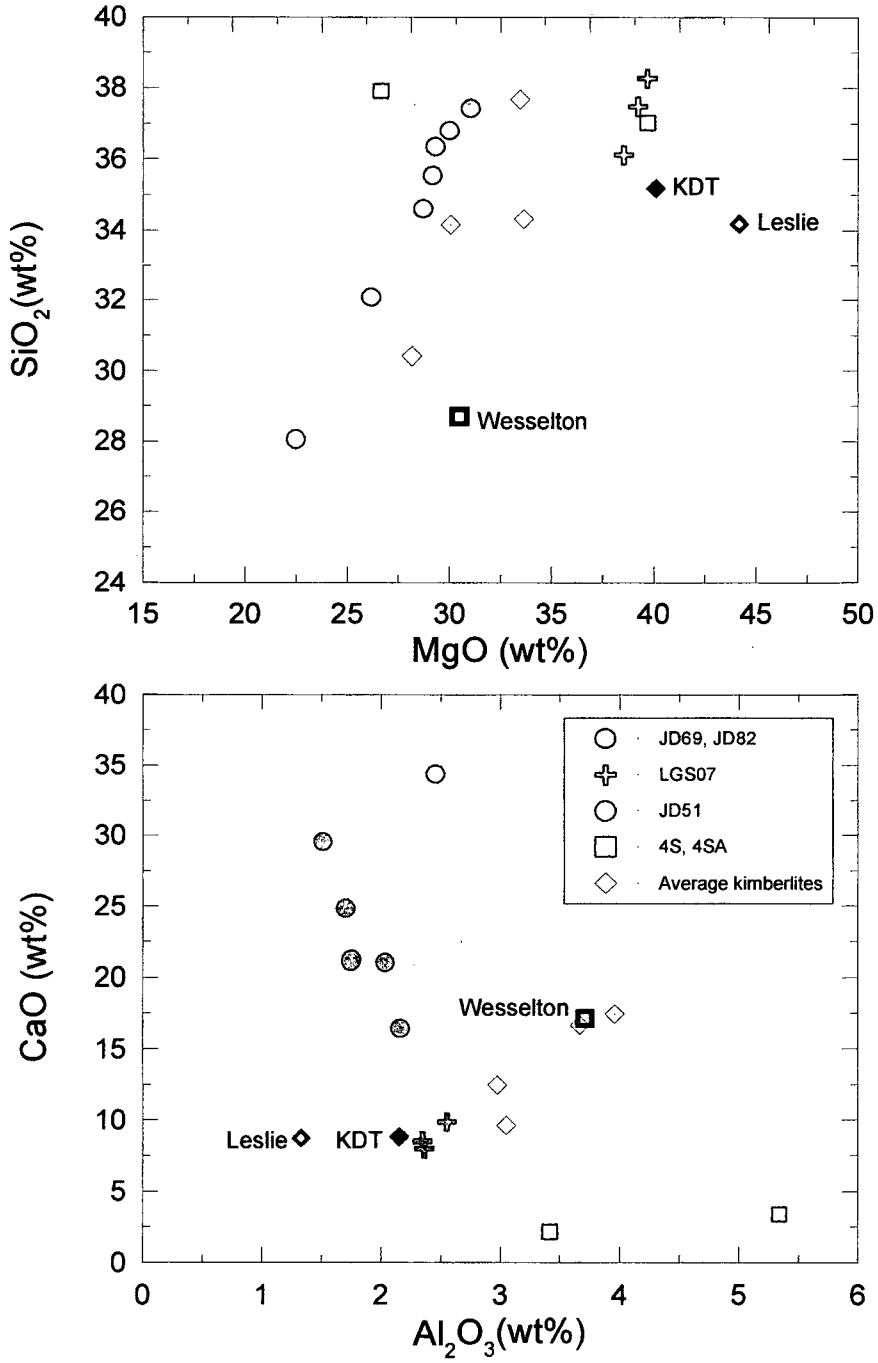

Figure 4.2 Volatile-normalized SiO_2 *vs.* MgO and CaO *vs.* Al_2O_3 plots for Jericho aphanitic samples (in green (uncontaminated) and red) and other 'primitive' kimberlite magmas worldwide (Wesselton: Shee 1986; Leslie: Berg and Carlson, 1998; KDT-Dutoitspan: Berg, 1998). Also shown are average kimberlite compositions (Scott et al., 1985; Clement, 1982; Ilupin and Lutz, 1971). See Table 4.2 for detailed compositions.

4.3 PRIMARY MAGMAS AT JERICHO

4.3.1 Primary characteristics of the Jericho primitive kimberlite samples

Given that samples JD69 and JD82 represent primitive melts from Jericho, how close are these compositions to the primary kimberlite magma? Due to the hybrid nature of kimberlites and the lack of quenched 'glassy' kimberlite, it is difficult to speculate on the nature of a kimberlite primary magma. In this section, I will discuss properties of the kimberlite magmas which are indicative of primary magma, and which properties of the primitive magmas are likely changed from the original primary magma.

The Jericho primitive magmas (Table 4.3) have high Mg#s, high Cr and Ni, and high incompatible elements and these properties directly reflect primary melt properties. Although some CO_2 devolatilization may have occurred during ascent, these samples still have much higher CO_2 contents than most kimberlites, and these values represent a minimum CO_2 content for the primary magma.

The olivine microphenocrysts in samples JD69 and JD82 have been completely serpentinized. The replacement of olivine by serpentine involves a volume increase, the addition of water, and either the addition of Si or the removal of Mg. The concentration of Fe in the olivine can also be affected. This serpentinization results in a change in the Si/Mg ratio, as demonstrated in Figs. 3.1a and 3.8. Unless the system is closed, serpentinization results in an increase in this ratio for the whole rock.

Table 4.3 *Compositions of primitive kimberlite magmas from the Jericho pipe*

	JD69			JD82		
Sample	69-1	69-2	69-3	82-1	82-2	82-3
SiO_2 (wt%)	24.15	27.00	29.06	28.83	28.13	30.31
TiO_2	0.51	0.51	0.49	0.57	0.71	0.77
Al_2O_3	1.14	1.33	1.38	1.39	1.61	1.75
Fe_2O_3	2.23	2.15	2.13	5.27	2.69	2.95
FeO	3.58	3.50	3.79	1.51	4.17	4.64
MnO	0.16	0.14	0.13	0.16	0.16	0.15
MgO	19.71	22.39	23.69	23.25	23.09	25.14
CaO	22.25	19.37	16.69	16.86	16.66	13.32
Na_2O	0.14	0.15	0.13	0.12	0.19	0.24
K_2O	0.33	0.43	0.45	0.43	0.46	0.42
P_2O_5	0.67	0.61	0.56	0.71	0.78	0.75
CO_2	16.91	14.01	12.97	12.39	12.06	9.80
H_2O+	6.40	7.10	6.40	6.00	6.70	7.50
H_2O-	0.71	0.76	0.76	1.15	1.04	1.05
Total	98.89	99.45	98.63	98.64	98.45	98.79
FeO(t)	5.59	5.43	5.71	6.25	6.59	7.29
Mg#	86.3	88.0	88.1	86.9	86.2	86.0
Cr (ppm)	1301	1312	1570	1513	1803	1891
Ba	2889	4026	7274	3351	2820	3318
Rb	23.8	30.0	30.7	26.8	29.3	27.6
Sr	948.9	692.8	571.7	498.5	423.4	297.2
Nb	168.7	165.4	142.6	182.0	207.5	231.8
Zr	71.6	71.3	67.8	73.0	93.8	108.8
Y	9.6	10.3	11.1	10.2	10.9	11.3
Pb	13.1	15.7	14.3	15.9	13.2	16.2
Ni	789	1099	1151	1291	1367	1396
V	87	87	95	90	85	87
Ga	1.9	1.8	b.d.	2.8	3.2	3.0
Th	18.5	16.6	15.0	19.8	25.7	28.8
U	1.0	b.d.	b.d.	b.d.	b.d.	b.d.

b.d. below detection (Detection limits for U and Th is 1.0 ppm)
Mg# = 100. Mg/(Mg + Fe2+) where Fe2+ is calculated from FeO(t).

4.3.2 Experimental determinations of primary kimberlite melts

The high concentrations of incompatible elements suggests kimberlites represent low-degree partial melts (Dalton and Presnall, 1998). The high LREE/HREE ratios and low Al concentrations in kimberlite necessitates that garnet is retained in the solid residua during melting (Mitchell, 1986). Therefore, most authors agree that the source rock for kimberlite magmas is a carbonate-bearing garnet lherzolite, although Edgar and Charbonneau (1993) were unable to produce orthopyroxene in their melting experiments of the Wesselton kimberlite.

Dalton and Presnall (1998) investigated the CaO-MgO-Al_2O_3-SiO_2-CO_2 system at 6 GPa. They started with a slightly modified lherzolite composition from Canil and Scarfe (1990) given in Table 4.4, and performed experiments near the liquidus where they determined the crystal and melt phases. The melt phase was composed of both quench Ca-Mg carbonates and quench silicate phases and they found that the melt compositions showed a systematic variation with temperature from carbonatitic at the solidus (1380°C) through intermediary compositions to kimberlitic 70-100°C above the solidus. The composition of this melt phase at different temperatures is given in Table 4.4. For their modelling of a lherzolite with 0.15wt% CO_2, they found that this continuous change occurs within the melting range 0-1 volume%.

The chemical composition of the Dalton and Presnall (1998) partial melts can be directly compared to the Jericho kimberlite samples. Although it is difficult to directly compare experimental with actual results, it may give us an insight into the nature of the primary kimberlite melt.

Table 4.4: *Compositions of partial melts determined by Dalton and Presnall (1998) and Canil and Scarfe (1990)*

T (°C)	P (GPa)	SiO_2	MgO	CaO	CO_2	Al_2O_3
Dalton and Presnall (1998)						
Starting Composition*		**46.85**	**42.61**	**2.77**	**4.8**	**2.97**
1380	6	5.79	20.91	28.03	44.61	0.66
1405	6	20.37	26.00	21.02	30.84	1.77
1430	6	24.38	27.43	18.34	26.97	2.88
1455	6	27.24	27.69	18.40	24.46	2.21
1480	6	32.45	28.42	17.26	18.65	3.21
1505	6	36.23	29.57	16.58	14.53	3.09
Canil and Scarfe (1990)						
Starting Composition		**43.18**	**44.27**	**8.08**	**4.4**	**-**
1320	5	45.87	46.27	10.37	-	
1410	5	33.06	49.10	7.26	11.00	
1360	7	48.61	44.72	8.12	-	
1380	7	43.70	48.30	8.67	1.70	
1450	7	30.88	45.06	8.36	12.22	
1420	9	37.14	50.81	7.93	1.43	

*Dalton and Presnall (1998) chose a starting composition which was close to Canil and Scarfe (1990) CCMAS1 composition but they added slightly more (4.8 wt%) CO_2. I have estimated their composition by normalizing the data for 4.8 wt% CO_2.

Fig. 4.3a shows the Dalton and Presnall (1990) partial melt data compared with the uncontaminated Jericho aphanitic kimberlite samples (primitive samples JD69 and JD82, and LGS07) and bulk macrocrystal Jericho kimberlite. The arrow indicates the direction from low partial melts (carbonatitic) to high partial melts (kimberlitic). It is clear that the Jericho primitive samples JD69 and JD82 plot somewhat closer, and on the other side of, the partial melts than the bulk macrocrystal samples and the 'microporphyritic' LGS07. It is therefore probable that the Jericho primitive samples represent primitive melts and the other samples have had olivine xenocrysts added to them. Fig. 4.3b shows the Jericho primitive magmas (and LGS07) with other worldwide primitive kimberlites and average worldwide kimberlites (Table 4.2). Once again, the

a) Jericho

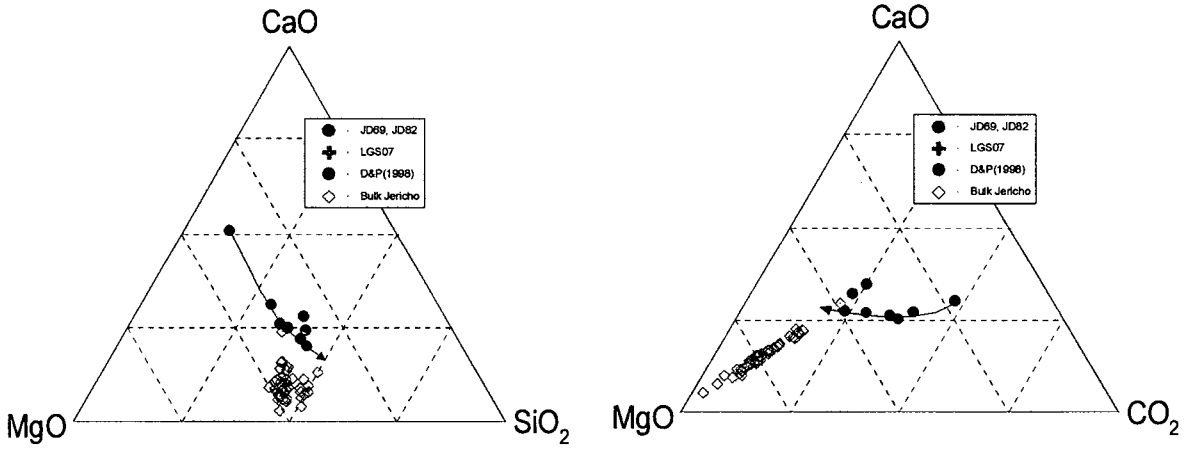

b) Worldwide

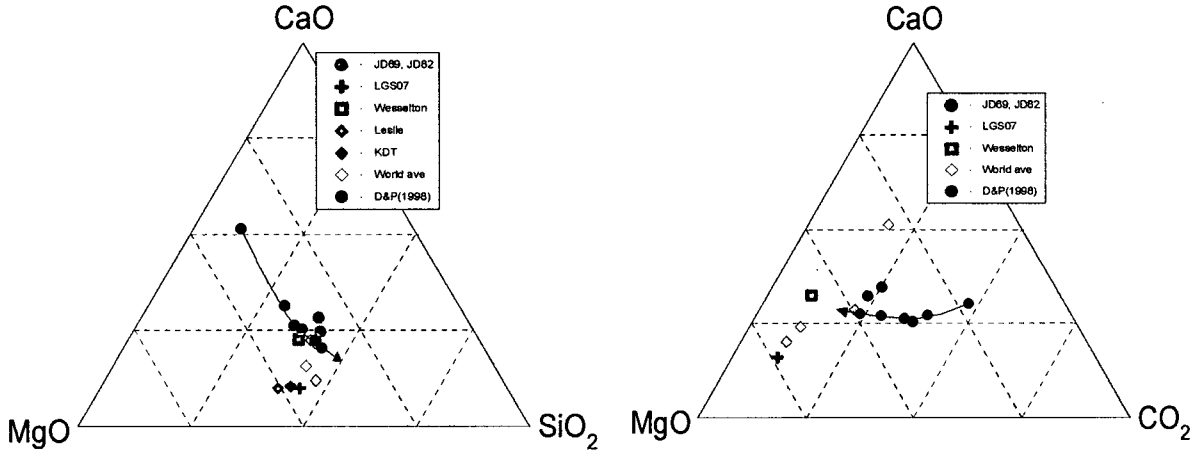

Figure 4.3 CaO-MgO-SiO_2 (left) and CaO-MgO-CO_2 (right) ternary plots for a) Jericho aphanitic and bulk macrocrystal kimberlite, and b) Jericho primitive kimberlites, worldwide primitive kimberlites and average worldwide kimberlites. The black arrow is from low to high temperature (higher degrees of partial melts) from Dalton and Presnall's (1990) melting experiments on a carbonated garnet lherzolite.

Jericho primitive samples plot very close to the Dalton and Presnall (1990) trend. The Wesselton kimberlite also plots close to this trend and therefore also may represent a good primitive kimberlite melt.

Canil and Scarfe (1990) also investigated melting of synthetic CO_2-bearing peridotites at varying temperatures and pressures. They produced partial melts at 5, 7 and 9 GPa within 100°C of the solidus and the results are given, along with the starting composition, in Table 4.4. They found that their partial melts formed at 5 and 7 GPa were not unlike that those of primary uncontaminated kimberlites in CaO-MgO-SiO_2 space. Kimberlites used for comparison were the Wesselton kimberlite (as mentioned in this thesis) and a Lesotho kimberlite from Eggler and Wendlandt (1979). The Lesotho kimberlite sample, however, has since been found to contain significant crustal contamination and is not a good representative of a primary kimberlite magma (Mitchell, 1995).

4.3.3 Origin of the Jericho primary magma

The geotherm established by Kopylova *et al.* (1998) from peridotite and pyroxenite data suggests that a kimberlite magma sampling these xenoliths must have been generated at depths greater than approximately 6.5 GPa and at temperatures greater than 1300°C (Fig. 4.4). These pressures and temperatures are similar to the 6 GPa and 1450-1500°C conditions Dalton and Presnall (1998) used to generate kimberlitic melts from a carbonated garnet lherzolite source. They show that the compositions of the Jericho primitive kimberlite samples could be primary kimberlite melts formed under these conditions. Canil and Scarfe (1990) also were able to produce kimberlite-like melts at 5 and 7 GPa but at lower temperatures (1320-1450°C), however the compositions of their partial melts are much more SiO_2 and MgO rich than Dalton and

Presnall's (1998) melts and are more similar to macrocrystal kimberlite than primary kimberlite melt.

In summary, Dalton and Presnall's (1998) partial melt experiments were performed at similar temperatures and pressures to the Jericho primary melt. The formation of kimberlitic partial melts at these temperatures and pressures suggest it's plausible that the Jericho primary kimberlite melt formed as a < 1 volume % partial melt from a carbonated garnet lherzolite source.

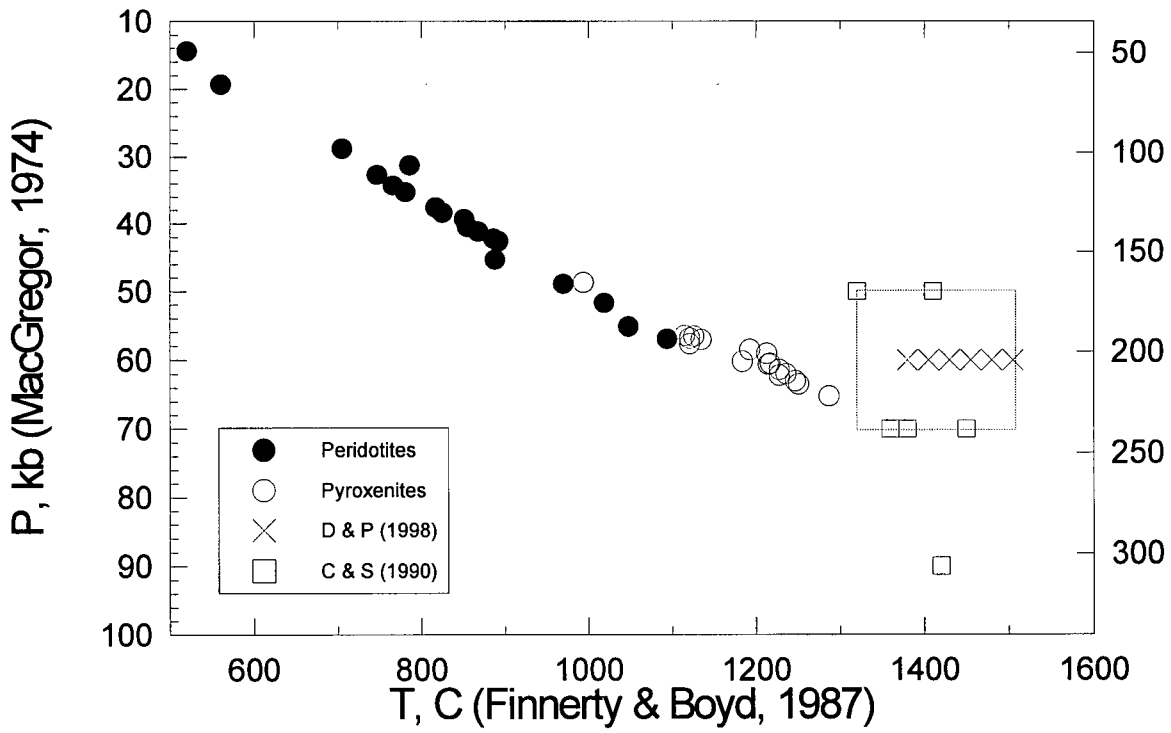

Figure 4.4 Equilibrium P-T estimates for the Jericho peridotites and pyroxenites (including porphyroclastic peridotites) using the methods of Finnerty and Boyd (1987) and MacGregor (1974). After Kopylova *et al.*, (1998). The dashed box encloses experimental partial melts which have kimberlitic compositions (Dalton and Presnall, 1998 (D&P, 1998) and Canil and Scarfe, 1990 (C&S, 1990)).

Chapter 5
CONCLUSIONS

For this study, six samples of aphanitic kimberlite (<3% macrocrysts) were collected from the Jericho kimberlite in an attempt to identify primitive, or even primary, kimberlite melts. As there is no evidence for quenched 'glassy' kimberlite, aphanitic kimberlite is the next best approximation of a primitive melt, as it is devoid of macrocrysts, which could be xenolithic. Based on macroscopic observations, the samples were divided into two groups. The first group is composed of three samples of 'chilled margin' kimberlite, and the second group consists of three samples of 'flow differentiated' kimberlite. The chilled margin samples are associated with the edges of thin macrocrystal Phase 1 kimberlite dykes. The flow differentiated samples are associated with the edge of the Phase 2 diatreme, and it is likely that crystals were removed from these samples by processes occurring at the margins of the kimberlite diatreme during emplacement.

Petrographically, three of the chilled margin samples (JD51, JD69 and JD82) are very similar with few microphenocrysts (<30%) set in a fine-grained matrix of predominantly serpentine and calcite. The flow differentiated samples (4S, 4SA and LGS07) have a higher proportion of microphenocrysts (50%) and these crystals are rounded, suggesting they may be xenocrysts which were milled during transport and emplacement.

Geochemically, all samples have high Mg#, Cr and Ni contents indicative of primary magmas. Samples JD51, JD69 and JD82 all have very high CO_2 contents, suggesting there was little degassing during emplacement. Sample LGS07 has a moderate CO_2 content and samples 4S

and 4SA have anomalously low CO_2 (<1 wt%) suggesting extensive degassing. Crustal contamination by the host granite (Contwoyto Batholith) is observed geochemically in samples 4S, 4SA and JD51 with elevated U and Th levels. Sample 4SA also has a pervasive secondary Fe- Si-rich alteration.

Geochemically and petrographically, the chilled margin samples JD69 and JD82 appear to be the closest example of a primary melt at Jericho to date. Primary characteristics of these melts include their Mg#, Cr, Ni and incompatible element contents. The CO_2 content of these samples represents a minimum value for the primary magma.

These primitive kimberlite samples have similar chemical compositions to other 'primitive' kimberlite magmas from Canada and South Africa. The Wesselton kimberlite, which some authors have referred to as the least fractionated kimberlite identified (Edgar et al., 1998; Edgar and Charbonneau, 1993; Mitchell, 1995) is somewhat similar to the two Jericho primitive samples.

The geochemical characteristics of Dalton and Presnall's (1998) partial melts of a carbonated garnet lherzolite at 6 GPa are similar to the composition of the Jericho primitive kimberlites. These partial melts are <1 vol% of the source rock and exist at temperatures between approximately 1450-1500°C. Given the Kopylova *et al.* (1998) geotherm for the Jericho peridotites and pyroxenites, which suggests the Jericho primary kimberlite magma originated from pressures of approximately 6.5 GPa (220 km), and at temperatures greater than 1300°C, results of their experiments are relevant. In the absence of contrary evidence, a carbonated garnet lherzolite source is plausible.

With the further collection of examples of primitive kimberlite worldwide, we may start to see differences in the nature of the primary magmas. These differences may give us an insight

into mantle composition and heterogeneity, and/or partial melting processes.

REFERENCES

Apter, D. B., Harper, F. J., Wyatt, B. A. & Smith, B. H. S. (1984). The Geology of the Mayeng Kimberlite Sill Complex, South Africa. In: Kornprobst, J. (ed.) *KIMBERLITES. I: Kimberlites and Related Rocks*. Vol. 11A, Developments in Petrology series, Elsevier, pp. 43-57.

Arima, M., Nakayama, K., Akaishi, M., Yamaoka, S. & Kanda, H. (1993). Crystallization of diamond from a silicate melt of kimberlite composition in high-pressure and high-temperature experiments. *Geology* **21**, 968-970.

Arima, M. & Inoue, M. (1995). High pressure experimental study on growth and resorption of diamond in kimberlite melt. *Ext. Abstr. VI Int. Kimberlite Conf.*, 8-10.

Berg, G. W. (1998). Geochemical Relations which reflect the History of Kimberlites from the Type area of Kimberley, South Africa. *7th Int. Kimb. Conf., Ext. Abstr. vol.* 76-78.

Berg, G. W. & Carlson, J. A. (1998) The Leslie Kimberlite Pipe of Lac de Gras, Northwest Territories, Canada: Evidence of Near Surface Hypabyssal Emplacement. *7th Int. Kimb. Conf., Ext. Abstr. vol.* 81-83.

Bhattacharji, S. (1967). Mechanics of flow differentiation in ultramafic and mafic sills. *Journal of Geology* **75**, 101-112.

Brey, G. P. and Ryabchikov, I. D. (1994). Carbon dioxide in strongly silica undersaturated melts and origin of kimberlite magmas. *Neues Jahrb. Mineral. Monatsh.* **10**, 449-463.

Canil, D. & Scarfe, C. M. (1990). Phase Relations in Peridotite + CO_2 Systems to 12 GPa: Implications for the Origin of Kimberlite and Carbonate Stability in the Earth's Upper Mantle. *Journal of Geophysical Research* **B10**, 15805-15816.

Chacko, T. (1993). Experimental studies of equilibrium oxygen and carbon isotopic fractionation factors between phases. In: Luth, R. W. (ed.) *Experiments at High Pressure and Applications to the Earth's Mantle*. Vol. 21, pp.357-384. Mineralogical Association of Canada.

Clayton, R. N. & Keiffer, S. W. (1991). Oxygen isotopic thermometer calculations. In: Taylor, H. P. Jr. et al. (eds) *Stable Isotope Geochemistry: A Tribute to Samuel Epstein*, Spec. Pub. No. 3, pp. 3- 10. The Geochemical Society.

Clement, C. R. (1982). A comparative geological study of some major kimberlite pipes in the Northern Cape and Orange Free State. Ph.D thesis, Univ. Cape Town.

Cookenboo, H. O. (1998) Emplacement history of the Jericho kimberlite pipe, northern Canada. *7th Int. Kimb. Conf., Ext. Abstr. vol.* 161-163.

Cookenboo, H. O., Orchard, M. & Daoud, D. (1998). Remnants of Paleozoic cover on the

Archean Canadian Shield: Limestone xenoliths from kimberlite in the central Slave Craton. Geology *(In press).*

Cui, Y. & Russell, J. K. (1995). Magmatic origins of calc-alkaline intrusions from the Coast Plutonic Complex, southwestern British Columbia. *Canadian Journal of Earth Sciences* **32**, 1643-1667.

Cullers, L. R., Mullenax, J., Dimarco, M. J. & Nordeng, S. (1982). The trace element content and petrogenesis of kimberlites in Riley County, Kansas, U.S.A. *American Mineralogist* **67**, 223-233.

Dalton, J. A. & Presnall, D. C. (1998) The continuum of primary carbonatitic-kimberlitic melt compositions in equilibrium with lherzolite: data from the system CaO-MgO-Al_2O_3-SiO_2-CO_2 at 6 GPa. *Journal of Petrology* (In press).

Davis, W. J. (1997). U-Pb zircon and rutile ages from granulite xenoliths in the Slave province: Evidence for mafic magmatism in the lower crust coincident with Proterozoic dike swarms. *Geology* **25**, 343-346.

Deines, P. & Gold, D. P. (1973). The isotopic composition of carbonatite and kimberlite carbonates and their bearing on the isotopic composition of deep-seated carbon. *Geochimica Cosmochimica Acta* **37**, 1709-1733.

Edgar, A. D. & Charbonneau, H. E. (1993). Melting experiments on a SiO_2-poor, CaO-rich aphanitic kimberlite from 5-10 GPa and their bearing on sources of kimberlite magmas *American Mineralogist* **78**, 132-142.

Edgar, A. D., Arima, M., Baldwin, D. K., Bell, D. R., Shee, S. R., Skinner, M. W. & Walker, E. C. (1988). High-pressure-high-temperature melting experiments on a SiO2-poor aphanitic kimberlite from the Wesselton mine, Kimberley, South Africa. *American Mineralogist* **73**, 524-533.

Edwards, D., Rock, N. M. S., Taylor, W. R., Griffin, B. J. & Ramsay, R. R. (1992). Mineralogy and Petrology of the Aries Diamondiferous Kimberlite Pipe, Central Kimberley Block, Western Australia. *Journal of Petrology* **33**, 1157-1191.

Eggler, D. H. & Wendlandt, R. F. (1979). Experimental studies on the relationship between kimberlite magmas and partial melting of peridotite. In: Boyd, F. R. & Meyer, H. O. A. (eds) *Kimberlites, diatremes and diamonds: Their geology, petrology and geochemistry*, Am. Geophys. Union, Washington, D. C., pp. 331-338..

Fesq, H. W., Kable, E. J. D. & Gurney, J. J. (1975). Aspects of the geochemistry of kimberlites from the Premier Mine and other South African occurrences, with particular reference to the rare earth elements. *Physics and Chemistry of the Earth* **9**, 686-707.

Girnis, A. V., Brey, G. P. & Ryabchikov, I. D. (1995). Origin of Group IA kimberlites: Fluid-saturated melting experiments at 45-55 kbar. *Earth. Planet. Sci. Lett.* **134**, 283-296.

Heaman, L. M., Creaser, R. A. & Cookenboo, H. O. (1998). Zircons from eclogite in the Jericho Kimberlite Pipe, northern Canada: Evidence for Proterozoic High Pressure Metamorphism Beneath the Slave Province. *7th Int. Kimb. Conf., Ext. Abstr. vol.* 325-327.

Hoffman, P. & Hall, L. (1993) Geology, Slave Craton and environs, District of Mackenzie, Northwest Territories, Geological Survey of Canada, Open File 2559.

Ilupin, I. P. & Lutz, B. G. (1971). The chemical composition of kimberlite and questions on the origin of kimberlite magmas. *Sovietskaya Geol.* **6**, 61-73 (in Russian).

Jenner, G. A., Longerich, H. P., Jackson, S. E. & Fryer, B. J. (1990). ICP-MS: a powerful tool for high-precision trace-element analysis in earth sciences: evidence from analysis of selected U.S.G.S. reference samples. In: (ed. P. J. Potts *et al.*) *Microanalytical methods in mineralogy and geochemistry. Chemical Geology* **83**, 133-148.

Kirkley, M. B., Smith, H. B. & Gurney, J. J. (1989). Kimberlite carbonates - a carbon and oxygen stable isotope study. *In* Ross *et al.* (eds) Kimberlites and Related Rocks, Geological Society of Australia Special Publication No. 14, vol. 1, pp. 264-281.

Kobelski, B. J., Gold, D. P. & Deines, P. (1979). Variations in stable isotope compositions for carbon and oxygen in some South African and Lesothan kimberlites. *In* Boyd and Meyer (eds) Kimberlites, Diatremes and Diamonds: Their Geology, Petrology and Geochemistry, American Geophysical Union, vol. 1, pp. 264-281.

Kopylova, M. G., Russell, J. K. & Cookenboo H. (1998). Petrography and Chemistry of the Jericho kimberlite (Slave Craton, Northern Canada) *7th Int. Kimb. Conf., Ext. Abstr. vol.* 449-451.

LeCheminant, A. N. & Heaman, L. M. (1989). Mackenzie igneous events, Canada: Middle Proterozoic hotspot magmatism associated with ocean opening. *Earth and Planetary Science Letters* **96**, 38-48.

Legault, M. I. & Charbonneau, B. W. (1993). Geophysical, geochemical, and petrographical study of the Contwoyto Batholith, Lupin gold mine area, Northwest Territories. In: *Current Research*, Part E. Geol. Surv. Canada, Paper 93-1E, p. 207-218.

Matsuhisa, Y., Goldsmith, J. R. & Clayton, R. N. (1979). Oxygen isotopic fractionation in the system quartz-albite-anorthite-water. *Geochimica Cosmochimica Acta* **43**, 1131-1140.

McDonough, W. F., Sun, S., Ringwood, A. E., Jagoutz, E. & Hofmann, A. W. (1992). Potassium, rubidium, and cesium in the Earth and Moon and the evolution of the mantle of the Earth. *Geochimica Cosmochimica Acta* **56**, 1001-1012.

Mitchell, R. H. (1986). *Kimberlites: Mineralogy, Geochemistry, and Petrology*. Plenum Press, New York, 442pp.

Mitchell, R. H. (1995). *Kimberlites, Orangeites, and Related Rocks*. Plenum Press, New York,

410pp.

Mitchell, R. H. (1997). *Kimberlites, Orangeites, Lamproites, Melilitites, and Minettes: A Petrological Atlas.* Almaz Press Inc., 243pp.

Nicholls, J. & Gordon, T. M. (1994). Procedures for the calculation of axial ratios on Pearce element-ratio diagrams. *Canadian Mineralogist* **32**, 969-977.

Nicholls, J. & Russell, J. K. (1991). Major-element chemical discrimination of magma-batches in lavas from Kilauea volcano, Hawaii, 1954-1971 eruptions. *Canadian Mineralogist* **29**, 981-993.

Pearce, T. H. (1968). A contribution to the theory of variation diagrams. *Contributions to Mineralogy and Petrology* **19**, 142-157.

Ringwood, A. E., Kesson, S. E., Hibberson, W. & Ware, N. (1992). Origin of kimberlites and related magmas. *Earth and Planetary Science Letters* **113**, 521-538.

Russell, J. K. & Nicholls, J. (1988). Analysis of petrologic hypotheses with Pearce element ratios. *Contributions to Mineralogy and Petrology* **99**, 25-35.

Russell, J. K. & Snyder, L. D. (1997). Petrology of picritic basalts from Kamloops, British Columbia: Primary liquids from a Triassic-Jurassic arc. *Canadian Mineralogist* **35**, 521-541.

Scott Smith, B. H. (1996). Kimberlites. *In* Mitchell, R. H. (ed.) Undersaturated Alkaline Rocks: Mineralogy, Petrogenesis, and Economic Potential. Mineralogical Society of Canada, Short Course Series v. 24, p.217-243.

Shee, S. R. (1986). The petrogenesis of the Wesselton mine kimberlites, Kimberley, South Africa. Ph. D. thesis, University of Cape Town, Cape Town, South Africa.

Sheppard, S. M. F. & Dawson, J. B. (1975). Hydrogen, carbon and oxygen isotope studies of megacryst and matrix minerals from Lesothan and South African kimberlites. *Physics and Chemistry of the Earth* **9**, 747-763.

Smith, C. B., Gurney, J. J., Skinner, E. M. W., Clement, C. R & Ebrahim, N. (1985). Geochemical character of southern African kimberlites: a new approach based upon isotopic constrains. *Transactions of the Geological Society of South Africa* **88**, 267-280.

Smyth, J. R. and Clayton, R. N. (1988) Correlation of oxygen isotope fractionation and electrostatic potentials in silicates. *Eos* **69**, 1514 (abstr.).

Smyth, J. R. (1989) Electrostatic characterization of oxygen sites in minerals. *Geochimica Cosmochimica Acta* **53**, 1101-1110.

Stanley, C. R. & Russell, J. K. (1989). Petrologic hypothesis testing with Pearce element ratio diagrams: derivation of diagram axes. *Contributions to Mineralogy and Petrology* **103**, 78-89.

Sun, S. S. (1980). Lead isotopic study of young volcanic rocks from mid-ocean ridges, ocean islands and island arcs. *In* Bailey et al. (eds) The evidence for chemical heterogeneity in the Earth's mantle, Philosophical Transactions of the Royal Society of London, Series A, 409-445.

Taylor, S. R. & McLennan, S. M. (1985). *The continental crust: its composition and evolution.* Blackwell, Oxford.

Taylor, W. R., Tompkins, L. A. & Haggerty, S. E. (1994). Comparative geochemistry of West African kimberlites: evidence for a micaceous kimberlite end member of sublithospheric origin. *Geochimica Cosmochimica Acta* **58**, 4017-4037.

van Breemen, O., King, J. E. & Davis, W. J. (1989). U-Pb zircon and monazite ages from plutonic rocks in the Contwoyto - Nose Lakes map area, central Slave province, District of Mackenzie. *In* Radiogenic age and isotope studies, Report 3, Geological Survey of Canada, Paper 89-2, p.29-38.

Appendix A: Calculation of modes using false colour imagery

False colour images of backscatter electron images were produced to help identify groundmass minerals, and to determine their modal abundances. Calcite, serpentine, olivine and apatite were identified; however, it was difficult to differentiate between the other accessory minerals due to their similar mean atomic numbers and low modal abundances. Once the colour image was produced, a histogram of the colour ranges was made, and the area under the curve represented the mode, in area per cent. Fig. A1 shows an example of a backscatter electron image of sample 4S (Fig. 2.9) and the colour enhanced image. Note that it does not differentiate between serpentine in the groundmass and serpentine forming rims around the olivine.

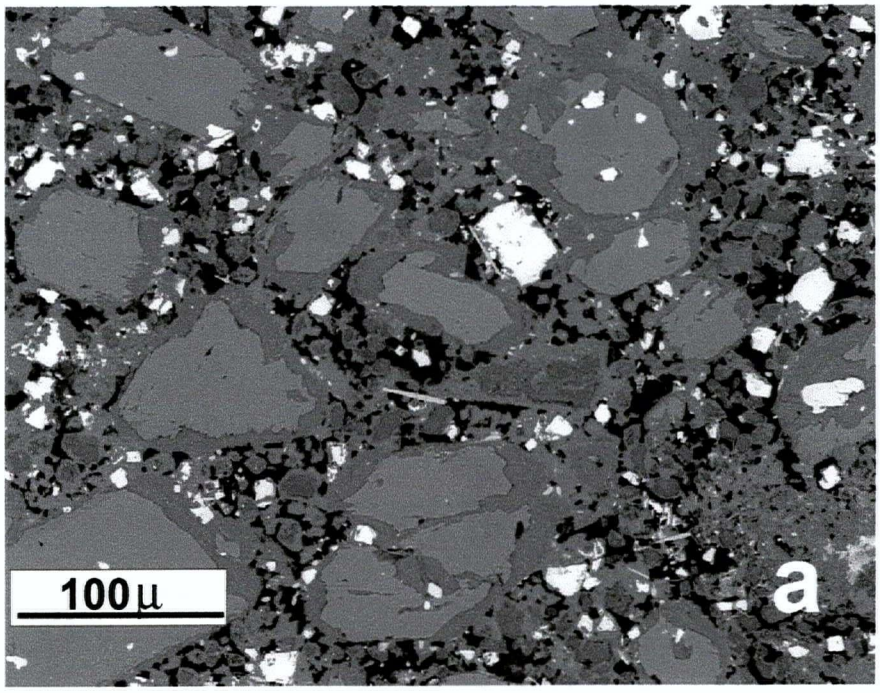

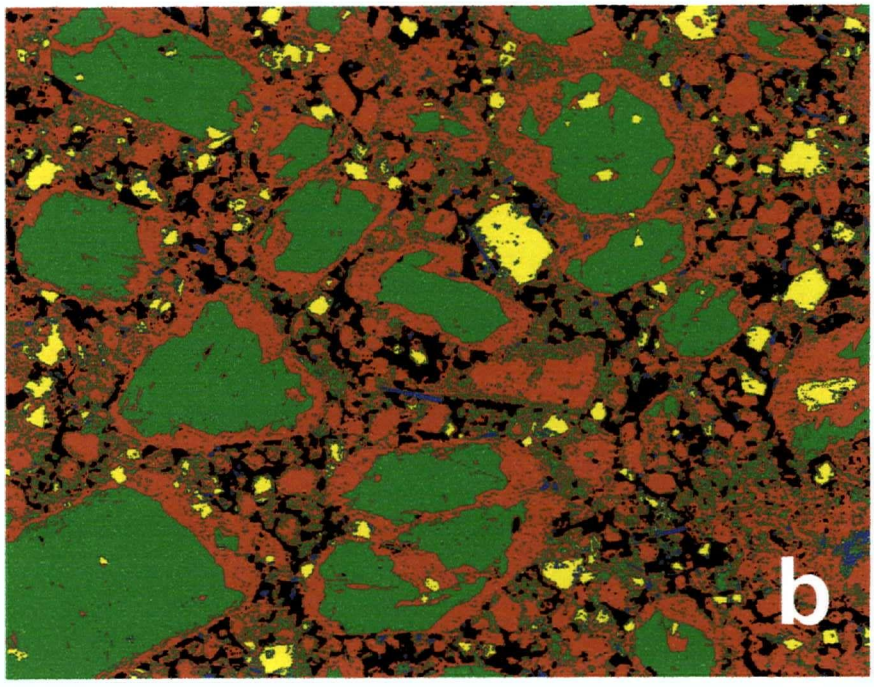

Figure A1. SEM backscatter electron micrographs of sample 4S. a) is the regular image and b) is the colour-enhanced image. Olivine microphenocrysts (green) have serpentinized rims (green), set in a groundmass of spinel and perovskite (yellow) and serpentine (red) and apatite laths (blue). The black space is void space and this rock has a microporosity.

Appendix B: Mineralogy of Jericho aphanitic kimberlite samples

Table B1: *Minor element chemistry and crystal morphology of kimberlite minerals*

Mineral	Minor elements*	Crystal morphology
Olivine	Fe, Mn	MC and MP: subhedral - rounded grains.
Serpentine	Fe	MP: pseudomorphs after rounded olivine grains, commonly highly strained; GM: primary anhedral mosaics.
Chlorite and clay minerals	Fe, Al	MP: pseudomorphs after rounded olivine grains, commonly highly strained.
Calcite	Sr	GM: typically occurs as primary anhedral mosaics. Rarely occurs as rhombic crystals (probably secondary).
Spinel + Ilmenite	Cr, Fe, Al, Ni	GM: Euhedral to subhedral cubic crystals. In JD51, JD69 and JD82 crystals are <20μ and in 4S, 4SA and LGS07 crystals are larger (<50μ).
Garnet		MC: rare grain sighted in JD69 with strongly developed kelyphitic rim.
Perovskite	Ti, Nb, Zr	GM: Euhedral to subhedral crystals.
Apatite	P, F	GM: Forms thin laths (up to 20μ).
Barite	Ba	GM: Euhedral to subhedral crystals.
Phlogopite	Ba	MP: rare grain sighted in JD69, strongly eroded.
Sulphides	Ni, Fe	GM: euhedral - cubic crystals.

*as observed from EDS spectra
MC = macrocrysts; MP = microphenocrysts; GM = groundmass

Appendix C: Treatment of Analytical Precision in Chemical Analyses

Major and trace elements

Major and trace elements were analysed for at the McGill University laboratories in Montreal, Canada. Their reported laboratory accuracy is within 1% for all major elements, except SiO_2 which has an accuracy of 0.5%. The trace element accuracy is reported as 5%. Instrument precision is within 0.6% relative, and overall laboratory precision is within 1.0% relative for beads and 0.65% relative for pellets. Detection limits are shown in Table C1. I adopted estimates of uncertainty of Russell and Snyder (1997) for the major elements because their samples were measured on the same XRF spectrometer at McGill University. For the trace elements, the overall laboratory precision was used. These results are shown in Table 3.1.

Table C1: Detection limits of major and trace elements (in ppm unless shown as relative percent, %)

SiO_2	60	MgO	95	BaO	17	Rb, Sr, Nb, Zr, Y,	1.0
TiO_2	35	CaO	15	Cr_2O_3	15	Pb, Ga, Th, U	
Al_2O_3	120	Na_2O	75	Ni	3		
Fe_2O_3*	30	K_2O	25	V	10	H_2O+	1.0%
MnO	30	P_2O_5	35			FeO, Fe_2O_3, H_2O,	0.01%

*Fe_2O_3 = total Fe calculated as Fe_2O_3

Rare earth elements

Based on replicate (N=3) analyses, precision is within 5% for all REE. The accuracy of these samples was determined by comparison with two standards (BHVO-1 and SY2), and is within 8%. The value of 1 standard deviation was determined for each REE from 3 duplicate analyses of JD51 (Table C2). The detection limit for the REE is shown in Table C2.

Table C2: *Details of rare earth element analyses of 3 duplicate analyses (of sample JD51) and 2 standards (BHVO-1 and SY2)*

	Detection Limit	51-1	51-2	51-3	1σ	BHVO-1		SY2	
						Meas.	Recom.	Meas.	Recom.
La	0.01	218.73	216.46	215.50	1.659	2.11	2.06	2.41	2.42
Ce	0.01	353.76	347.14	347.66	3.681	15.65	15.8	69.66	75
Pr	0.01	34.81	33.76	33.84	0.584	37.96	39	160.8	175
Nd	0.04	109.48	108.18	106.73	1.376	5.37	5.7	20.12	18.8
Sm	0.02	12.59	12.56	12.67	0.057	6.39	6.4	17.2	17
Eu	0.01	2.95	2.86	2.92	0.046	0.89	0.96	2.77	2.5
Gd	0.03	8.03	7.78	7.95	0.128	5.3	5.2	19.77	18
Tb	0.01	0.56	0.55	0.55	0.0058	6.21	6.2	15.74	16.1
Dy	0.01	2.76	2.75	2.76	0.0058	25.1	25.2	76.72	73
Ho	0.01	0.4	0.39	0.39	0.0058	0.97	0.99	4.49	3.8
Er	0.03	0.83	0.82	0.77	0.032	2.59	2.4	14.78	12.4
Tm	0.01	0.09	0.09	0.09	0.0000	0.34	0.33	2.46	2.1
Yb	0.03	0.43	0.47	0.48	0.026	1.95	2.02	17.59	17
Lu	0.01	0.07	0.06	0.06	0.006	0.28	0.291	2.9	2.7

Stable Isotopes

The value of 1 standard deviation was determined for each of the stable isotope data from 4 duplicate analyses of JD69 for the calcite fraction and 2 duplicate analyses of JD69 for the silicate fraction. (Table C3).

Table C3: *Duplicate analyses and standard deviations of stable isotope data (in ‰)*

	Calcite fraction					Silicate fraction			
	JD69-2				1σ	JD69-2		1σ	JD69 (no HCl)
Yield*	2.6	2.9	2.9	2.9	**0.2**	13.9	15.2	**0.9**	11.7
$\delta^{13}C_{PDB}$	-4.5	-4.6	-4.6	-4.6	**0.1**	-	-	-	-
$\delta^{18}O_{SMOW}$	16.1	15.9	15.7	15.9	**0.2**	5.2	7.2	**1.4**	4.7

*Yield is in micromoles of O_2/mg sample

The calcite fractions have relatively low errors (1 - 2%) but the silicate fractions have very high errors (6-27%). The $\delta^{18}O_{SMOW}$ errors are very high such that these values should be treated with caution. There is a good correlation between CO_2 content (wt%) and the yield of the calcite fraction (Fig. C1) which suggests the extraction of the calcite was successful. There is no

obvious correlation between SiO_2 content and the yield of the silicate fraction (Fig. C1). The presence of calcite affects the oxygen isotope ratios of the silicate fraction (K. Kyser, pers. comm.). This can be illustrated with sample JD69 where two splits were treated with HCl (removing the calcite) and one split was not treated (leaving calcite present). The split not treated gave the lowest yield, not surprisingly since calcite was also present, and correspondingly the lowest $\delta^{18}O_{SMOW}$.

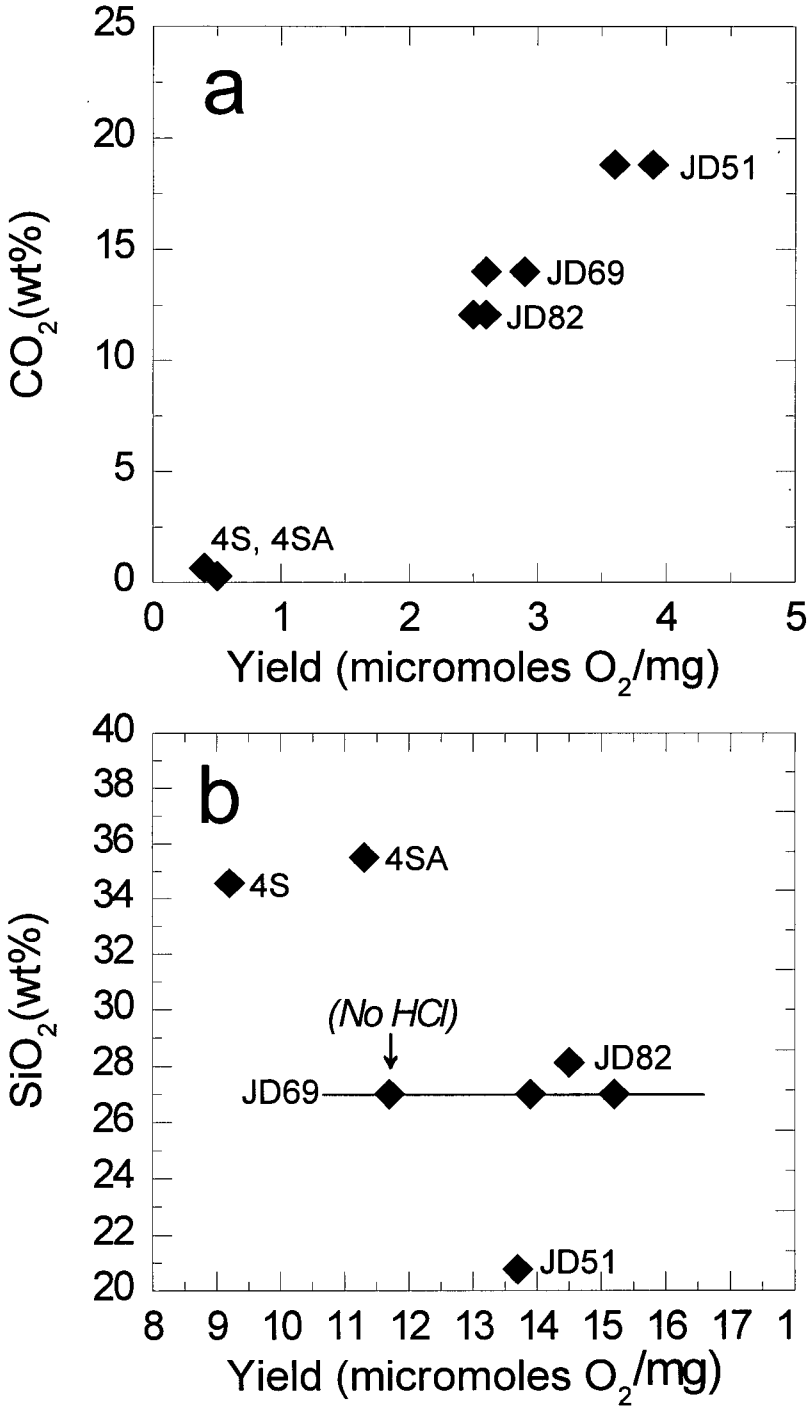

Figure C1. a) Measured CO_2 content (wt%) vs. yield of carbonate from sample. b)Oxygen isotope ratios of silicate fractions as a function of SiO_2 (wt%).

Appendix D: Major and trace element bulk geochemistry of the Jericho kimberlite (extended results of Kopylova *et al.*, 1998).

Chemical compositions of Phase 1 kimberlite is shown in Table D1, Phase 2 kimberlite in Table D2, Phase 3 kimberlite in Table D3, and kimberlite autoliths in Table D4. Analyses were performed by Chemex labs in Vancouver, Canada.

Table D1: *Phase 1 kimberlite samples (N=15)*

	Phase 1														
	1	2	3	4	5	6	7	8	9	10	11	12	13	14	15
SiO_2 (wt%)	34.95	34.07	33.50	30.65	31.65	34.95	32.43	32.55	34.18	31.42	34.87	33.36	32.19	30.86	33.97
TiO_2	0.60	0.91	0.78	0.79	0.64	1.23	0.82	0.78	1.22	0.95	1.18	0.80	1.28	1.11	1.79
Al_2O_3	1.44	1.46	1.71	1.45	2.00	1.90	1.69	1.79	1.88	2.04	2.43	2.08	1.67	1.58	1.56
Fe_2O_3	1.69	2.33	2.90	1.75	2.02	3.09	2.02	2.41	2.07	2.77	3.50	2.18	2.83	3.00	2.98
FeO	6.48	5.74	4.96	5.24	5.11	5.35	5.37	5.47	6.03	4.61	5.82	5.66	5.71	5.41	5.75
MnO	0.17	0.16	0.15	0.15	0.15	0.18	0.13	0.15	0.17	0.15	0.20	0.14	0.17	0.18	0.17
MgO	36.76	37.43	37.41	34.02	36.94	38.40	35.53	37.33	35.39	34.31	31.25	37.76	33.38	38.00	37.90
CaO	6.18	5.68	5.53	10.86	8.30	2.27	8.16	6.82	6.62	8.93	6.53	6.13	8.42	6.94	4.53
Na_2O	0.14	0.17	0.11	0.07	0.10	0.05	0.09	0.10	0.18	0.13	0.14	0.10	0.20	0.07	0.09
K_2O	0.20	0.22	0.11	0.10	0.12	0.09	0.14	0.07	0.39	0.19	0.20	0.10	0.18	0.05	0.22
P_2O_5	0.51	0.40	0.35	0.32	0.32	0.54	0.36	0.39	0.35	0.40	0.65	0.39	0.49	0.53	0.42
CO_2	4.36	4.00	3.67	8.21	6.23	1.06	6.09	4.99	5.06	6.49	4.22	4.29	5.98	4.29	2.24
H_2O+	4.06	5.23	6.43	4.45	4.47	8.46	5.30	5.31	3.87	5.75	5.13	4.64	4.44	5.76	6.32
H_2O-	0.73	0.81	1.04	0.76	0.71	0.90	0.45	0.41	0.99	0.52	2.84	0.75	0.84	0.77	0.61
Total	98.27	98.61	98.65	98.82	98.76	98.47	98.58	98.57	98.40	98.66	98.96	98.38	97.78	98.55	98.55
LOI	9.71	9.54	11.25	13.15	11.36	10.49	11.63	10.60	10.15	12.73	12.10	9.70	11.80	10.84	9.16
C.I.	0.98	0.94	0.94	0.94	0.91	0.96	0.96	0.92	1.00	0.97	1.18	0.94	1.01	0.85	0.93
Ilm Index	0.23	0.23	0.22	0.22	0.20	0.24	0.22	0.22	0.25	0.23	0.32	0.22	0.28	0.24	0.27
Fe_2O_3/FeO	0.26	0.41	0.58	0.33	0.40	0.58	0.38	0.44	0.34	0.60	0.60	0.39	0.50	0.55	0.52
Si/Mg	0.74	0.70	0.69	0.70	0.66	0.70	0.71	0.68	0.75	0.71	0.86	0.68	0.75	0.63	0.69
Mg#	89.1	89.5	89.8	89.9	90.5	89.4	89.8	89.7	88.9	89.6	86.1	89.8	87.8	89.3	88.9
Cr (ppm)	1916	1916	1847	1437	1642	2053	1505	1505	2326	1642	2532	1847	2258	2121	2121
Ba	1470	1340	1360	1400	1305	1645	1520	1525	1635	1495	3660	1525	1735	1655	1290
Rb	38	42	20	22	18	18	26	16	52	34	32	18	30	12	50
Sr	756	552	426	494	410	220	532	582	642	484	1160	564	772	756	306
Nb	136	132	124	116	88	162	122	128	152	128	224	132	172	182	152
Zr	75	57	54	48	45	75	54	63	66	81	102	60	72	72	60
Y	6	6	6	6	4	10	6	8	8	8	10	8	8	8	6
Pb	13	6	4	4	4	8	3	4	7	4	17	6	5	4	3
Ni	1550	1500	1450	1300	1300	1250	1300	1400	1500	1200	1350	1350	1550	1300	1450
F	530	590	370	980	430	270	550	470	570	690	750	700	460	650	350
S (%)	0.13	0.18	0.20	0.12	0.05	0.10	0.06	0.09	0.10	0.07	0.05	0.05	0.07	0.09	0.06

See Table D4 for notes

Table D2: *Phase 2 kimberlite samples (N=10)*

	Phase 2									
	1	2	3	4	5	6	7	8	9	10
SiO_2 (wt%)	30.12	34.86	34.07	35.85	36.87	36.11	35.29	37.16	35.87	36.26
TiO_2	1.49	0.84	0.86	0.70	0.65	0.90	0.59	0.58	0.73	0.59
Al_2O_3	3.80	2.36	2.28	2.44	2.89	2.46	3.50	2.73	2.46	2.68
Fe_2O_3	3.04	2.76	2.88	2.58	2.53	2.49	2.75	2.16	2.97	2.65
FeO	6.44	4.19	4.23	3.69	4.10	4.44	3.90	4.22	4.72	3.85
MnO	0.20	0.12	0.13	0.10	0.12	0.13	0.13	0.11	0.16	0.12
MgO	30.82	25.71	29.40	30.84	32.75	32.48	29.06	33.17	31.99	29.95
CaO	9.87	9.31	8.16	5.28	4.81	6.71	6.85	2.97	5.87	5.77
Na_2O	0.20	0.12	0.19	0.11	0.18	0.18	0.15	0.16	0.20	0.13
K_2O	0.27	0.62	0.58	0.57	0.80	0.92	0.62	0.42	0.61	0.79
P_2O_5	0.67	0.15	0.26	0.20	0.24	0.37	0.23	0.15	0.55	0.19
CO_2	6.93	6.23	5.76	3.78	2.82	4.11	4.66	1.76	3.85	4.11
H_2O+	3.97	7.37	7.48	9.25	8.55	5.50	9.01	10.75	6.20	8.46
H_2O-	0.57	3.48	1.75	3.66	1.52	0.77	1.66	2.51	2.87	1.67
Total	98.39	98.12	98.03	99.05	98.83	97.57	98.40	98.85	99.05	97.22
LOI	11.20	16.89	15.77	16.76	13.03	11.19	16.14	14.77	12.81	15.45
C.I.	1.09	1.39	1.20	1.20	1.16	1.13	1.29	1.18	1.16	1.24
Ilm Index	0.34	0.28	0.25	0.21	0.20	0.22	0.23	0.20	0.24	0.22
Fe_2O_3/FeO	0.47	0.66	0.68	0.70	0.62	0.56	0.71	0.51	0.63	0.69
Si/Mg	0.76	1.05	0.90	0.90	0.87	0.86	0.94	0.87	0.87	0.94
Mg#	85.7	87.3	88.5	90.1	90.2	89.7	89.0	90.6	88.5	89.5
Cr (ppm)	1847	2532	1574	1232	1711	1779	1368	1642	1847	1711
Ba	1735	1115	1070	645	715	2600	935	370	1720	825
Rb	28	62	68	58	68	108	64	44	80	78
Sr	512	204	450	430	238	608	296	264	734	396
Nb	180	124	92	72	88	128	80	58	154	72
Zr	102	60	51	48	45	72	63	39	81	48
Y	12	8	6	6	8	8	10	6	10	8
Pb	11	6	4	2	4	7	5	5	9	3
Ni	1150	1300	1400	1350	1350	1300	1000	1400	1600	1300
F	540	540	500	280	290	960	600	200	760	440
S (%)	0.29	0.35	0.12	0.09	0.07	0.04	0.03	0.04	0.10	0.06

See Table D4 for notes

Table D3: *Phase 3 kimberlite samples (N=8)*

	Phase 3							
	1	2	3	4	5	6	7	8
SiO_2 (wt%)	34.79	35.31	32.91	33.86	33.40	35.36	30.49	32.12
TiO_2	0.55	0.57	1.29	0.85	0.73	0.62	0.52	0.79
Al_2O_3	1.72	1.47	1.64	1.39	1.54	2.03	2.39	2.26
Fe_2O_3	2.34	2.28	2.17	2.29	4.04	2.35	1.95	3.07
FeO	5.00	5.27	5.68	5.00	3.39	5.05	3.94	4.23
MnO	0.13	0.12	0.13	0.13	0.14	0.12	0.12	0.15
MgO	37.23	36.37	36.22	36.39	36.49	36.51	30.85	31.08
CaO	4.64	4.71	6.96	6.39	5.18	4.15	10.60	8.31
Na_2O	0.08	0.09	0.07	0.06	0.24	0.11	0.04	0.11
K_2O	0.13	0.19	0.11	0.16	0.24	0.17	0.09	0.16
P_2O_5	0.10	0.07	0.26	0.14	0.28	0.13	0.25	0.24
CO_2	4.14	3.70	5.39	5.06	3.85	3.15	8.18	6.12
H_2O+	6.73	6.69	5.24	6.50	9.90	7.53	7.34	7.84
H_2O-	0.57	1.40	0.59	0.91	1.10	0.56	1.67	1.37
Total	98.15	98.24	98.66	99.13	100.52	97.84	98.43	97.85
LOI	11.42	11.81	10.81	12.51	13.72	11.48	17.32	15.98
C.I.	0.98	1.00	0.95	0.96	0.95	1.02	1.06	1.10
Ilm Index	0.20	0.21	0.24	0.22	0.21	0.21	0.20	0.25
Fe_2O_3/FeO	0.47	0.43	0.38	0.46	1.19	0.47	0.49	0.73
Si/Mg	0.72	0.75	0.70	0.72	0.71	0.75	0.77	0.80
Mg#	90.3	89.9	89.4	90.2	90.3	90.1	90.6	88.8
Cr (ppm)	2053	1642	1505	1505	1642	3216	1163	1779
Ba	430	270	1250	505	780	395	1540	1225
Rb	18	24	16	26	38	24	12	20
Sr	112	168	336	232	274	142	334	326
Nb	62	72	108	86	106	66	72	100
Zr	33	36	51	33	48	33	36	48
Y	4	6	8	2	6	6	6	8
Pb	6	4	5	3	5	4	2	2
Ni	1700	1750	1450	1550	1600	1550	1200	1300
F	180	320	420	290	320	250	770	600
S (%)	0.20	0.17	0.18	0.12	0.12	0.12	0.12	0.10

See Table D4 for notes

Table D4: *Kimberlite autolith samples (N=10)*

	Autoliths									
	1	2	3	4	5	6	7	8	9	10
SiO_2 (wt%)	31.08	29.36	33.26	29.83	31.21	29.19	33.54	28.85	34.16	24.65
TiO_2	1.22	1.07	1.04	0.82	1.00	0.85	1.17	0.84	1.16	1.09
Al_2O_3	2.84	1.94	1.84	2.04	2.16	1.70	1.85	2.09	1.55	2.15
Fe_2O_3	3.72	2.97	2.33	2.97	2.96	3.38	2.25	3.29	2.33	3.12
FeO	5.05	4.98	5.42	4.29	5.26	4.73	5.34	4.35	5.24	4.19
MnO	0.23	0.18	0.15	0.14	0.18	0.17	0.19	0.17	0.14	0.16
MgO	31.39	32.51	35.71	30.68	35.47	31.93	36.18	31.19	36.96	27.12
CaO	6.36	10.20	7.44	10.68	8.44	11.63	6.69	11.48	5.24	16.47
Na_2O	0.12	0.07	0.16	0.14	0.19	0.07	0.11	0.11	0.11	0.11
K_2O	0.13	0.09	0.14	0.15	0.12	0.12	0.26	0.13	0.15	0.15
P_2O_5	0.64	0.53	0.53	0.47	0.57	0.48	0.36	0.46	0.23	0.54
CO_2	4.33	8.21	5.24	7.85	5.83	8.84	4.84	8.54	3.85	12.06
H_2O+	9.44	6.30	4.49	6.99	4.88	5.43	5.48	5.91	7.01	5.98
H_2O-	3.20	1.13	0.75	1.24	0.66	0.59	0.75	1.24	0.72	0.86
Total	99.75	99.54	98.50	98.29	98.93	99.11	99.01	98.65	98.85	98.65
LOI	16.15	14.59	10.73	16.58	11.18	14.44	11.13	15.83	11.38	19.16
C.I.	1.08	0.96	0.98	1.03	0.94	0.96	0.97	0.99	0.96	0.98
Ilm Index	0.30	0.27	0.24	0.25	0.25	0.27	0.23	0.26	0.23	0.29
Fe_2O_3/FeO	0.74	0.60	0.43	0.69	0.56	0.72	0.42	0.76	0.45	0.75
Si/Mg	0.77	0.70	0.72	0.75	0.68	0.71	0.72	0.72	0.72	0.70
Mg#	87.0	88.3	89.4	88.7	88.9	88.0	89.8	88.4	90.0	87.4
Cr (ppm)	2189	1779	1916	1779	1984	1437	2463	1642	2053	1711
Ba	n.a.	n.a.	1640	1985	955	1530	1435	1735	n.a.	2600
Rb	n.a.	n.a.	32	30	30	22	32	26	n.a.	28
Sr	n.a.	n.a.	584	574	500	462	334	584	n.a.	692
Nb	n.a.	n.a.	152	144	196	140	162	140	n.a.	170
Zr	n.a.	n.a.	66	72	84	69	57	66	n.a.	78
Y	n.a.	n.a.	8	10	12	10	6	8	n.a.	10
Pb	7	n.a.	2	7	n.a.	8	7	n.a.	3	6
Ni	1400	n.a.	1200	1200	n.a.	1450	1650	n.a.	1550	910
F	600	590	610	700	760	990	340	850	210	1080
S (%)	0.14	0.05	0.06	0.11	0.08	0.07	0.07	0.09	0.12	0.01

Notes:

n.a. = not analysed for

C.I. (Contamination Index) = $(SiO_2 + Al_2O_3 + Na_2O)/(MgO + 2K_2O)$, after Clement (1982).

Ilm. I. (Ilmenite Index) = $(FeO(t) + TiO_2)/(MgO + 2K_2O)$, after Taylor *et al.* (1994).

Mg# = 100. $Mg/(Mg + Fe^{2+})$ where Fe^{2+} is calculated from FeO(t).

Cr (ppm) was recalculated from Cr_2O_3 (wt%).

LOI = Loss on ignition

Appendix E: Calculation of theoretical yields, whole rock $\delta^{18}O_{SMOW}$, and mineral-mineral fractionation factors for stable isotope results.

1. CALCULATION OF THEORETICAL YIELDS

The theoretical yields for the carbonate and silicate fractions were calculated for each sample from geochemical and modal analyses, and compared to the extracted yield.

Carbonate fraction

Based on EDS analysis, all carbonate in the samples exists as calcite. Only Sr was identified as an impurity (approximately 1 wt% of the calcite, as determined from geochemical analyses).

To extract the calcite, it is reacted with phosphoric acid which releases CO_2 and leaves Ca and O behind in solution. Therefore, to calculate the theoretical yields of the carbonate fractions, the CO_2 wt% of the rock was divided by the total wt% of the sample analysed. The results are shown in Table E1.

Silicate fraction

Two methods have been used to calculate the theoretical yields of the silicate fraction, and the results are shown in Table E1. As calcite was removed from these samples prior to analysis, approximately 95% of the sample consists of silicates.

Method 1: Summation of oxides

For each oxide in the sample (excluding CaO and CO_2 which have been removed as calcite, and H_2O-), the μmol O_2 was determined per total amount of sample (ie. the sum of the oxide wt). The μmol O_2 for each oxide was summed and divided by the total amount of sample to determine the

μmol O_2 /mg sample of the silicate fraction, which are the units of the extracted yield.

Method 2: Using modes of serpentine and olivine

For each sample, the mode of olivine and serpentine has been determined (see Table 2.1). As these two minerals comprise nearly 100% of the silicate fraction, the modal proportions were used to calculate the theoretical yield. For these calculations, pure serpentine [$Mg_3Si_2O_5(OH)_4$] and pure forsterite [Mg_2SiO_4] compositions were assumed. Firstly, the modes (calculated in 2 dimensions) were converted to vol.% (3 dimensions) presuming the same mode in the third dimension. Secondly, the mass was calculated using density data ($\rho_{serpentine}$ = 2.55g/cm^3; $\rho_{forsterite}$ = 3.22g/cm^3), and normalized to 100%. Thirdly, the mass values were converted to mol O_2/mg sample and added to give the total yield, knowing that 1 mol forsterite = 2 mol O_2, and 1 mol serpentine = 4.5 mol O_2.

Table E1: *Measured and theoretical yields (in μmol O_2/mg sample)*

	Measured yield		Theoretical yield		
	Carb.	Sil.	Carb.	Sil.[1]	Sil.[2]
JD51	3.8	13.7	4.3	15.0	16.2
JD69	2.9	14.6	3.2	15.4	16.2
JD82	2.6	14.5	2.7	15.1	16.2
4S	-	9.2	-	14.3	15.5
4SA	-	11.3	-	13.8	15.4

Carb. = carbonate fraction; Sil. = silicate fraction.
[1] Calculated by summing oxides (Method 1)
[2] Calculated using modes of serpentine and olivine (Method 2)

The theoretical yields of Method 2 are higher than that of Method 1. Method 1 is probably a more accurate calculation, but similar yields were produced using Method 2 even though several assumptions had to be made.

2. CALCULATION OF $\delta^{18}O_{SMOW}$ FOR THE WHOLE ROCK.

Whole rock $\delta^{18}O$ values are presented in Table E2. To calculate $\delta^{18}O$ of the whole rock, I used the following equation:

$$\delta^{18}O_{rock} = \Sigma\ \delta^{18}O_{mineral} \cdot X_O$$

where $\delta^{18}O$ of each mineral is multiplied by the proportion of Oxygen atoms in the mineral (X_O). For samples JD51, JD69 and JD82, which are predominantly calcite and serpentine the equation is:

$$\delta^{18}O_{rock} = \Sigma\ \delta^{18}O_{calcite} \cdot X_{O(calcite)} + \delta^{18}O_{serpentine} \cdot X_{O(serpentine)}$$

Note that all $\delta^{18}O$ values are relative to the SMOW standard. $X_{O(mineral)}$ = [#moles mineral in sample] x [#O in mineral]. Then, because $\Sigma X_{O(minerals)}$ must equal 1, the values are normalized to 1. For samples 4S and 4SA, which have insignificant calcite, the whole rock essentially equals the proportion of serpentine.

Table E2: *Whole rock $\delta^{18}O$ values*

	$X_{O(calcite)}$ (#O = 3)	$X_{O(serpentine)}$ (#O = 9)	$\delta^{18}O_{rock}$ (‰)
JD51	0.43	0.57	11.81
JD69	0.32	0.68	9.37
JD82	0.28	0.72	9.17
4S	0	1	4.2
4SA	0	1	11.9

$\delta^{18}O_{calcite}$ and $\delta^{18}O_{serpentine}$ values are presented in Table 5.

3. CALCULATION OF MINERAL-MINERAL FRACTIONATION FACTORS

If calcite and serpentine were in equilibrium in the groundmass, the calculation of calcite-serpentine fractionation factors allows an estimation of the temperature of equilibrium. To calculate the fractionation factors between calcite, forsterite, serpentine, CO_2 and H_2O, the following equations were used (where $x = 10^6 T_{(K)}^{-2}$).:

From Clayton and Kieffer (1991):

$$\Delta_{quartz\text{-}calcite} = 0.335x + 0.05x^2 - 0.0035x^3$$

$$\Delta_{quartz\text{-}forsterite} = 3.79x - 0.228x^2 + 0.0091x^3$$

From Chacko (1993):

$$\Delta_{quartz\text{-}CO_2} = -4.346x + 0.802x^2 - 0.0507x^3$$

From Clayton and Kieffer (1991) with Matsuhisa *et al.* (1979):

$$\Delta_{quartz\text{-}H_2O} = 0.2617 + 0.451x + 0.714x^2 + 0.0019x^3$$

In order to estimate $\Delta_{quartz\text{-}serpentine}$, values from Smyth (1989) and Smyth and Clayton (1988) were used to determine:

$$\Delta_{quartz\text{-}lizardite} = 1.20x$$

All fractionation factors were calculated relative to quartz, and made relative to calcite by the following relationship:

$$\Delta_{quartz\text{-}calcite} - \Delta_{quartz\text{-}mineral} = \Delta_{mineral\text{-}calcite}$$

A $\Delta_{mineral\text{-}calcite}$ against temperature plot demonstrates the temperature dependence (Fig. E1). If serpentine and calcite were in equilibrium they would have a maximum $\Delta_{serpentine\text{-}calcite}$ of 3‰ (at 200°C) to less than 1 at higher temperatures.

$$\Delta_{serpentine\text{-}calcite} = \delta^{18}O_{calcite} - \delta^{18}O_{serpentine}$$

For JD51, JD69 and JD82, the values are 8.4, 9.9 and 9.9‰ respectively. These high values indicate that serpentine and calcite either were not in equilibrium during crystallization, or have later had their oxygen isotopes affected by alteration.

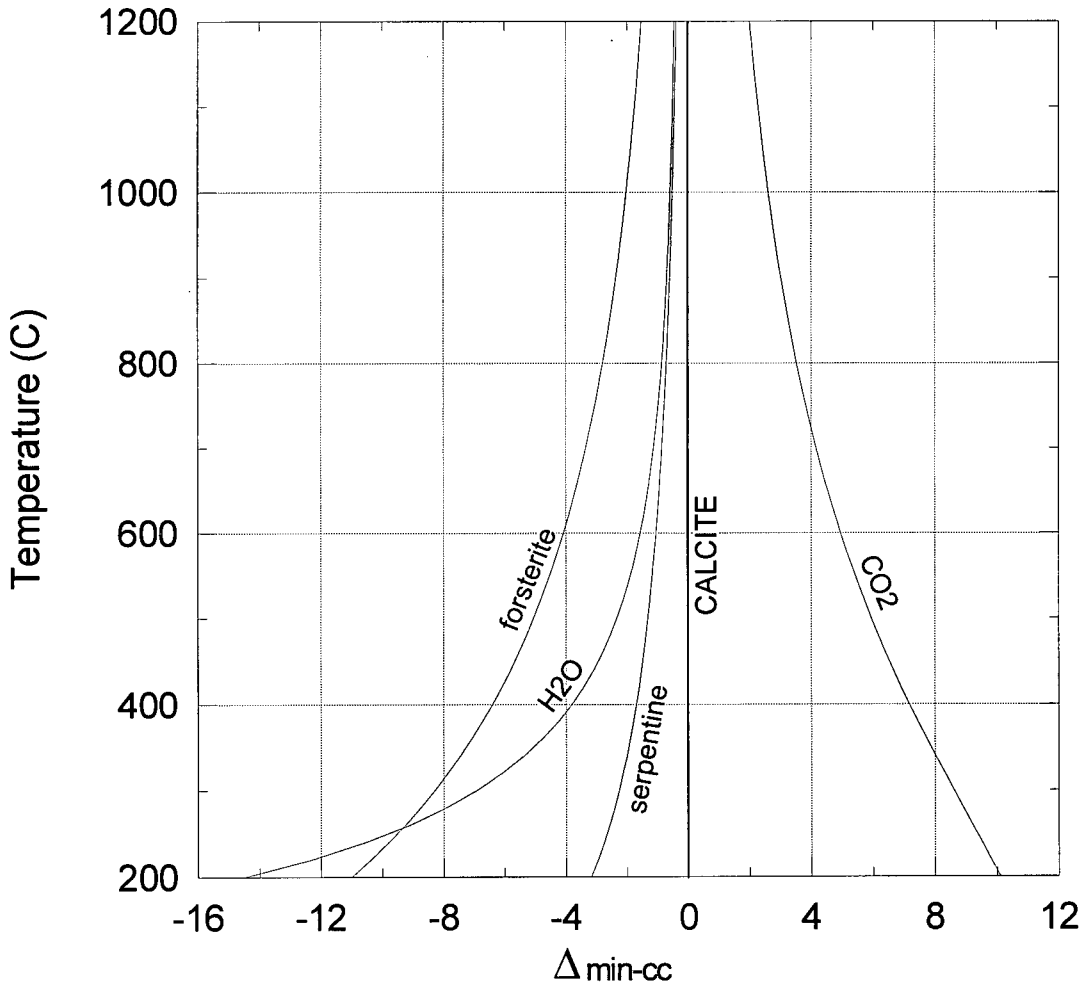

Figure E1 Fractionation curves between forsterite, serpentine, H_2O, CO_2 and calcite. $\Delta_{min\text{-}cc}$ is the fractionation between a mineral and calcite.

Appendix F: Geochemistry of the Contwoyto Batholith granite.

Table F1: *Average (N=50) values for major, minor and trace elements of the Contwoyto Batholith granite, after Legault and Charbonneau (1993) and B. Davis (pers. comm.)*

Oxide	Avg. value (wt%)	Element	Avg. value (ppm)	REE* (ppm)	Value (ppm)
SiO_2	72.57	Ba	535	La	18.82
TiO_2	0.15	Ce	41	Ce	39.90
Al_2O_3	15.04	La	23	Pr	4.68
FeO(t)	1.14	Pb	15	Nd	17.10
MnO	0.01	Rb	170	Sm	3.53
MgO	0.40	Sr	144	Eu	0.53
CaO	0.83	Th	11	Gd	2.81
Na_2O	4.30	U	6	Tb	0.32
K_2O	4.56	Zr	90	Dy	1.48
P_2O_5	0.21	Nb*	12.4	Ho	0.26
				Er	0.64
				Tm	0.08
				Yb	0.49
				Lu	0.07

*Nb and REE values are from B. Davies pers. comm. from a sample of the Contwoyto Batholith collected at 458700E and 7312800N. The Jericho kimberlite is located approximately between 478050 - 478200E and 7319345 - 7319745N.

Appendix G: Primordial mantle and chondrite compositions

Primordial mantle and chondrite values were used for normalizations of multi-element and REE plots. These values are listed in Table G1.

Table G1: *Primordial mantle values (McDonough et al, 1992) and chondrite values (Taylor and McLennan, 1985).*

	Primordial mantle	Chondrite
Rb	0.635	
Ba	6.99	
Th	0.084	
U	0.021	
K	240	
Nb	0.713	
La	0.708	0.367
Ce	1.833	0.957
Sr	21.1	
Nd	1.366	0.711
P*	90.4	
Hf	0.309	
Zr	11.2	
Sm	0.444	0.231
Ti	1280	
Tb	0.108	0.058
Y	4.55	
Pb	0.071	
Pr	0.137	
Eu		0.087
Gd		0.306
Dy		0.381
Ho		0.085
Er		0.249
Tm		0.036
Yb*	0.372	0.248
Lu*	0.057	0.038

*Primordial mantle values for P are from Sun (1980) and for Yb and Lu are from Taylor and McLennan (1985).